N 70 23454

NASA CR 109341

Study of a Design Modification to the Infrared Multidetector Spectrometer for the Nimbus "F" Experiment

By: B. D. Henderson

CASE FILE COPY

JET PROPULSION LABORATORY
CALIFORNIA INSTITUTE OF TECHNOLOGY
PASADENA, CALIFORNIA

FINAL REPORT

Study of a Design Modification
to the
Infrared Multidetector Spectrometer
for the
Nimbus "F" Experiment

By: B. D. Henderson

Contract No. 952673

February 27, 1970

Prepared for:

California Institute of Technology
Jet Propulsion Laboratory
4800 Oak Grove Drive
Pasadena, California 91103

Beckman® INSTRUMENTS, INC.
ADVANCED TECHNOLOGY OPERATIONS
FULLERTON, CALIFORNIA • 92634

TABLE OF CONTENTS

SECTION		PAGE
1	INTRODUCTION	1
2	FINAL PERFORMANCE REQUIREMENTS	3
3	MONOCHROMATOR	6
	1. Monochromator Ray Trace Procedures	10
	2. Selecting Grating Offset Angle and Grating Constant	12
	3. Final Monochromatic Design	26
	4. Single Line Entrance Slit	28
	5. Double Entrance Slits	35
	6. Spectral Image Aberrations	40
	7. Collimating Mirror	67
4	DETECTOR FOREOPTICS	70
	1. Aperture Stops for Detector Foreoptics	71
	2. Detector Location	89
5	TELESCOPE AND SCAN MIRROR	115
	Telescope Paraboloid Mirror and Auxillary Mirror	120
	Scan Mirror Location	133
6	FIXED FIELD DETECTORS	137
7	RADIATION COOLING SHIELD	138
8	MONOCHROMATOR ERROR ANALYSES	141
	1. Entrance Slit Locational Accuracy	141
	2. Grating Locational Accuracy	142
	3. Collimating Mirror Locational Accuracy	142
	4. Collimating Mirror Focal Length	142
9	CONCLUSION	145
10	REFERENCES	148

LIST OF ILLUSTRATIONS

FIGURE NO.		PAGE
1	Spectrometer Overall Dimensions and Location on Nimbus Ring	5
2	Three-View Drawing of the Axis System Used for the Ray-Trace of the Monochromator	7
3	Plot of λ vs. W for Commercial Gratings	9
4	Ray Starting Points in the (X_o, Y_o, Z_o) Axis System	16
5	Plot of Spectral Image Surface Aberrations for Grating Offset Angles of 25° and 30°	19
6	Plot of W vs. Wavelength, λ, for Grating Offset Angles of 25° and 30°	21
7	Graphical Determination of the Best Grating Offset Angle $\alpha_{2,3}$ and the Best Grating Constant	25
8	Entrance Slit Starting Points in the (X_o, Y_o, Z_o) Axis System of the Final Monochromator	37
9	Spectral Image for E4 Starting Point, W = 0.7903, λ = 3.7633	58
10	" " " W = 0.8533, λ = 4.0633	59
11	" " " W = 0.8953, λ = 4.2633	60
12	" " " W = 0.9163, λ = 4.3633	61
13	" " " W = 0.9373, λ = 4.4633	62
14	" " " W = 0.9583, λ = 4.5633	63
15	" " " W = 1.0633, λ = 5.0633	64
16	" " " W = 1.1685, λ = 5.5633	65
17	" " " W = 1.2733, λ = 6.0633	66
18	Optically Used Areas on Collimating Mirror Surface	68
19	Three-View Drawing of Axis Systems for Ray Trace of Detector Foreoptics	72
20	Spectral Image of Main Entrance Slit and Detector Lens Center and Cross Section W = .777 λ = 3.7 μ	76
21	" " " W = .840 λ = 4.0 μ	77
22	" " " W = .882 λ = 4.2 μ	78
23	" " " W = .903 λ = 4.3 μ	79
24	" " " W = .924 λ = 4.4 μ	80
25	" " " W = .945 λ = 4.5 μ	81
26	" " " W =1.050 λ = 5.0 μ	82
27	" " " W =1.155 λ = 5.5 μ	83
28	" " " W =1.260 λ = 6.0 μ	84
29	Comparison of Spectral Images for the Main Entrance Slit	85
30	Templates Used to Determine Optical Center Lines for Detector Lenses	87
31	Plan View of Detector Lens Locations Relative to Spectral Image Surface	90

LIST OF ILLUSTRATIONS (Continued)

FIGURE NO.		PAGE
32	25-Ray Spot Images of the Center and Four Corners of the Diffraction Grating Formed on the Detector $\lambda = 3.7\ \mu$	101
33	" " " $\lambda = 4.0\ \mu$	102
34	" " " $\lambda = 4.2\ \mu$	103
35	" " " $\lambda = 4.3\ \mu$	104
36	" " " $\lambda = 4.4\ \mu$	105
37	" " " $\lambda = 4.5\ \mu$	106
38	" " " $\lambda = 5.0\ \mu$	107
39	" " " $\lambda = 5.5\ \mu$	108
40	" " " $\lambda = 6.0\ \mu$	109
41	Expanded 25-Ray Spot Image for G1 Starting Point on Diffraction Grating	110
42	" " G2 "	111
43	" " G3 "	112
44	" " G4 "	113
45	" " G5 "	114
46	Plan View of Axes Used for Ray Trace of Telescope System	117
47	Telescope Angular Field-of-View--Sixteen 100-Ray Angular Images for the Sixteen Starting Points on the Two Entrance Slits. All Dimensions in Radians	121
48	Telescope Angular Field-of-View--Expanded 100-Ray Angular Image for Starting Point B1 on the Main Entrance Slit	123
49	" " B2 "	124
50	" " B3 "	125
51	" " B4 "	126
52	" " E1 "	127
53	" " E2 "	128
54	" " E3 "	129
55	" " E4 "	130
56	Optically Used Area on Paraboloid Telescope Mirror	131
57	Scan Mirror Location, Boundary Rays are Exhibited for Spectrometer Scan Angles, of 28° and 112°	133
Drawing 1	Plan View of Spectrometer	146
Drawing 2	Side View of Spectrometer	147

LIST OF TABLES

TABLE NO.		PAGE
1	Definitions for the Monochromator Axis System	13
2	Definitions for the Dimensional Parameters Which are Used to Specify the Linear and Rotational Transformations to Successive Axis Systems	14
3	Dimensional Parameters for the Preliminary Monochromator Using a 25° Grating Offset	17
4	Four Ray Starting Points for the Preliminary Monochromator Using a 25° Grating Offset	17
5	Dimensional Parameters for the Preliminary Monochromator Using a 30° Grating Offset	18
6	Four Ray Starting Points for the Preliminary Monochromator Using a 30° Grating Offset	18
7	The Coordinator of the Four Corners of the Grating Ruled Area	18
8	Spectral Image Surface Locations, Z_5 Coordinates, as a Function of Grating Offset Angle, Grating Constant, and Wavelength	22
9	Spectral Image Surface Width and Optical Width of Collimating Mirror for Various Grating Constants, and for 25° and 30° Grating Offsets. The Wavelength Range in all Cases is 3.5 μ to 6.5 μ	23
10	Best Grating Offset Angle and the Resultant Spectral Image Surface Spread and Optical Width of Collimating Mirror for the 3.7 μ to 6.0 μ Wavelength Range	27
11	Dimensional Parameters for the Final Monochromator Ray Trace	27
12	Four Ray Starting Points on Single-Line Entrance Slit for the Final Monochromator	29
13	Spectral Image Surface Characteristics, Entrance Slit Starting Point A1	30
14	" " " A2	31
15	" " " A3	32
16	" " " A4	33
17	Definition of Terminology Used for Spectral Image Characteristic Tables	34
18	Sixteen Entrance Slit Starting Points for the Two Entrance Slits of the Final Monochromator	38
19	Spectral Image Surface Characteristics, Starting Point B1	41
20	" " " B2	42
21	" " " B3	43
22	" " " B4	44
23	" " " C1	45
24	" " " C2	46
25	" " " C3	47
26	" " " C4	48
27	" " " D1	49
28	" " " D2	50
29	" " " D3	51
30	" " " D4	52

LIST OF TABLES (Continued)

TABLE NO.		PAGE
31	Spectral Image Surface Characteristics, Starting Point E1	53
32	" " " E2	54
33	" " " E3	55
34	" " " E4	56
35	W Values and Equivalent Wavelengths Used for the Ray Trace of the Two Entrance Slits	57
36	Definitions for the Axis Systems Used to Ray-Trace the Detector Foreoptics	73
37	Five Ray Starting Points on Grating Ruled Surface That are Used to Ray-Trace Detector Foreoptics	74
38	Dimensional Parameters for the Axis System Used to Ray-Trace the Detector Foreoptics	74
39	Location of Aperture Stops Relative to (X_2', Y_2', Z_2') Axis System, Aperture Stop Size, and Index of Refraction of Detector Lens	88
40	Diffraction Grating Image Characteristics on Emersed Detector W = .777 λ = 3.7 μ for 210 L/MM Grating	91
41	" W = .840 λ = 4.0 μ "	92
42	" W = .882 λ = 4.2 μ "	93
43	" W = .903 λ = 4.3 μ "	94
44	" W = .924 λ = 4.4 μ "	95
45	" W = .945 λ = 4.5 μ "	96
46	" W = 1.050 λ = 5.0 μ "	97
47	" W = 1.155 λ = 5.5 μ "	98
48	" W = 1.260 λ = 6.0 μ "	99
49	Definitions for the Axis System Used to Ray-Trace the Telescope System	118
50	Dimensional Parameter for Telescope System	119
51	Angular Field Image Characteristics for the Paraboloid Telescope, and the α_8'' and β_8'' Angular Displacements Required to Match the Angular Centroids for the Starting Points Along the Outer Edges of the Two Entrance Slits	122
52	Length of Scan Mirror Required for Mirror Spectrometer View Angles	134
53	Axial Ray Error Analysis for Final Monochromator	143
54	100-Ray Error Analysis for Final Monochromator	144

SECTION 1

INTRODUCTION

The California Institute of Technology Jet Propulsion Laboratory (JPL) has contracted Beckman Instruments, Inc. (Contract No. 952673) to perform an optical ray trace analysis of an infrared multidetector spectrometer which has been designed for a Nimbus "F" experiment. The purpose of this ray trace analysis is to delineate optimal optical design modifications to the four major parts of the spectrometer: the Monochromator, Detector Foreoptics, Telescope and Scanning Mirror, and Radiation Cooling Shields for the Detectors.

The final monochromator optical design which is presented in this report is based heavily on the monochromator design for a proposed Mars fly-by spectrometer. The optical ray trace analysis for that monochromator and its telescope was performed in 1964 by Henderson (1), and Henderson and Zerucha (2), (3), and that instrument was constructed at JPL; Schaper and La Porte (4) and Schaper (5), and successfully tested in a balloon flight in 1967; Shaw, McClatchey, and Schaper (6), and again in 1969 McClatchey and Shaw (7).

The final monochromator design detailed in this report differs from the Mars fly-by monochromator in the following respects:

1. The angular offset of the grating normal from the collimating mirror axis is now 26° rather than 30°.

2. The new grating constant is 210 1/mm rather than 240 1/mm.

3. A dimensionally wider spectral image surface is now provided for the detectors, the new width being 7 inches. Similarly, a dimentionally wider collimating mirror is required. The used width of the new collimating mirror, not including supporting areas, is 8.75 inches.

4. Two entrance slits are now used rather than one. In addition, these two slits are curved in the direction of the optical axis so their spectral images match the curved edges formed by the intersection of the front spherical surface of each detector lens with the rectangular body of the lens.

The computer ray trace analyses which have been performed for this study are purely mathematical model-building procedures. The monochromator and its multiple detector system are very complex and require the analysis of hundreds of optical images in reaching an optimal design. The final monochromator spectral image surface is defined in this report by 180 separate images, each formed by 100 rays, for a total of 18,000 rays. Each of these 180 images is further described in numerical tables by six parameters. So, 1080 numerical values are used in this report to describe the final spectral image surface. Similarly, the detector foreoptics and the detector locations are defined by 45 images of 25 rays each, and each of these images is described by seven parameters.

The many preliminary ray traces that were performed to reach the final optimal design demanded a comparative analysis of thousands of numerical values. For this reason, the major engineering information of this report is found in its many numerical tables. The Figures that are presented in this report have generally been developed directly from the numerical tables.

NOTE

All dimensions in this report are in inches unless otherwise specified.

SECTION 2

FINAL PERFORMANCE REQUIREMENTS

The goal of the optical analysis presented in this report has been to find the optimal design for a multidetector grating spectrometer capable of the following performance characteristics:

1. The final monochromator design from this study is similar to the monochromator described in the Phase II Final Report (2), JPL Contract 950880. The specified wavelength range at the beginning of this study was 3.5 μ to 6.5 μ with a resolving power, $\frac{\lambda}{\Delta\lambda} = 100$ at 4.3 μ. The wavelength range, however, was reduced to 3.7 μ to 6.0 μ at the preliminary design review meeting to maximize the spectral image spread. This permits the use of wider slits, resulting in a greater radiant through-put.

2. This optical study is to develop a practical method for each detector at the spectral image surface to receive the radiant flux from two separate spectral bands on a reciprocal time basis. The numerical difference between the central wavelengths for these two spectral bands is to be 1/2, 1-1/2, or 2-1/2, etc. spectral bandwidths. Of course, only one of these numerical difference coefficients is to be used in the final design.

3. The detector foreoptics were designed to give a maximum spectral radiant through-put to the detector, with a minimum of stray light.

4. A telescope will have a focal length of roughly 10 inches, and will form an earth image on the entrance slits. This telescope needs to be physically folded with an additional mirror to fit within the spectrometer's allowable dimensions.

5. A field-of-view scanning mirror must be provided which permits the telescope to scan the earth through ±22° at right-angles to the Nimbus orbit. The same scanning mirror must rotate to a position where the telescope can view space.

6. The radiation cooling shield for cooling the detectors must receive the minimum possible radiation from both the earth and the Nimbus structure at all times.

7. Four or five individual detectors with a 4 μ to 5 μ bandwidth sensitivity must continuously view separate but equal parts of the field-of-view. Their total field-of-view coverage should be the full field-of-view of the monochromator.

8. The maximum allowable spectrometer size is shown in Figure 1, and its weight should not be much greater than 15 pounds.

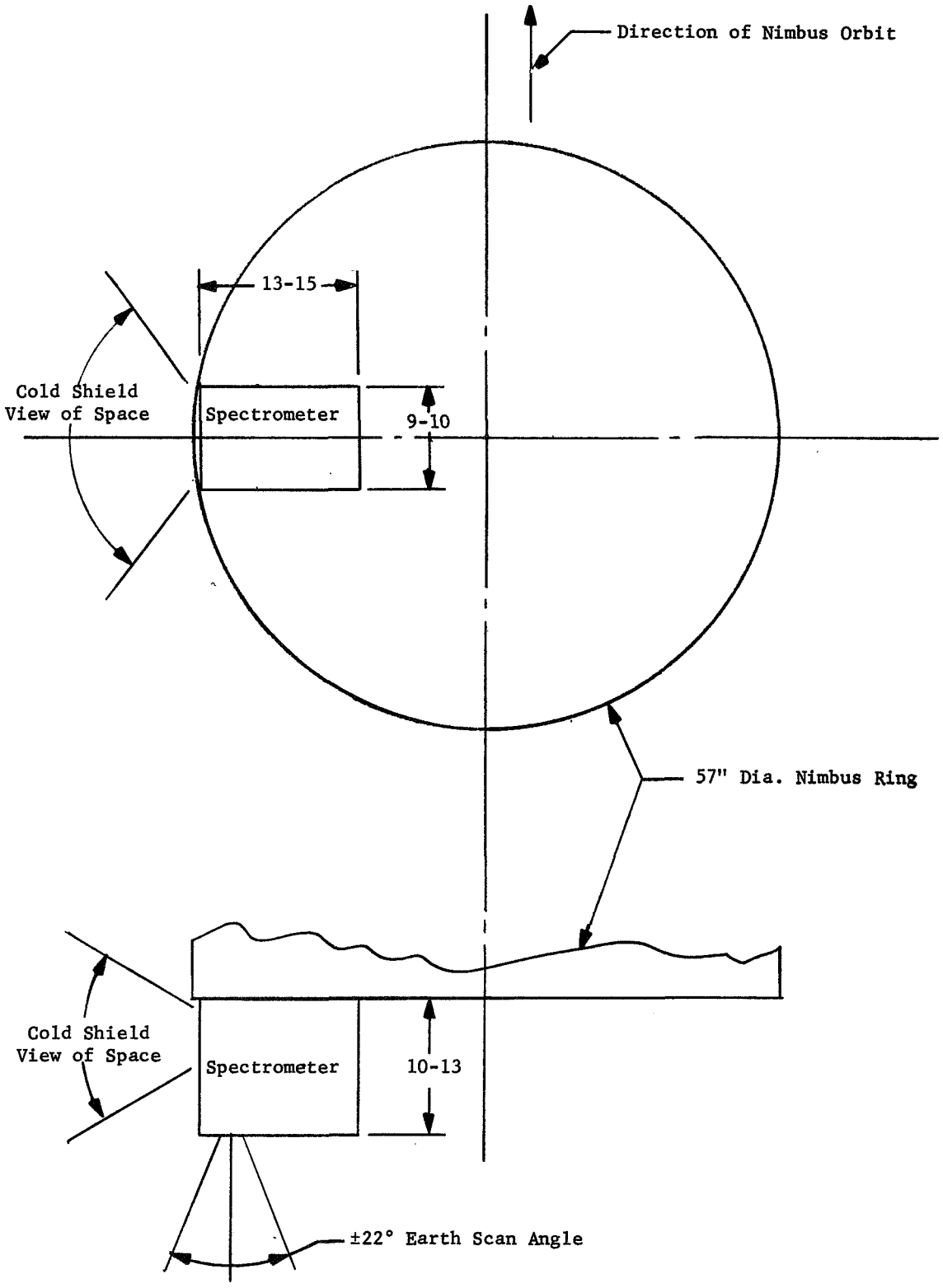

Figure 1. Spectrometer Overall Dimensions and Location on Nimbus Ring

SECTION 3

MONOCHROMATOR

The optical analysis of the monochromator is presented first in this report since it is the heart of the spectrometer system. Before the detector fore-optics, the telescope system, or the radiant cooling shield could be properly designed, it was necessary to completely finalize the monochromator design.

The monochromator consists of only the entrance slits, grating, collimating mirror, and spectral image surface. All the optical ray traces for the monochromator use the axis systems which are shown as a three-view drawing in Figure 2. The dimensions between the origins of these axis systems are in inches. The ray trace program requires that each optical surface be in a separate axis system, and that each axis system be defined geometrically, relative to its previous axis system.

All the monochromator ray traces commence with the entrance slits which are in the (X_o, Y_o, Z_o) axis system. The rays are then traced, in turn, to the paraboloid collimator mirror in the (X_1, Y_1, Z_1) axis system; the diffraction grating in the (X_2, Y_2, Z_2) axis system; the Y_3-Z_3 plane of the (X_3, Y_3, Z_3) axis system which is a mathematical facility; the collimating mirror again in the (X_4, Y_4, Z_4) axis system; and finally the spectral image plane in the (X_5, Y_5, Z_5) axis system.

All the monochromator axis systems have the same angular orientation except the grating axis system, (X_2, Y_2, Z_2). The grating normal which is parallel to the X_2-axis is displaced through the angle α_2, as shown in Figure 2. Rays may be diffracted from the grating at any angles between ±90° from the grating normal. The actual diffraction angle is in part determined by a computer input value, W, where

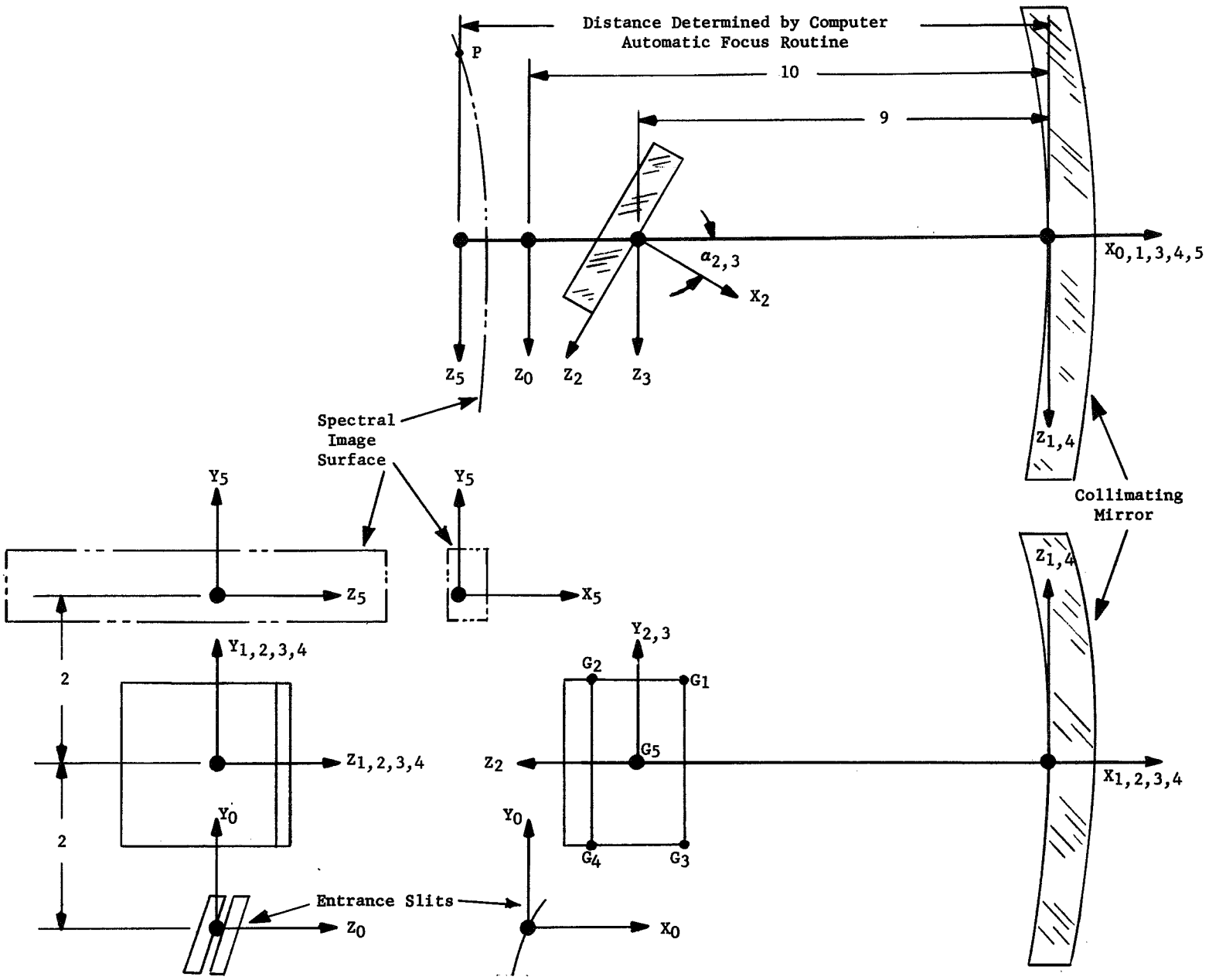

Figure 2. Three-View Drawing of the Axis System Used for the Ray-Trace of the Monochromator.

$$W = \frac{N\lambda k}{1000} \quad \text{(dimensionless)} \tag{1}$$

where N = ± grating order

λ = wavelength of light in μ

k = grating constant in lines/mm

The monochromator has been ray-traced for a number of input W values, but N, λ, and k are never computer inputs. This gives generalized optical performance for the monochromator as a function of only W and the grating angle α_2. Thus, the same ray-traced monochromator performance can be utilized for any wavelength region by selecting the proper N, λ, and k from equation (1). Figure 3 shows the graphical solution of equation (1), giving λ vs. W for a number of commercially available grating constants, k. N = 1 for Figure 3.

The (X_3, Y_3, Z_3) axis system has the same origin as the (X_2, Y_2, Z_2) axis system of the grating. The X_3-axis is, however, rotated back to coincidence with the collimating mirror axis. The (X_3, Y_3, Z_3) axis system is used to facilitate defining mathematically the (X_4, Y_4, Z_4) axis system of the collimating mirror relative to the (X_2, Y_2, Z_2) axis system of the grating.

The same collimating mirror is used in both the (X_1, Y_1, Z_1) axis system, and the (X_4, Y_4, Z_4) axis system. These two axis systems (Figure 2) are identical and will generally be referred to as the $(X_{1,4}, Y_{1,4}, Z_{1,4})$ axis system. Multiple subscripts are also used on a single axis in Figure 2, when all the axes with those subscripts are coincident in that view.

The spectral image surface is defined by the (X_5, Y_5, Z_5) axis system. In its simplest form, the spectral image surface can probably best be described as the locus of the focal points for all ray starting points on any line segment or on one edge of a slit in the (X_o, Y_o, Z_o) axis system and for all wavelengths within the prescribed wavelength range. When astigmatic images are involved, as is nearly always the case for a reflective monochromator, the focus condition selected is the one which minimizes the optical aberrations measured in the

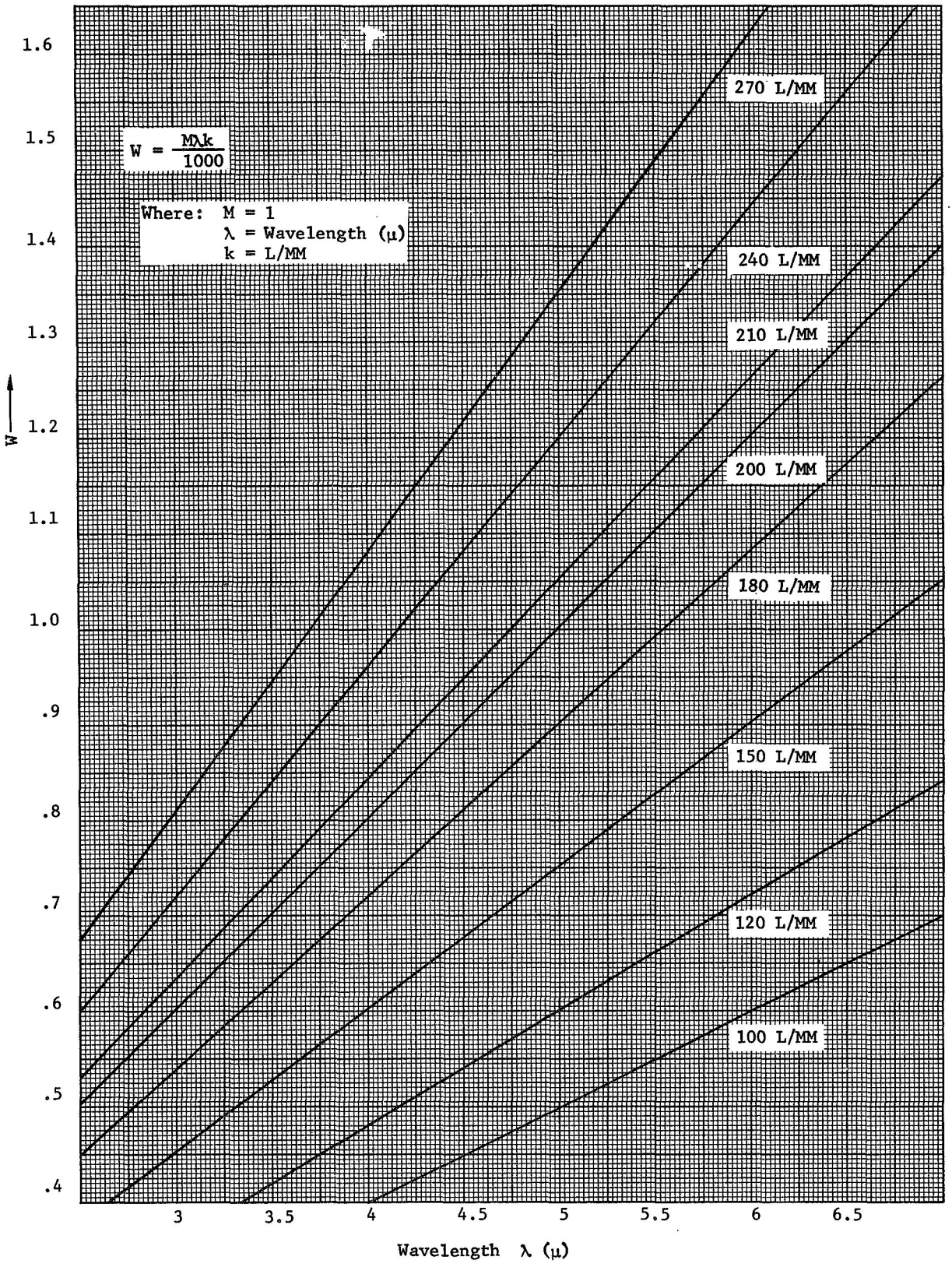

Figure 3. Plot of λ vs. W for Commercial Gratings

direction of wavelength dispersion. This description says that a spectral image surface represents the sharpest images of one edge of an entrance slit for all applicable wavelengths. The other edge of the same entrance slit must then create a separate spectral image surface. Similarly for multiple entrance slits, separate spectral image surfaces are created for each slit edge.

The final monochromator design which is described in this report has four highly irregular spectral image surfaces representing the separate edges of two entrance slits. The major ray trace effort of this contract has been devoted to finding the entrance slit shapes which optimize these four spectral image surfaces, and thus produce the best possible spectral resolution at each detector.

1. MONOCHROMATOR RAY TRACE PROCEDURES

The following steps are used to trace rays from the entrance slits to the spectral image surface, and determine the three-dimensional centroids for each focus so produced:

a. The entrance slits are represented by a sufficient number of discrete ray starting points which are selected in the (X_o, Y_o, Z_o) axis system.

b. One hundred rays are traced from each of these starting points to the diffraction grating.

c. The rays in each family of 100 rays, commencing from a single point on the entrance slit, are so directed from their starting point that every 100-ray family intersects the diffraction grating ruled surface (the Y_2-Z_2 plane) in the same uniform 10 x 10 rectangular array which accurately matches the boundaries of the grating ruled area. The grating ruled area thus becomes the aperture stop of the monochromator.

d. At the diffraction grating, each of the 100-ray families from a separate entrance slit starting point will be diffracted from the grating at a large number of different diffraction angles, where each diffraction angle depends on the input W value. Thus, the

number of diffracted 100-ray families has increased by the product of the number of ray starting points and the number of W values.

e. Each diffracted 100-ray family has a best focus at some location in the (X_5, Y_5, Z_5) axis system. This best focus location depends on both the W value used for the diffraction grating and the location of the starting point for its 100 rays in the (X_o, Y_o, Z_o) axis system. The computer determines the best focus location for each diffracted 100-ray family by moving the origin of the (X_5, Y_5, Z_5) axis system along its own X_5-axis until the best-focus condition exists on the Y_5-Z_5 plane. The computer defines a best focus for a 100-ray intersection with the Y_5-Z_5 plane when their total least square deviation from the Z_5 centroid measured in the direction of dispersion (the Z_5 direction) is a minimum.

f. Once the computer has found the best image for a 100-ray family, the computer calculates and prints out the following information about the image:

1. The X_4 coordinate of the origin of the (X_5, Y_5, Z_5) axis system. This is the distance of the Y_5-Z_5 plane from the collimating mirror, and will generally be referred to as a_5.

2. The Y_5 coordinate of the Y_5 centroid for the 100-ray image.

3. The Z_5 coordinate of the Z_5 centroid for the 100-ray image.

4. The Y_5 spread or numerical difference between the smallest and largest Y_5 values for a 100-ray image, called ΔY_5.

5. The Y_5 spread or numerical difference between the smallest and largest Y_5 values for the 80 rays having the smallest deviation from the centroid Y_5, called 80% ΔY_5.

6. The Z_5 spread or numerical difference between the smallest and largest Z_5 values for a 100-ray image, called ΔZ_5.

7. The Z_5 spread or numerical difference between the smallest and largest Z_5 values for the 80 rays having the smallest deviation from the Z_5 centroid, called 80% ΔZ_5.

By using these ray-trace procedures, the exact three-dimensional location of the centroid for the best focus can be determined for any combinations of entrance slit starting point location and diffracting grating W value. The final monochromator design analysis which will be described in this report utilized all combinations of nine different W values and 20 entrance slit starting points. The specific nine W values were selected to give good definition of the spectral image surface relative to the desired wavelength range.

The monochromator axis systems which are shown in Figure 2 and which are used for all ray traces are rigorously defined in Table 1. The definitions for the dimensional parameters which are used to transform to successive axis systems are given in Table 2.

2. SELECTING GRATING OFFSET ANGLE AND GRATING CONSTANT

At the beginning of the monochromator study, it was not obvious what the grating offset angle, α_2, and the grating constant, k, should be. It was, therefore, necessary to perform a preliminary study of the spectral image surface characteristics for several different grating offset angles. The first preliminary ray traces used only nine rays from one starting point in the (X_o, Y_o, Z_o) axis system, and ray-traced the monochromator for all combinations of nine W values and three different grating offset angles:

$$\alpha_2 = 25°, 30°, \text{ and } 35°$$

These preliminary ray traces showed that reasonably desirable wavelength positioning was obtained on the spectral image surface for the 3.5 μ to 6.5 μ wavelength range for α_2 = 25° and 30°, but not for 35°.

Table 1. Definitions for the Monochromator Axis Systems

(X_o, Y_o, Z_o)	ENTRANCE SLITS--The two entrance slits do not lie in any plane, so they are defined by three-dimensional coordinates in the (X_o, Y_o, Z_o) system.
(X_1, Y_1, Z_1) (X_4, Y_4, Z_4)	PARABOLOID COLLIMATING MIRROR--These two axis systems are identical and will generally be referred to as the $(X_{1,4}, Y_{1,4}, Z_{1,4})$ axis system. The apex of the paraboloid collimating mirror is tangential to the $Y_{1,4}$-$Z_{1,4}$ plane at the origin of the $(X_{1,4}, Y_{1,4}, Z_{1,4})$ axis system. The focus of the paraboloid collimating mirror is located on the negative $X_{1,4}$-axis.
(X_2, Y_2, Z_2)	DIFFRACTION GRATING--The ruled surface of the grating is in the Y_2-Z_2 plane, and the grating rulings are parallel to the Y_2-axis.
(X_3, Y_3, Z_3)	MATHEMATICAL AXIS SYSTEM--This axis system has the same origin as the (X_2, Y_2, Z_2) axis system, and is used only as a mathematical aid.
(X_5, Y_5, Z_5)	SPECTRAL IMAGE SURFACES--These are the spectral images of the entrance slit edges in the (X_5, Y_5, Z_5) axis system.

Table 2. Definitions for the Dimensional Parameters Which are Used to Specify the Linear and Rotational Transformations to Successive Axis Systems.

a_n	The X_{n-1} coordinate for the origin of the (X_n, Y_n, Z_n) axis system in the $(X_{n-1}, Y_{n-1}, Z_{n-1})$ axis system.
b_n	The Y_{n-1} coordinate for the origin of the (X_n, Y_n, Z_n) axis system measured in the $(X_{n-1}, Y_{n-1}, Z_{n-1})$ axis system.
c_n	The Z_{n-1} coordinate for the origin of the (X_n, Y_n, Z_n) axis system measured in the $(X_{n-1}, Y_{n-1}, Z_{n-1})$ axis system.
α_n	The angular displacement of the X_n axis from the X_{n-1} axis measured in the X_{n-1}-Z_{n-1} plane. This angle is positive when the X_n axis is moved toward the positive Z_{n-1} axis, and negative when moved toward the negative Z_{n-1} axis.
β_n	The angular displacement of the X_n axis from the X_{n-1} axis measured in the X_{n-1}-Y_{n-1} plane. This angle is positive when the X_n axis is moved toward the positive Y_{n-1} axis, and negative when moved toward the negative Y_{n-1} axis.
γ_n	The angular displacement of the Z_n axis from the Z_{n-1} axis measured in the Y_{n-1}-Z_{n-1} plane. This angle is positive when the Z_n axis is moved toward the positive Y_{n-1} axis, and negative when moved toward the negative Y_{n-1} axis.

Next, more precise ray traces were performed for the 25° and 30° grating offset angles using 100-ray families from four starting points in the (X_o, Y_o, Z_o) axis system. These four starting points were essentially in a line. The line they represent was tilted from parallelism with the Y_o-axis in order to obtain a spectral image of this line in the (X_5, Y_5, Z_5) axis system, which is as nearly parallel to the Y_5-axis as possible for all nine W values. Several repeat ray traces were required while changing the locations of the four starting points in the (X_o, Y_o, Z_o) axis system until the best image was found in the (X_5, Y_5, Z_5) axis system. The final four starting point coordinates in the (X_o, Y_o, Z_o) axis system for both the 25° and 30° grating offset angles are shown in Figure 4.

Tables 3 and 4 give, respectively, the monochromator dimensional parameters and the ray starting points for the 25° grating offset, and Tables 5 and 6 give, respectively, the monochromator dimensional parameters and the ray starting points for the 30° grating offset. Table 7 lists the coordinates of the four corners of the grating ruled area in the (X_2, Y_2, Z_2) axis system. These corners are titled G1, G2, G3, and G4, respectively. The center of the grating is titled G5. Both monochromators were ray-traced for the following W values: .6, .7, .8, .85, .9, 1.0, 1.1, 1.2, and 1.3.

Figure 5 is a composite graph showing the magnitude of the optical aberrations on the spectral image surface for both the 25° and 30° grating offsets. Two types of aberration measurements are shown. These are:

1. The maximum Z_5 spread for each 100-ray family, ΔZ_5

2. The Z_5 spread represented by the 80 rays of each 100-ray family, which have the smallest deviation from the Z5 centroid, 80% ΔZ_5.

Both types of aberration measurements are shown in Figure 5 for ray starting points A'1, A"1, A'4, and A"4 for both the 25° and 30° grating offsets.

There is little difference in aberrations for the 25° and 30° grating offsets, as shown in Figure 5. Further, over much of the spectral image surface, the

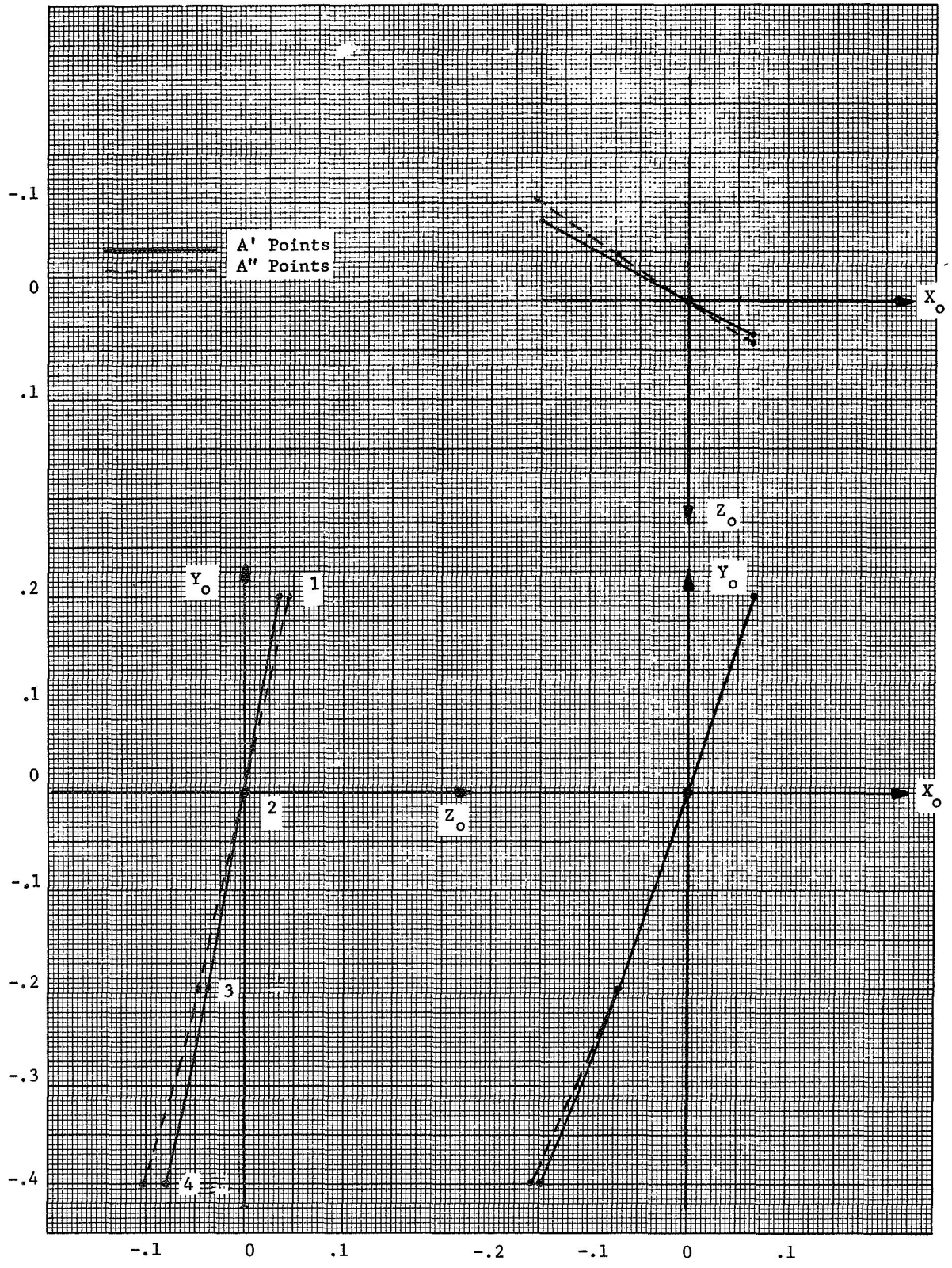

Figure 4. Ray Starting Points in the (X_o, Y_o, Z_o) Axis System

Table 3. Dimensional Parameters for the Preliminary Monochromator Using a 25° Grating Offset

Axis Subscript	a	b	c	α	β	γ
1	10.0	0	2.0	0	0	0
2	- 9.0	0	0	25.0°	0	0
3	0	0	0	-25.0°	0	0
4	9.0	0	0	0	0	0
5	Determined by Automatic Focus	0	2.0	0	0	0

Table 4. Four Ray Starting Points for the Preliminary Monochromator Using a 25° Grating Offset

Starting Points	X_o	Y_o	Z_o
A'1	.065	.200	.035
A'2	0	0	0
A'3	-.073	-.200	-.038
A'4	-.149	-.400	-.080

Table 5. Dimensional Parameters for the Preliminary Monochromator Using a 30° Grating Offset.

Axis Subscript	a	b	c	α	β	γ
1	10.0	0	2.0	0	0	0
2	- 9.0	0	0	30°	0	0
3	0	0	0	-30°	0	0
4	9.0	0	0	0	0	0
5	Determined by Automatic Focus	0	2.0	0	0	0

Table 6. Four Ray Starting Points for the Preliminary Monochromator Using a 30° Grating Offset.

Starting Points	X_o	Y_o	Z_o
A"1	.066	.200	.044
A"2	0	0	0
A"3	-.071	-.200	-.049
A"4	-.155	-.400	-.103

Table 7. The Coordinator of the Four Corners of the Grating Ruled Area

Grating Corner	X_2	Y_2	Z_2
G1	0	1.38	-1.59
G2	0	1.38	1.59
G3	0	-1.38	-1.59
G4	0	-1.38	1.59

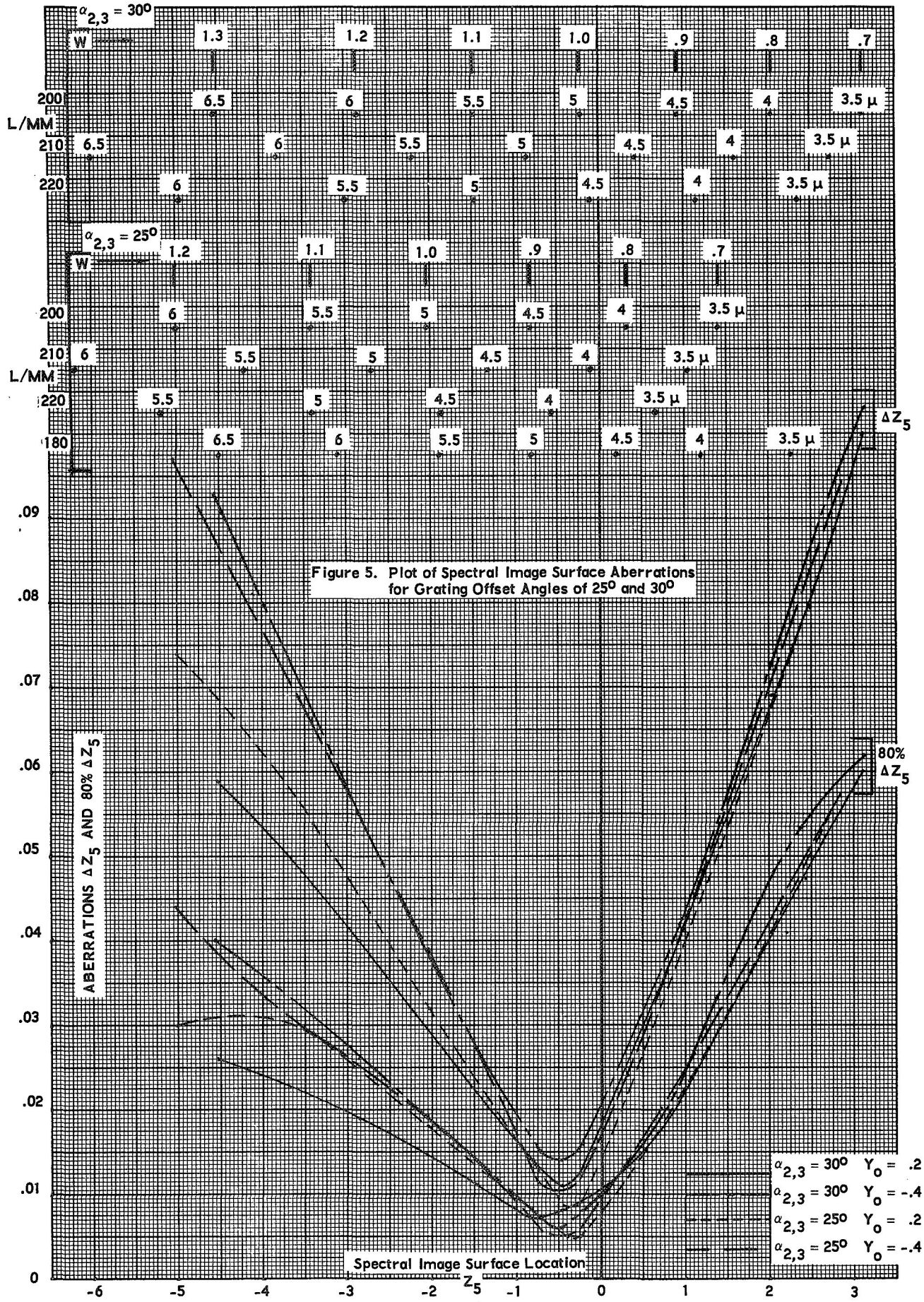

Figure 5. Plot of Spectral Image Surface Aberrations for Grating Offset Angles of 25° and 30°

A'1 and A"1 starting points give nearly the same size aberrations as the A'4 and A"4 starting points. Of course, this is no longer true at large, negative Z_5 coordinates.

At the top of Figure 5 are shown the Z_5 coordinates for the respective W values used to ray-trace the 25° and 30° grating offset monochromators. Besides the two W value scales, a number of wavelength scales that apply for commercially available grating constants are shown. In determining these wavelength scales, the ray-traced values of Z_5 were plotted against the input W values for the corresponding 25° and 30° grating offsets, as shown in Figure 6. The W value represented by a given wavelength, λ, and grating constant, k, was found by solving

$$W_{\lambda k} = \frac{\lambda k}{1000}, \text{ where } N = 1 \qquad (2)$$

or by referring to Figure 3. The proper Z_5 coordinate is then found for the given λ and k from Figure 6, using $W_{\lambda k}$. Table 8 also shows the same Z_5 coordinates for the given λ, k, and grating offset angles as shown at the top of Figure 5.

Figure 5 and Table 8 give considerable information for selecting the best grating offset angle and the best grating constant. Wavelength scales in Figure 5 and Table 8 show the true width of the spectral image surface in inches for any given wavelength range. Further, the collimating mirror optical width must be approximately two inches wider than the spectral image surface to prevent ray vignetting.

This says that if the width of the monochromator enclosure is to be held below 10 inches, then the optical width of the collimating mirror should not be much greater than 9 to 9.5 inches. The spectral image surface width should then be no greater than 7 to 7.5 inches.

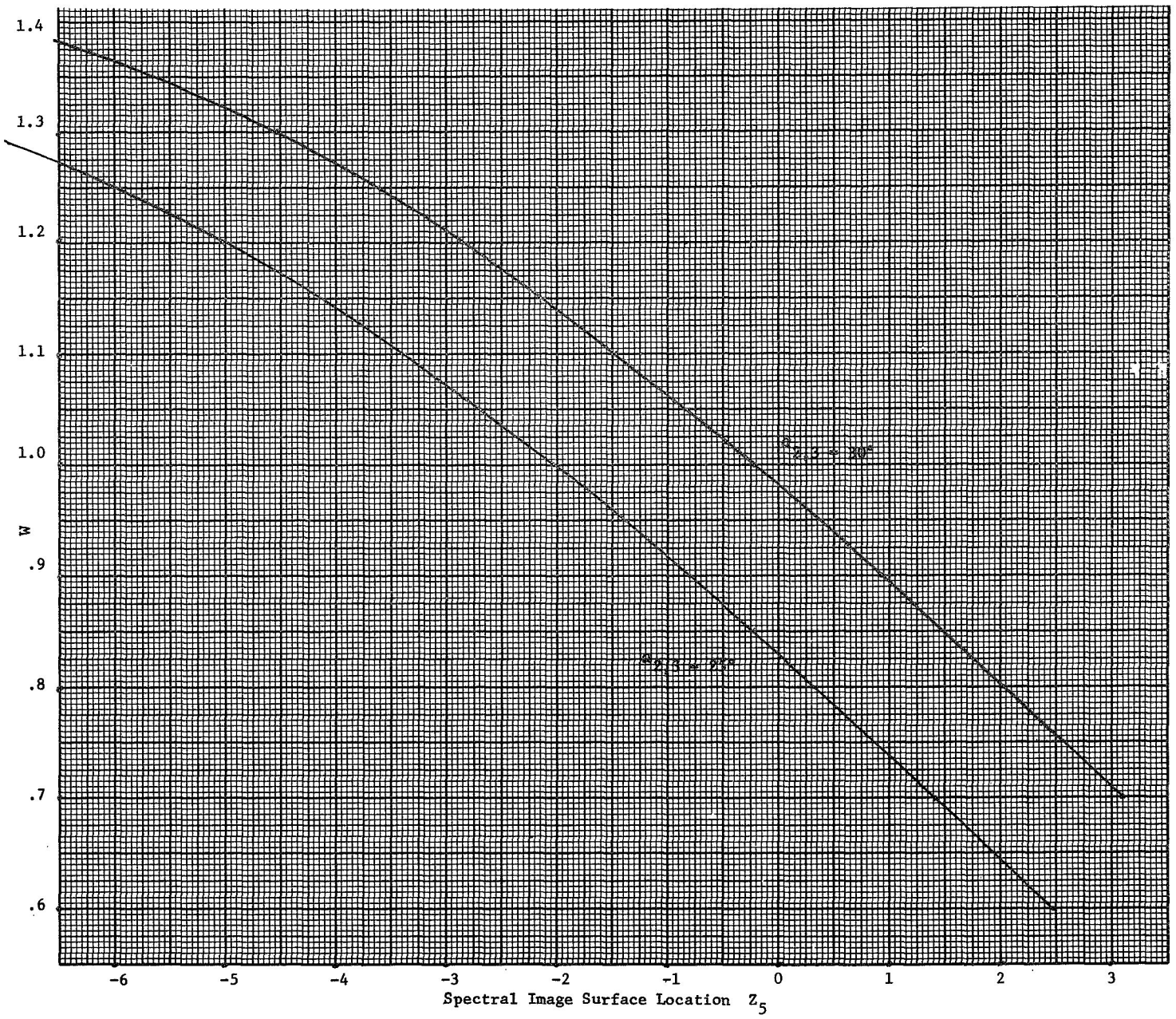

Figure 6. Plot of W vs. Wavelength, λ, for Grating Offset Angles of 25° and 30°

Table 8. Spectral Image Surface Locations, Z_5 Coordinates, as a Function of Grating Offset Angle, Grating Constant, and Wavelength

Grating Offset Angle	25°						30°					
Grating Constant L/MM	200		210		220		200		210		220	
λ	$W_{\lambda k}$	Z_5	$W_{\lambda k}$	Z_5	$W_{\lambda k}$	Z_5	$W_{\lambda k}$	Z_5	$W_{\lambda k}$	Z_5	$W_{\lambda k}$	Z_5
3.5	.7	1.409	.735	1.03	.770	.65	.7	3.104	.735	2.73	.770	2.35
4.0	.8	.321	.840	- .12	.880	- .57	.8	2.030	.840	1.60	.880	1.15
4.5	.9	- .817	.945	-1.33	.990	-1.88	.9	.926	.945	.43	.990	- .10
5.0	1.0	-2.039	1.050	-2.70	1.100	-3.40	1.0	- .230	1.050	- .85	1.100	-1.48
5.5	1.1	-3.399	1.155	-4.20	1.210	-5.18	1.1	-1.476	1.155	-2.20	1.210	-3.00
6.0	1.2	-5.005	1.260	-6.20	1.320		1.2	-2.871	1.260	-3.80	1.320	-4.95
6.5	1.3	-7.154	1.365		1.430		1.3	-4.544	1.365	-6.00	1.430	

During these preliminary monochromator studies, the expected wavelength range was 3.5 μ to 6.5 μ. The spectral image surface widths for this wavelength range are listed in Table 9, along with the expected optical width of the collimating mirror.

Table 9. Spectral Image Surface Width and Optical Width of Collimating Mirror for Various Grating Constants, and for 25° and 30° Grating Offsets. The Wavelength Range in all Cases is 3.5 μ to 6.5 μ.

Grating Offset Angle α_2	Grating Constant, k 1/mm	Spectral Image Surface Width Inches	Optical Width of Collimating Mirror Inches
25°	180	6.72	8.8
	200	8.56	10.6
	210	9.0	11.0
	220	9.0	11.0
30°	200	7.65	9.7
	210	8.73	10.7
	220	9.0	11.0

The only acceptable optical widths for the collimating mirror shown in Table 9 are for the 180 1/mm grating used at a 25° offset angle and the 200 1/mm grating used at a 30° offset angle. Figure 5 shows that in both of these cases the 4.3 μ region lies well to the right of the minimum aberration region which is near $Z_5 = -.50$.

Based upon the preliminary monochromator design information which is summarized in Figure 5 and Tables 8 and 9, the experimenter for this Nimbus "F" experiment modified the monochromator final performance specifications as follows:

1. The new wavelength range is to be 3.7 μ to 6.0 μ.

2. The 4.3 μ spectral image is to be located roughly at $Z_5 = -.50$, where the aberrations are a minimum.

This reduced wavelength range is sufficient for the Nimbus "F" experiment, and yet it permits a greater linear dispersion on the spectral image surface. This means wider entrance slits can be used to give a higher radiant through-put. Further, the 4.3 μ spectral image is to be formed at or near $Z_5 = -.50$, which is the location on the spectral image surface having minimum aberrations. A dozen or more adjacent detectors will be located on the spectral image surface to define the CO_2 band about 4.3 μ. It is desirable for these detectors to encounter the smallest aberrations possible, so the aberrations will have a minimal effect on the spectral response function of each detector.

It is obvious from Figure 5 and Table 8 that neither the 25° nor 30° grating offsets are proper for these new specifications. Figure 7 was developed as a means of finding the optimal grating offset angle. In Figure 7, the grating offset angle is plotted versus the Z_5 coordinates on the spectral image surface. For both the 25° and 30° grating offset angles, the Z_5 values are plotted for all combinations of three grating constants

200 1/mm
210 1/mm
220 1/mm

and three wavelengths

3.7 μ
4.3 μ
6.0 μ

The corresponding points at 25° and 30° are connected by straight lines, which is a sufficiently good approximation for this purpose. The ideal grating offset angle for each of the three grating constants is given by the intersection of their 4.3 μ lines with $Z_5 = -.50$. The total Z_5 spread on the spectral image

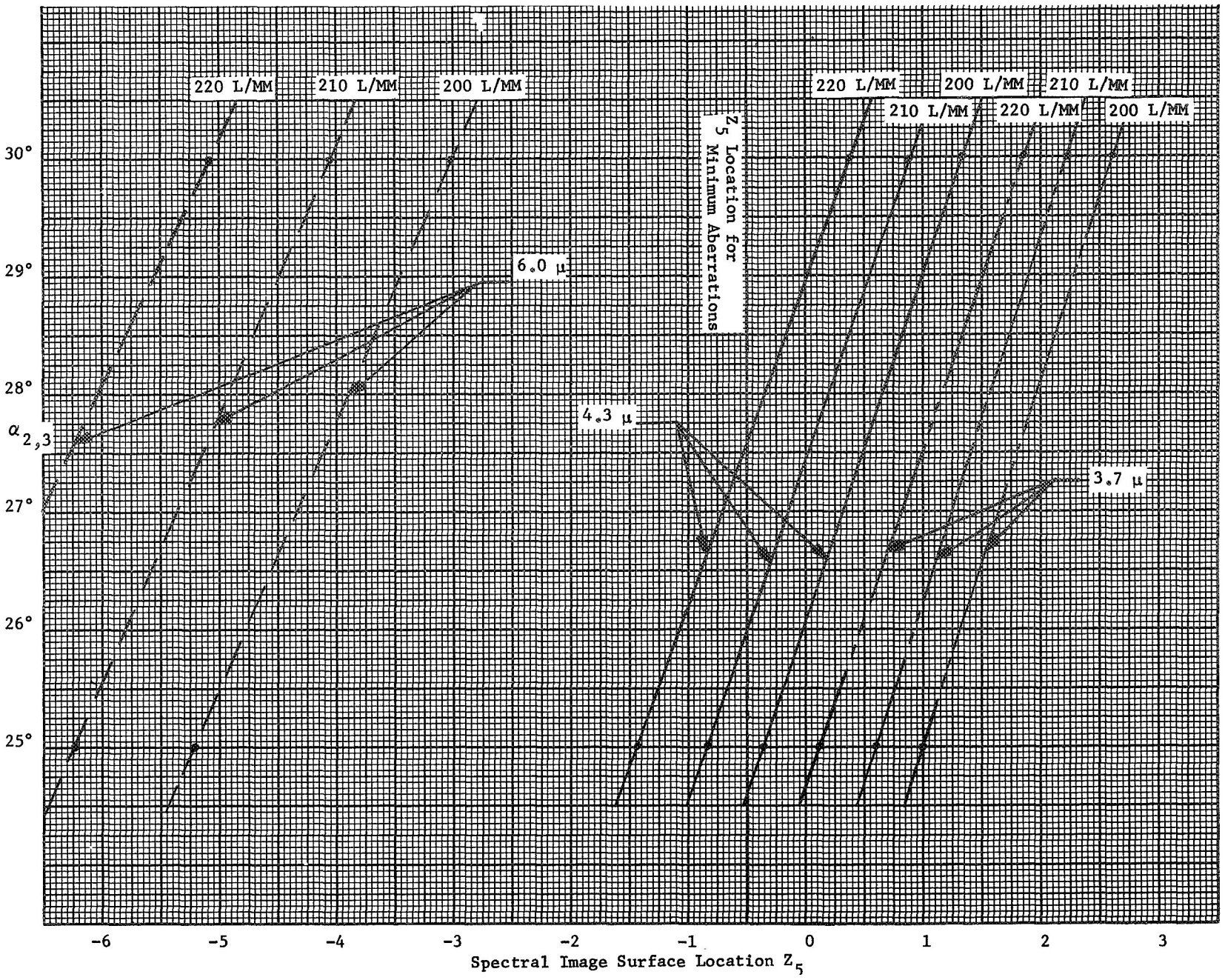

Figure 7. Graphical Determination of the Best Grating Offset Angle, $\alpha_{2,3}$, and the Best Grating Constant

surface for the 3.7 μ to 6.0 μ wavelength range can then be read off for that grating offset angle.

Table 10 lists the best grating offset angle for each of the three grating constants and the resultant spectral image surface spread, and collimator mirror optical width for the 3.7 μ to 6.0 μ wavelength range.

Of these three possible choices, the 220 1/mm grating requires a 27.5° offset angle. However, it requires too large a collimating mirror optical width.

The 210 1/mm grating requires a 26° offset angle, and it uses 8.8 inches for the collimating mirror optical width. A 210 1/mm grating having a first-order blaze at 4.3 μ is a cataloged item by one manufacturer.

The 200 1/mm grating requires a 24.6° grating offset angle, and it uses 8.3 inches for the collimating mirror optical width. However, this is less dispersion than the 210 1/mm grating. Therefore, the 210 1/mm grating with a 26° offset angle will be used for the final monochromator design and for the remainder of this report.

3. FINAL MONOCHROMATIC DESIGN

The axis systems which are used to ray trace the final monochromator are identical to those used for the preliminary monochromator studies which have been discussed in the previous paragraphs of this section. Again, Figure 2 and Table 1 define the axis systems that are used for all monochromator ray traces, and Table 2 defines the monochromatic dimensional parameters. Table 11 gives the dimensional parameters of the final monochromator which differs from Tables 3 and 5 only in the values of α_2 and α_3, which have now become 26° and -26°, respectively.

The grating ruled area for the final monochromator is 2.76 inches measured along the grating rulings, and 3.18 inches measured across the rulings. This is the same size grating ruled area as used for both the preliminary monochromators, and also for the monochromator of the Phase II Study Final Report.[2]

Table 10. Best Grating Offset Angle and the Resultant Spectral Image Surface Spread and Optical Width of Collimating Mirror for the 3.7 μ to 6.0 μ Wavelength Range

Grating Constant, k (1/mm)	Best Grating Offset Angle for 4.3 μ	Spectral Image Surface Width Inches	Optical Width of Collimating Mirror Inches
200	24.6°	6.25	8.3
210	26.0°	6.75	8.8
220	27.5°	7.70	9.7

Table 11. Dimensional Parameters for the Final Monochromator Ray Trace

Axis Subscript	a	b	c	α	β	γ
1	10.0	0	2.0	0	0	0
2	- 9.0	0	0	26.0°	0	0
3	0	0	0	-26.0°	0	0
4	9.0	0	0	0	0	0
5	Determined by Automatic Focus	0	2.0	0	0	0

Table 7 thus defines the coordinates of the four corners of grating ruled area on the Y_2-Z_2 plane, and this ruled area is the aperture stop of the monochromator.

At a 26° grating offset, the 3.18-inch grating width subtends a projected width of 2.86 inches measured on the Y_3-Z_3 plane, which is perpendicular to the paraboloid axis. This gives the grating a nearly square projection for those rays which are dispersed to Z_5 = -.50 on the spectral image surface which is the spectral location for 4.3 μ.

4. SINGLE LINE ENTRANCE SLIT

The initial ray traces for the final monochromator used 100-ray families from the four starting points in the (X_o, Y_o, Z_o) axis system listed in Table 12. These four starting points, A1, A2, A3, and A4 have nearly the same values as A'1, A'2, A'3, and A'4, respectively, for the preliminary monochromator, with a 25° grating offset and A"1, A"2, A"3, and A"4, respectively, for the preliminary monochromator with a 30° grating offset. In all three cases, the four starting points define a single line in the (X_o, Y_o, Z_o) axis system which produces a spectral image which is substantially parallel to the Y_5 axis for most of the spectral image surface of its respective monochromator. The A1, A2, A3, A4 set of points would fall between the A'1, A'2, A'3, A'4 and the A"1, A"2, A"3, A"4 sets of points in Figure 4. Tables 13, 14, 15, and 16 describe the focussed spectral images for starting points A1, A2, A3, and A4, respectively. In all cases, the spectral images are described for 3.7, 4.0, 4.2, 4.3, 4.4, 4.5, 5.0, 5.5, and 6.0 μ, assuming a 210 1/mm grating constant.

Tables 13, 14, 15, and 16 have the same format. Above each of these tables is shown the starting point coding A1, A2, etc., followed by the X_o, Y_o, and Z_o coordinates of that starting point. The column headings for these tables are described in Table 17.

Tables 13, 14, 15, and 16 are accurate to within ±.001 inch for every value given. These tables give substantially all the spectral image information that can be gained from a ray trace of these four points. Similar tables to

Table 12. Four Ray Starting Points on Single-Line Entrance Slit for the Final Monochromator.

Starting Points	X_o	Y_o	Z_o
A1	.065	.200	.037
A2	0	0	0
A3	-.073	-.200	-.040
A4	-.150	-.400	-.085

Table 13. Spectral Image Surface Characteristics

Entrance Slit Starting Point--A1 X_o = .065 Y_o = .2 Z_o = .037

W_1	λ_1 210 L/MM Grating	a_5	a_5 Comparison A1 - A2	Centroid Z_5	Centroid Z_5 Comparison A1 - A2	Centroid Y_5	ΔY_5	ΔZ_5	80% ΔZ_5
.777	3.7	-10.368	.003	.918	-.002	-.188	.052	.038	.021
.840	4.0	-10.353	.002	.221	-.002	-.191	.044	.020	.010
.882	4.2	-10.365	.000	- .255	.000	-.191	.038	.008	.006
.903	4.3	-10.377	.000	- .498	.000	-.191	.034	.010	.006
.924	4.4	-10.394	-.001	- .744	.000	-.190	.032	.013	.007
.945	4.5	-10.417	-.002	- .994	.000	-.188	.031	.016	.008
1.050	5.0	-10.621	-.007	-2.314	.003	-.169	.046	.036	.019
1.155	5.5	-11.051	-.015	-3.816	.006	-.129	.062	.058	.026
1.260	6.0	-11.959	-.038	-5.674	.013	-.050	.090	.075	.031
Should have value			.000		.000	-.200			

Table 14. Spectral Image Surface Characteristics

Entrance Slit Starting Point--A2 $X_o = 0$ $Y_o = 0$ $Z_o = 0$

W_1	λ_1 210 L/MM Grating	a_5		Centroid Z_5		Centroid Y_5	ΔY_5	ΔZ_5	80% ΔZ_5
.777	3.7	-10.371		.920		.012	.060	.039	.022
.840	4.0	-10.355		.223		.008	.052	.021	.012
.882	4.2	-10.365		- .255		.008	.046	.009	.005
.903	4.3	-10.377		- .498		.009	.042	.008	.005
.924	4.4	-10.393		- .744		.010	.039	.011	.006
.945	4.5	-10.415		- .994		.012	.035	.014	.008
1.050	5.0	-10.614		-2.317		.033	.044	.036	.024
1.155	5.5	-11.036		-3.822		.077	.056	.059	.027
1.260	6.0	-11.921		-5.687		.166	.075	.084	.033
Should have value						.000			

Table 15. Spectral Image Surface Characteristics

Entrance Slit Starting Point--A3 $X_o = -.073$ $Y_o = -.2$ $Z_o = -.040$

W_1	λ_1 210 L/MM Grating	a_5	a_5 Comparison A3 - A2	Centroid Z_5	Centroid Z_5 Comparison A3 - A2	Centroid Y_5	ΔY_5	ΔZ_5	80% ΔZ_5
.777	3.7	-10.374	-.003	.922	.002	.212	.070	.040	.023
.840	4.0	-10.356	-.001	.223	.000	.207	.061	.021	.011
.882	4.2	-10.365	.000	- .255	.000	.207	.055	.009	.007
.903	4.3	-10.376	.001	- .498	.000	.208	.051	.008	.005
.924	4.4	-10.391	.002	- .745	-.001	.209	.047	.009	.007
.945	4.5	-10.412	.003	- .996	-.002	.212	.043	.013	.010
1.050	5.0	-10.606	.008	-2.321	-.004	.234	.041	.040	.019
1.155	5.5	-11.017	.019	-3.831	-.009	.283	.049	.065	.028
1.260	6.0	-11.877	.055	-5.703	-.016	.381	.058	.099	.049
Should have value			.000		.000	.200			

Table 16. Spectral Image Surface Characteristics

Entrance Slit Starting Point--A4 X_o = -.150 Y_o = -.4 Z_o = -.085

W_1	λ_1 210 L/MM Grating	a_5	a_5 Comparison A4 - A2	Centroid Z_5	Centroid Z_5 Comparison A4 - A2	Centroid Y_5	ΔY_5	ΔZ_5	80% ΔZ_5
.777	3.7	-10.381	-.010	.925	.005	.411	.079	.040	.022
.840	4.0	-10.361	-.006	.225	.002	.406	.071	.021	.013
.882	4.2	-10.368	-.003	- .254	.001	.406	.064	.013	.006
.903	4.3	-10.378	-.001	- .498	.000	.407	.061	.011	.006
.924	4.4	-10.393	.000	- .745	-.001	.408	.057	.013	.007
.945	4.5	-10.413	.002	- .996	-.002	.411	.053	.016	.010
1.050	5.0	-10.601	.013	-2.324	-.007	.435	.043	.045	.021
1.155	5.5	-11.002	.034	-3.838	-.016	.489	.042	.074	.032
1.260	6.0	-11.836	.085	-5.719	-.032	.596	.042	.116	.048
Should have value			.000		.000	.400			

Table 17. Definition of Terminology Used for Spectral Image Characteristic Tables

W_1	The set of W values used for the ray traces of both the single line slit and the main entrance slit.
λ_1	The equivalent wavelengths for W_1 with a 210 1/mm grating constant: 3.7, 4.0, 4.2, 4.3, 4.4, 4.5, 5.0, 5.5, and 6.0 μ.
a_5	The X_4 coordinate for the origin of the (X_5, Y_5, Z_5) axis system. The origin of the (X_5, Y_5, Z_5) axis system is linearly transformed along its own X_5-axis by the computer until a best focus is obtained for each 100-ray family on the Y_5-Z_5 plane. This focus minimizes the least square Z_5 deviation about the Z_5 centroid. Thus, a_5 gives the distance of the Y_5-Z_5 plane from the collimating mirror apex for a best focus.
a_5 Comparison	This column is used to compare the numerical difference between the values of a_5 from the two Tables noted by starting point code.
Centroid Z_5	This is the Z_5 coordinate of the Z_5 centroid for all 100 rays in a focussed spectral image.
Centroid Z_5 Comparison	This column is used to compare the numerical difference between the centroid Z_5 values from the two Tables noted by starting point code.
Centroid Y_5	This is the Y_5 coordinate of the Y_5 centroid for all 100 rays in a focussed spectral image.
ΔY_5	This is the Y_5 spread or numerical difference between the largest and smallest Y_5 values in a focussed spectral image.
ΔZ_5	This is the Z_5 spread or numerical difference between the largest and smallest Z_5 values in a focussed spectral image.
80% ΔZ_5	This is the Z_5 spread for those 80 rays which produce the least square deviation about the Z_5 centroid.

to these had to be made up for trial values for A1, A2, A3, and A4 starting points before the best set of four starting points could be determined. The final set of A1, A2, A3, and A4 starting points given in Table 12 produces a spectral image at 4.3 μ which is parallel to the Y_5-axis within ±.001 inch.

Tables 13, 14, 15, and 16 show that the spectral images of the four starting points are no longer parallel to Y_5 at 5.5 μ and 6.0 μ. However, nothing can be done about this. The four tables do show precisely the spectral image surface coordinates and its deviations from an ideal plane or cylindrical image surface.

5. DOUBLE ENTRANCE SLITS

The single-line entrance slit which was analyzed in the preceding section is useful in defining the entrance slit when a metal mask is to be shaped in the form of the spectral image surface, and a number of discrete vertical exit slits are cut through it. Such mask-type exit slits are not practical for this monochromator. This is because the adjacent detectors on the spectral image surface must have no physical gap between them. In this manner, adjacent detectors have spectral band passes with a common half-power wavelength value. It is impractical to place the detectors side by side since the detectors would have to be too large for a good S/N ratio. However, detector lenses can be made rectangular when viewed along their optical axis, and can be stacked side by side against one another. This, then, insures that the half-power wavelengths for adjacent detectors will be substantially coincident.

The rectangular lenses then become the exit slits of the monochromator. The intersection of the spherical front lens face with the rectangular body of the lens produces, in effect, a slit edge which is curved severely along the X_5 axis. If the lens for the 4.3 μ detector has a rectangular cross-section of .6 inch measured on the Y_5 axis and .1 inch measured on the Z_5 axis, and if the entrance slit edges are designed to produce images parallel to the Y_5 axis, as is the case for starting points A1, A2, A3, and A4, then some parts of the lens' defining edge would be out of focus by as much as ±.043 inch.

To correct for this focal error, the entrance slits of the final monochromator have been curved along the X_o axis, so the entrance slit images will match the curved edges of the rectangular detector lenses.

Figure 8 is a plot of the entrance slits for the final monochromator. Points B1, B2, B3, B4, C1, C2, C3, and C4 define the main entrance slit, and are used as 100-ray family starting points for ray traces for the main entrance slit. Points D1, D2, D3, D4, E1, E2, E3, and E4 define the second slit which produces overlapping wavelengths at each detector. These latter points are used as 100-ray family starting points for ray traces for the second slit. Figure 8 also shows in dashed lines the single line slit represented by points A1, A2, A3, and A4. Table 18 gives the (X_o, Y_o, Z_o) axis system coordinates for the sixteen starting points used for the two entrance slits, as shown in Figure 8.

Each entrance slit has an effective width of .1 inch. That is the Z_o coordinate difference between comparable B and C starting points, and D and E starting points is .1 inch. For example:

$$B1-C1 = .1 \text{ inch}$$

as measured on the Z_o axis.

An entrance slit width of .1 inch gives the spectrometer a resolving power greater than 100 at 4.3 μ. To be exact, the resolving power is

$$R = \frac{4.3\ \mu}{\Delta\lambda} \quad \text{for a .1-inch entrance slit} \tag{3}$$

The spectral dispersion on the spectral image plane in the vicinity of 4.3 μ can be found by using the numerical difference in Z_5 centroid values between 4.2 μ and 4.4 μ, as found in the "centroid Z_5" column of Table 14 for the A2 starting point. Then,

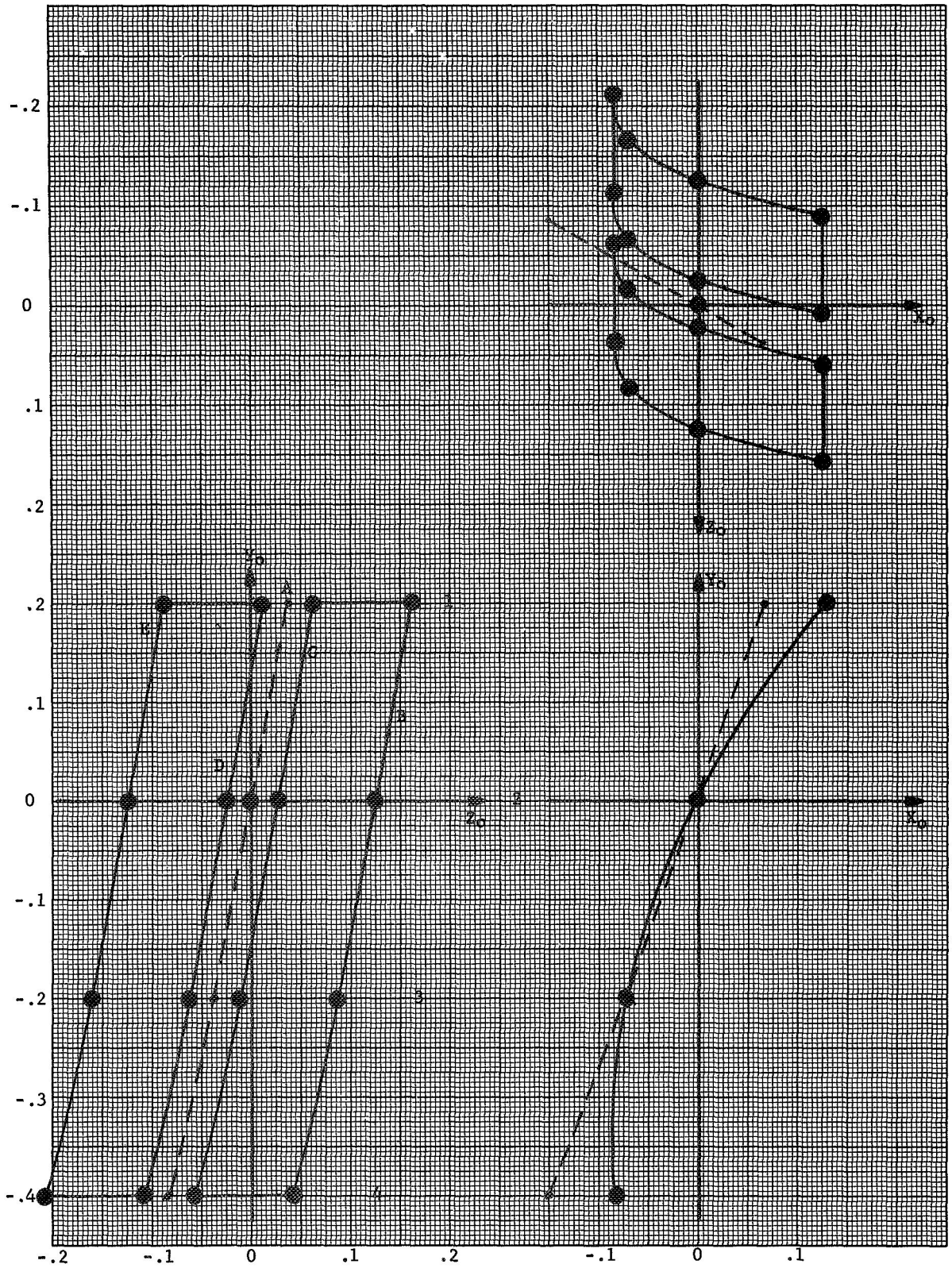

Figure 8. Entrance Slit Starting Points in the (X_o, Y_o, Z_o) Axis System of the Final Monochromator

Table 18. Sixteen Entrance Slit Starting Points for the Two Entrance Slits of the Final Monochromator

Starting Points	X_o	Y_o	Z_o
B1	.127	.2	.160
B2	0	0	.125
B3	-.070	-.2	.085
B4	-.083	-.4	.040
C1	.127	.2	.060
C2	0	0	.025
C3	-.070	-.2	-.015
C4	-.083	-.4	-.060
D1	.127	.2	.010
D2	0	0	-.025
D3	-.070	-.2	-.065
D4	-.083	-.4	-.110
E1	.127	.2	-.090
E2	0	0	-.125
E3	-.070	-.2	-.165
E4	-.083	-.4	-.210

$$\Delta\lambda = \frac{(4.4\ \mu - 4.2\ \mu) \times .1}{Z_5(4.2\ \mu) - Z_5(4.4\ \mu)} \tag{4}$$

$$= \frac{.2 \times .1}{-.255 - (-.744)}$$

$$= .0409\ \mu/.1 \text{ inch of spectral image}$$

Finally:

$$R = \frac{4.3}{.0409} = 105$$

The second entrance slit is to be used on a time-share basis with the main slit. When the second slit is used, it produces a different wavelength distribution on the spectral image surface. It should produce a spectral bandpass on a specific detector lens, in an array of uniform width detector lenses, which has a center wavelength which is 1/2 $\Delta\lambda$, 1-1/2 $\Delta\lambda$, 2-1/2 $\Delta\lambda$, etc., different than the center wavelength for that detector when the main slit is used. $\Delta\lambda$ is the spectral bandwidth of acceptance of the specific detector.

To accomplish the 1/2 $\Delta\lambda$ wavelength difference requires the entrance slit to be moved laterally along the Z_o axis .05 inch. However, it will probably not be desirable to use a moving entrance slit for this experiment.

To accomplish the 1-1/2 $\Delta\lambda$ wavelength difference requires the center of the second slit to be displaced -.15 inch along the Z_o axis from the center of the main slit, and for a 2-1/2 $\Delta\lambda$ wavelength difference requires the second slit to be moved -.25 inch from the main slit, etc.

The 1-1/2 $\Delta\lambda$ shift for the second slit has been selected for the final monochromator since it is enough shift for a good physical separation of the slits, yet it is not so great as to deteriorate the spectral image or to require a lot wider collimating mirror to handle the rays through the second slit. This second slit is actually shaped identical to the main slit, as shown in Figure 8

and Table 18. The major goal for the final monochromator ray traces has been to develop two entrance slit shapes which produce identically focussed images on the edges of each rectangular detector lens.

Tables 19 through 34 define the spectral image characteristics for the sixteen starting points on the two entrance slits, and they have the same format as Tables 13, 14, 15, and 16 for starting points A1, A2, A3, and A4, respectively. Again, Table 17 defines the terminology used in the tables. The ray starting points B2, C2, D2, and E2 are used as the reference points for the four edges of the two entrance slits. The other three ray starting points for each edge of the entrance slits were finalized by trial and error runs at 4.3 μ for the main slit, and at 4.3633 μ for the second slit, until the spectral images of these points had the best possible focal match with the rectangular edges of the detector lens, and the spectral images of four reference points B2, C2, D2, and E2. The deviations from ideal which exist at other wavelengths cannot be further controlled.

Table 35 shows the nine W_1 values used for the main slit ray traces and the comparable wavelengths for the 210 1/mm grating, and the resultant nine W_2 values for the second slit which has a -.15 inch Z_o displacement from the main slit. The comparable wavelengths are also given for this second slit.

6. SPECTRAL IMAGE ABERRATIONS

Tables 19 through 34 give the magnitude of the optical aberrations along both the Z_5 and Y_5 axis. It is, however, the Z_5 aberrations which modify spectral bandpass shapes received by each detector. Without aberrations, these spectral bandpasses should be triangular in shape. Optical aberrations round the triangular peak and spread the base of the triangle over a greater wavelength range.

Figures 9 through 17 show 100-ray spot diagrams for the aberrations on the spectral image surface for the nine W values. The spot diagrams are plotted for the E4 starting point on the second slit, since this starting point is the

Table 19. Spectral Image Surface Characteristics

Entrance Slit Starting Point--B1 X_o = .127 Y_o = .2 Z_o = .160

W_1	λ_1 210 L/MM Grating	a_5	a_5 Comparison B1 - B2	Centroid Z_5	Centroid Z_5 Comparison B1 - B2	Centroid Y_5	ΔY_5	ΔZ_5	80% ΔZ_5
.777	3.7	-10.426	-.058	.799	.000	-.186	.053	.038	.022
.840	4.0	-10.436	-.078	.098	.000	-.189	.049	.023	.012
.882	4.2	-10.446	-.074	- .382	.000	-.189	.041	.010	.009
.903	4.3	-10.457	-.070	- .627	.000	-.188	.037	.012	.008
.924	4.4	-10.479	-.073	- .875	.000	-.186	.037	.015	.008
.945	4.5	-10.507	-.077	-1.127	.001	-.184	.037	.018	.010
1.050	5.0	-10.746	-.097	-2.463	.002	-.163	.054	.037	.021
1.155	5.5	-11.243	-.140	-3.994	.004	-.120	.078	.057	.026
1.260	6.0	-12.327	-.252	-5.916	.005	-.033	.132	.080	.037
Should have value			-.072		.000	-.200			

Table 20. Spectral Image Surface Characteristics

Entrance Slit Starting Point--B2 $X_o = 0$ $Y_o = 0$ $Z_o = .125$

W_1	λ_1 210 L/MM Grating	a_5	a_5 Comparison B2 - A2	Centroid Z_5	Centroid Z_5 Comparison B2 - A2	Centroid Y_5	ΔY_5	ΔZ_5	80% ΔZ_5
.777	3.7	-10.368	.003	.799	-.121	.011	.062	.037	.023
.840	4.0	-10.358	-.003	.098	-.125	.008	.053	.019	.010
.882	4.2	-10.372	-.007	- .382	-.127	.008	.047	.009	.006
.903	4.3	-10.387	-.010	- .627	-.128	.009	.043	.008	.005
.924	4.4	-10.406	-.013	- .875	-.131	.011	.039	.011	.007
.945	4.5	-10.430	-.015	-1.128	-.134	.013	.036	.014	.008
1.050	5.0	-10.649	-.035	-2.465	-.148	.036	.044	.038	.018
1.155	5.5	-11.103	-.067	-3.998	-.176	.084	.056	.060	.026
1.260	6.0	-12.075	-.154	-5.921	-.234	.179	.079	.092	.037
Should have value			.000		-.125	.000			

Table 21. Spectral Image Surface Characteristics

Entrance Slit Starting Point--B3 $X_o = -.070$ $Y_o = -.2$ $Z_o = .085$

W_1	λ_1 210 L/MM Grating	a_5	a_5 Comparison B3 - B2	Centroid Z_5	Centroid Z_5 Comparison B3 - B2	Centroid Y_5	ΔY_5	ΔZ_5	80% ΔZ_5
.777	3.7	-10.372	-.004	.801	.002	.211	.071	.038	.022
.840	4.0	-10.361	-.003	.098	.000	.207	.062	.019	.011
.882	4.2	-10.374	-.002	- .382	.000	.207	.055	.011	.006
.903	4.3	-10.387	.000	- .628	-.001	.209	.052	.010	.005
.924	4.4	-10.406	.000	- .876	-.001	.210	.048	.012	.007
.945	4.5	-10.430	.000	-1.129	-.001	.213	.044	.016	.010
1.050	5.0	-10.642	.007	-2.469	-.004	.238	.041	.042	.021
1.155	5.5	-11.087	.016	-4.006	-.008	.291	.048	.068	.029
1.260	6.0	-12.031	.044	-5.937	-.016	.396	.062	.108	.046
Should have value			.000		.000	.200			

Table 22. Spectral Image Surface Characteristics

Entrance Slit Starting Point--B4 $X_o = -.083$ $Y_o = -.4$ $Z_o = .040$

W_1	λ_1 210 L/MM Grating	a_5	a_5 Comparison B4 - B2	Centroid Z_5	Centroid Z_5 Comparison B4 - B2	Centroid Y_5	ΔY_5	ΔZ_5	80% ΔZ_5
.777	3.7	-10.440	-.072	.804	.005	.413	.080	.041	.028
.840	4.0	-10.430	-.072	.100	.002	.409	.072	.022	.013
.882	4.2	-10.445	-.073	- .382	.000	.410	.066	.013	.008
.903	4.3	-10.460	-.073	- .628	-.001	.411	.062	.011	.005
.924	4.4	-10.479	-.073	- .877	-.002	.413	.059	.013	.007
.945	4.5	-10.504	-.074	-1.131	-.003	.416	.055	.015	.011
1.050	5.0	-10.728	-.079	-2.475	-.010	.443	.046	.042	.019
1.155	5.5	-11.195	-.092	-4.019	-.021	.502	.056	.071	.032
1.260	6.0	-12.201	-.126	-5.966	-.045	.619	.082	.114	.049
Should have value			-.072		.000	.400			

Table 23. Spectral Image Surface Characteristics

Entrance Slit Starting Point--C1 X_o = .127 Y_o = .2 Z_o = .060

W_1	λ_1 210 L/MM Grating	a_5	a_5 Comparison C1 - C2	Centroid Z_5	Centroid Z_5 Comparison C1 - C2	Centroid Y_5	ΔY_5	ΔZ_5	80% ΔZ_5
.777	3.7	-10.427	-.056	.896	.000	-.186	.053	.040	.022
.840	4.0	-10.417	-.061	.198	.000	-.189	.044	.022	.011
.882	4.2	-10.432	-.066	- .279	.001	-.189	.039	.011	.009
.903	4.3	-10.447	-.068	- .522	.001	-.188	.036	.013	.008
.924	4.4	-10.466	-.070	- .769	.001	-.187	.037	.016	.009
.945	4.5	-10.491	-.073	-1.019	.002	-.185	.037	.019	.010
1.050	5.0	-10.715	-.094	-2.344	.002	-.166	.053	.038	.020
1.155	5.5	-11.181	-.132	-3.853	.004	-.124	.076	.058	.027
1.260	6.0	-12.183	-.233	-5.727	.006	-.043	.124	.080	.033
Should have value			-.072		.000	-.200			

Table 24. Spectral Image Surface Characteristics

Entrance Slit Starting Point--C2 $X_o = 0$ $Y_o = 0$ $Z_o = .025$

W_1	λ_1 210 L/MM Grating	a_5	a_5 Comparison C2 - B2	Centroid Z_5	Centroid Z_5 Comparison C2 - B2	Centroid Y_5	ΔY_5	ΔZ_5	80% ΔZ_5
.777	3.7	-10.371	-.003	.896	.097	.012	.061	.039	.021
.840	4.0	-10.356	.002	.198	.100	.008	.052	.020	.011
.882	4.2	-10.366	.006	- .280	.102	.008	.046	.009	.005
.903	4.3	-10.379	.008	- .523	.104	.009	.043	.008	.005
.924	4.4	-10.396	.010	- .770	.105	.010	.039	.011	.006
.945	4.5	-10.418	.012	-1.021	.107	.012	.035	.014	.008
1.050	5.0	-10.621	.028	-2.346	.119	.033	.044	.036	.019
1.155	5.5	-11.049	.054	-3.857	.141	.079	.056	.059	.029
1.260	6.0	-11.950	.125	-5.733	.188	.168	.076	.085	.034
Should have value			.000		.100	.000			

Table 25. Spectral Image Surface Characteristics

Entrance Slit Starting Point--C3 X_o = -.070 Y_o = -.2 Z_o = -.015

W_1	λ_1 210 L/MM Grating	a_5	a_5 Comparison C3 - C2	Centroid Z_5	Centroid Z_5 Comparison C3 - C2	Centroid Y_5	ΔY_5	ΔZ_5	80% ΔZ_5
.777	3.7	-10.376	-.005	.898	.002	.212	.070	.040	.022
.840	4.0	-10.359	-.003	.198	.000	.207	.061	.021	.011
.882	4.2	-10.369	-.003	- .280	.000	.207	.055	.010	.006
.903	4.3	-10.380	-.001	- .524	-.001	.208	.051	.008	.005
.924	4.4	-10.397	-.001	- .771	-.001	.210	.047	.010	.006
.945	4.5	-10.418	.000	-1.022	-.001	.212	.044	.013	.010
1.050	5.0	-10.616	.005	-2.350	-.004	.235	.041	.040	.020
1.155	5.5	-11.035	.014	-3.866	-.009	.285	.049	.066	.029
1.260	6.0	-11.914	.036	-5.749	-.016	.384	.060	.100	.042
Should have value			.000		.000	.200			

Table 26. Spectral Image Surface Characteristics

Entrance Slit Starting Point--C4 X_o = -.083 Y_o = -.4 Z_o = -.060

W_1	λ_1 210 L/MM Grating	a_5	a_5 Comparison C4 - C2	Centroid Z_5	Centroid Z_5 Comparison C4 - C2	Centroid Y_5	ΔY_5	ΔZ_5	80% ΔZ_5
.777	3.7	-10.444	-.073	.901	.005	.414	.079	.043	.024
.840	4.0	-10.429	-.073	.200	.002	.409	.071	.024	.013
.882	4.2	-10.440	-.074	- .280	.000	.409	.065	.012	.008
.903	4.3	-10.452	-.073	- .524	-.001	.410	.062	.009	.005
.924	4.4	-10.470	-.074	- .772	-.002	.412	.058	.011	.008
.945	4.5	-10.493	-.075	-1.024	-.003	.415	.055	.014	.010
1.050	5.0	-10.701	-.080	-2.357	-.011	.440	.046	.039	.019
1.155	5.5	-11.141	-.092	-3.879	-.022	.496	.056	.067	.036
1.260	6.0	-12.075	-.125	-5.777	-.044	.606	.078	.106	.053
Should have value			-.072		.000	.400			

Table 27. Spectral Image Surface Characteristics

Entrance Slit Starting Point--D1 X_o = .127 Y_o = .2 Z_o = .010

W_2	λ_2 210 L/MM Grating	a_5	a_5 Comparison D1 - B1	Centroid Z_5	Centroid Z_5 Comparison D1 - B1	Centroid Y_5	ΔY_5	ΔZ_5	80% ΔZ_5
.7903	3.7633	-10.422	.004	.799	.000	-.186	.050	.037	.019
.8533	4.0633	-10.432	.004	.098	.000	-.189	.046	.021	.011
.8953	4.2633	-10.442	.004	- .381	.001	-.188	.038	.012	.008
.9163	4.3633	-10.453	.004	- .626	.001	-.188	.037	.015	.008
.9373	4.4633	-10.475	.004	- .874	.001	-.186	.037	.018	.010
.9583	4.5633	-10.502	.005	-1.126	.001	-.184	.037	.021	.012
1.0633	5.0633	-10.741	.005	-2.462	.001	-.163	.055	.041	.023
1.1683	5.5633	-11.236	.007	3.993	.001	-.120	.079	.061	.028
1.2733	6.0633	-12.314	.013	-5.914	.002	-.033	.132	.084	.036
Should have value			.000		.000	-.200			

Table 28. Spectral Image Surface Characteristics

Entrance Slit Starting Point--D2 $X_o = 0$ $Y_o = 0$ $Z_o = -.025$

W_2	λ_2 210 L/MM Grating	a_5	a_5 Comparison D2 - B2	Centroid Z_5	Centroid Z_5 Comparison D2 - B2	Centroid Y_5	ΔY_5	ΔZ_5	80% ΔZ_5
.7903	3.7633	-10.366	.002	.799	.000	.011	.059	.036	.020
.8533	4.0633	-10.356	.002	.098	.000	.008	.050	.017	.010
.8953	4.2633	-10.371	.001	- .382	.000	.008	.043	.008	.004
.9163	4.3633	-10.385	.002	- .627	.000	.009	.040	.010	.006
.9373	4.4633	-10.404	.002	- .876	-.001	.011	.036	.013	.008
.9583	4.5633	-10.428	.002	-1.128	.000	.013	.034	.016	.009
1.0633	5.0633	-10.646	.003	-2.465	.000	.036	.046	.039	.023
1.1683	5.5633	-11.100	.003	-3.998	.000	.084	.057	.062	.025
1.2733	6.0633	-12.068	.007	-5.921	.000	.179	.080	.087	.036
Should have value			.000		.000	.000			

Table 29. Spectral Image Surface Characteristics

Entrance Slit Starting Point--D3 $X_o = -.070$ $Y_o = -.2$ $Z_o = -.065$

W_2	λ_2 210 L/MM Grating	a_5	a_5 Comparison D3 - B3	Centroid Z_5	Centroid Z_5 Comparison D3 - B3	Centroid Y_5	ΔY_5	ΔZ_5	80% ΔZ_5
.7903	3.7633	-10.372	.000	.800	-.001	.211	.068	.036	.021
.8533	4.0633	-10.360	.001	.098	.000	.207	.059	.018	.010
.8953	4.2633	-10.373	.001	- .383	-.001	.208	.052	.007	.005
.9163	4.3633	-10.387	.000	- .628	.000	.209	.049	.009	.006
.9373	4.4633	-10.405	.001	- .877	-.001	.211	.045	.011	.007
.9583	4.5633	-10.429	.001	-1.130	-.001	.213	.041	.015	.009
1.0633	5.0633	-10.641	.001	-2.470	-.001	.238	.043	.042	.023
1.1683	5.5633	-11.086	.001	-4.007	-.001	.291	.050	.067	.027
1.2733	6.0633	-12.029	.002	-5.939	-.002	.396	.063	.103	.042
Should have value			.000		.000	.200			

Table 30. Spectral Image Surface Characteristics

Entrance Slit Starting Point--D4 $X_o = -.083$ $Y_o = -.4$ $Z_o = -.110$

W_2	λ_2 210 L/MM Grating	a_5	a_5 Comparison D4 - B4	Centroid Z_5	Centroid Z_5 Comparison D4 - B4	Centroid Y_5	ΔY_5	ΔZ_5	80% ΔZ_5
.7903	3.7633	-10.439	.001	.803	-.001	.413	.077	.040	.021
.8533	4.0633	-10.430	.000	.099	-.001	.409	.069	.021	.011
.8953	4.2633	-10.444	.001	- .383	-.001	.410	.063	.009	.005
.9163	4.3633	-10.459	.001	- .629	-.001	.411	.059	.010	.006
.9373	4.4633	-10.479	.000	- .879	-.002	.413	.056	.013	.008
.9583	4.5633	-10.504	.000	-1.132	-.001	.416	.052	.016	.010
1.0633	5.0633	-10.728	.000	-2.477	-.002	.444	.047	.042	.021
1.1683	5.5633	-11.195	.000	-4.021	-.002	.502	.058	.069	.032
1.2733	6.0633	-12.200	.001	-5.969	-.003	.620	.083	.108	.046
Should have value			.000		.000	.400			

Table 31. Spectral Image Surface Characteristics

Entrance Slit Starting Point--E1 X_o = .127 Y_o = .2 Z_o = -.090

W_2	λ_2 210 L/MM Grating	a_5	a_5 Comparison E1 - C1	Centroid Z_5	Centroid Z_5 Comparison E1 - C1	Centroid Y_5	ΔY_5	ΔZ_5	80% ΔZ_5
.7903	3.7633	-10.425	.002	.896	.000	-.186	.052	.039	.020
.8533	4.0633	-10.414	.003	.198	.000	-.189	.041	.021	.011
.8953	4.2633	-10.429	.003	- .279	.000	-.189	.036	.012	.008
.9163	4.3633	-10.444	.003	- .522	.000	-.188	.037	.015	.010
.9373	4.4633	-10.463	.003	- .769	.000	-.187	.037	.018	.011
.9583	4.5633	-10.488	.003	-1.019	.000	-.185	.037	.022	.013
1.0633	5.0633	-10.711	.004	-2.344	.000	-.166	.054	.041	.026
1.1683	5.5633	-11.176	.005	-3.853	.000	-.124	.077	.062	.029
1.2733	6.0633	-12.174	.009	-5.727	.000	-.043	.124	.084	.040
Should have value			.000		.000	-.200			

Table 32. Spectral Image Surface Characteristics

Entrance Slit Starting Point--E2 $X_o = 0$ $Y_o = 0$ $Z_o = -.125$

W_2	λ_2 210 L/MM Grating	a_5	a_5 Comparison E2 - C2	Centroid Z_5	Centroid Z_5 Comparison E2 - C2	Centroid Y_5	ΔY_5	ΔZ_5	80% ΔZ_5
.7903	3.7633	-10.370	.001	.895	-.001	.012	.058	.038	.019
.8533	4.0633	-10.355	.001	.197	-.001	.008	.049	.019	.010
.8953	4.2633	-10.366	.000	- .281	-.001	.008	.043	.008	.007
.9163	4.3633	-10.378	.001	- .524	-.001	.009	.039	.011	.006
.9373	4.4633	-10.395	.001	- .771	-.001	.010	.036	.014	.008
.9583	4.5633	-10.417	.001	-1.021	.000	.012	.034	.017	.011
1.0633	5.0633	-10.620	.001	-2.347	-.001	.033	.046	.038	.021
1.1683	5.5633	-11.047	.002	-3.858	-.001	.079	.058	.061	.026
1.2733	6.0633	-11.948	.002	-5.734	-.001	.168	.077	.082	.033
Should have value			.000		.000	.000			

Table 33 . Spectral Image Surface Characteristics

Entrance Slit Starting Point--E3 X_o = -.070 Y_o = -.2 Z_o = -.165

W_2	λ_2 210 L/MM Grating	a_5	a_5 Comparison E3 - C3	Centroid Z_5	Centroid Z_5 Comparison E3 - C3	Centroid Y_5	ΔY_5	ΔZ_5	80% ΔZ_5
.7903	3.7633	-10.376	.000	.896	-.002	.212	.067	.038	.021
.8533	4.0633	-10.360	-.001	.197	-.001	.207	.058	.019	.010
.8953	4.2633	-10.369	.000	- .282	-.002	.207	.052	.008	.005
.9163	4.3633	-10.381	-.001	- .525	-.001	.208	.048	.009	.006
.9373	4.4633	-10.397	.000	- .773	-.002	.210	.045	.012	.008
.9583	4.5633	-10.418	.000	-1.024	-.002	.212	.041	.015	.011
1.0633	5.0633	-10.617	-.001	-2.352	-.002	.235	.044	.040	.020
1.1683	5.5633	-11.036	-.001	-3.867	-.001	.285	.051	.065	.036
1.2733	6.0633	-11.915	-.001	-5.752	-.003	.384	.062	.095	.039
Should have value			.000		.000	.200			

Table 34. Spectral Image Surface Characteristics

Entrance Slit Starting Point--E4 X_o = -.083 Y_o = -.4 Z_o = -.210

W_2	λ_2 210 L/MM Grating	a_5	a_5 Comparison E4 - C4	Centroid Z_5	Centroid Z_5 Comparison E4 - C4	Centroid Y_5	ΔY_5	ΔZ_5	80% ΔZ_5
.7903	3.7633	-10.444	.000	.899	-.002	.414	.076	.042	.021
.8533	4.0633	-10.429	.000	.198	-.002	.409	.068	.023	.011
.8953	4.2633	-10.440	.000	- .282	-.002	.409	.062	.010	.006
.9163	4.3633	-10.453	-.001	- .526	-.002	.410	.059	.011	.006
.9373	4.4633	-10.470	.000	- .774	-.002	.412	.055	.014	.007
.9583	4.5633	-10.493	.000	-1.026	-.002	.415	.052	.016	.010
1.0633	5.0633	-10.702	-.001	-2.359	-.002	.440	.048	.039	.019
1.1683	5.5633	-11.143	-.002	-3.881	-.002	.496	.058	.065	.030
1.2733	6.0633	-12.079	-.004	-5.781	-.004	.606	.079	.100	.041
Should have value			.000		.000	.400			

Table 35. W Values and Equivalent Wavelengths Used for the Ray Trace of the Two Entrance Slits

W_1	λ_1 for 210 1/mm	W_2	λ_2 for 210 1/mm
.777	3.7	.7903	3.76333
.840	4.0	.8533	4.06333
.882	4.2	.8953	4.26333
.903	4.3	.9163	4.36333
.924	4.4	.9373	4.46333
.945	4.5	.9583	4.56333
1.050	5.0	1.0633	5.06333
1.155	5.5	1.1683	5.56333
1.260	6.0	1.2733	6.06333

NIMS MONOCHROMATOR F/3.5 10 INCH FL. 26 DEGREE GRATING 12-18-69

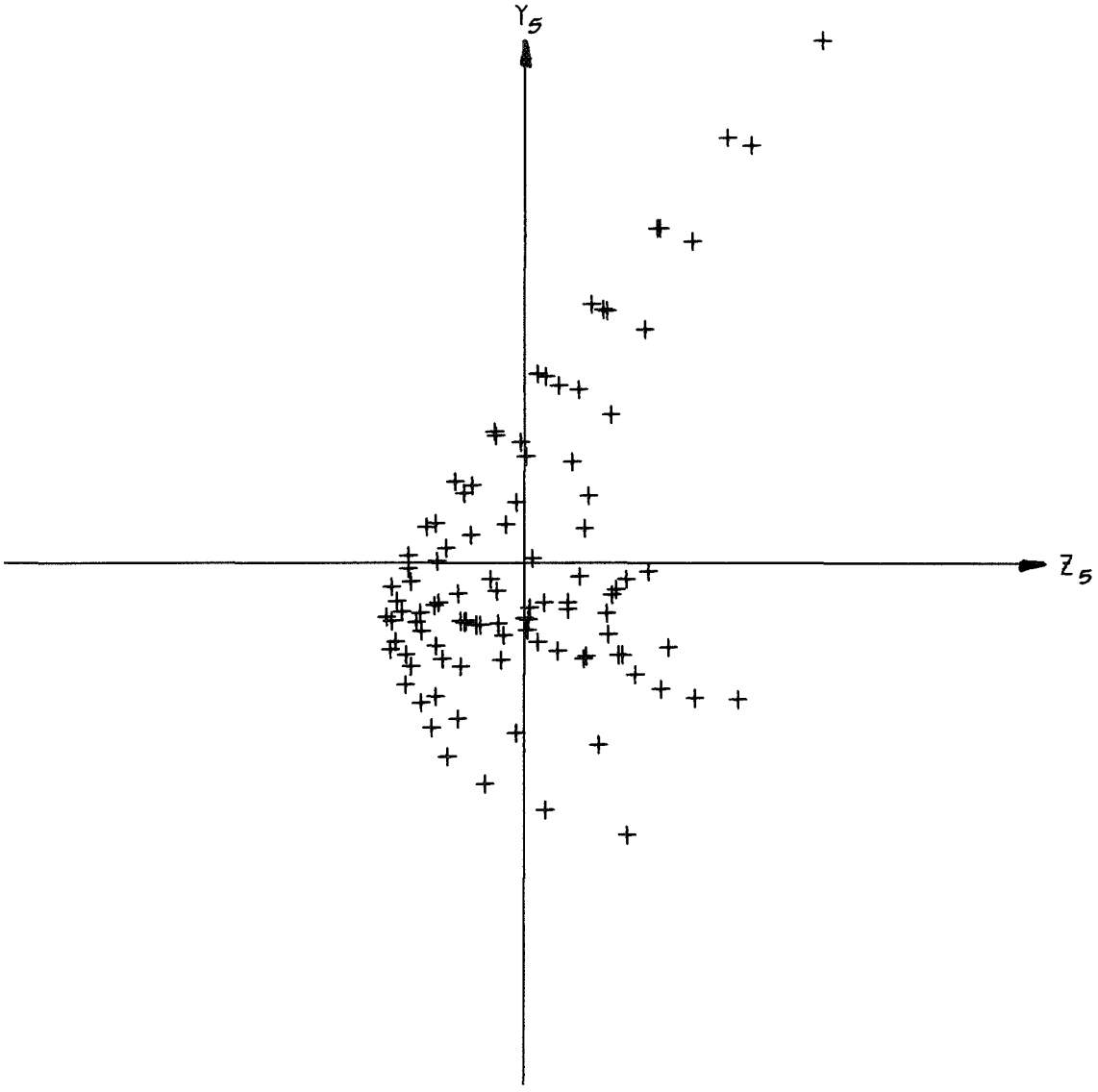

		MAX	MIN	
Z HALF AXIS LENGTH 0.050	Z =	0.028	-0.013	SURFACE NO.
Y HALF AXIS LENGTH 0.050	Y =	0.050	-0.026	5

Figure 9. Spectral Image for E4 Starting Point
W = 0.7903 λ = 3.7633

NIMS MONOCHROMATOR F/3.5 10 INCH FL. 26 DEGREE GRATING 12-18-69

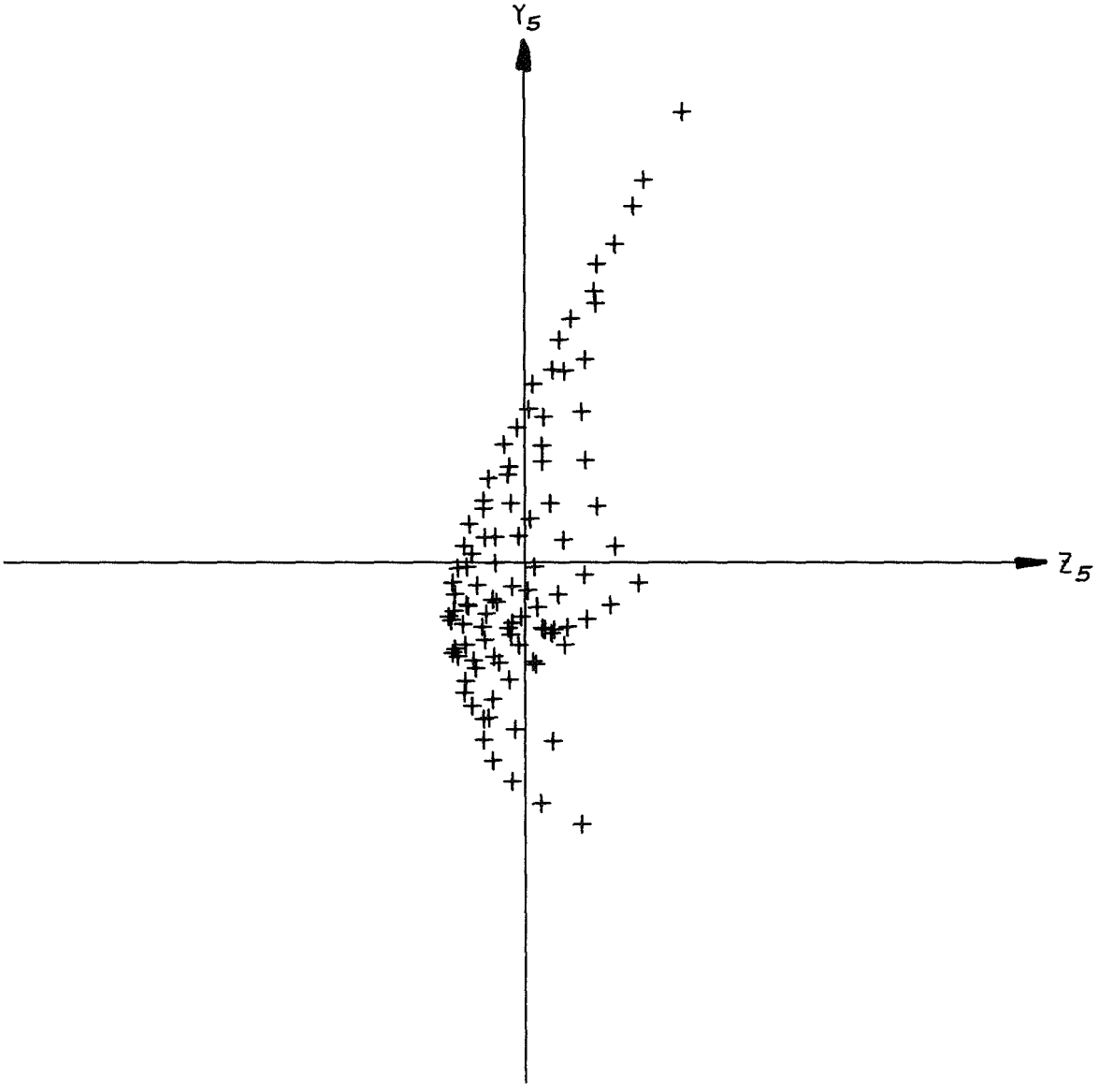

			MAX	MIN	
Z HALF AXIS LENGTH	0.050	Z =	0.015	-0.007	SURFACE NO.
Y HALF AXIS LENGTH	0.050	Y =	0.043	-0.025	5

Figure 10. Spectral Image for E4 Starting Point
W = 0.8533 λ = 4.0633

NIMS MONOCHROMATOR F/3.5 10 INCH FL. 26 DEGREE GRATING 12-18-69

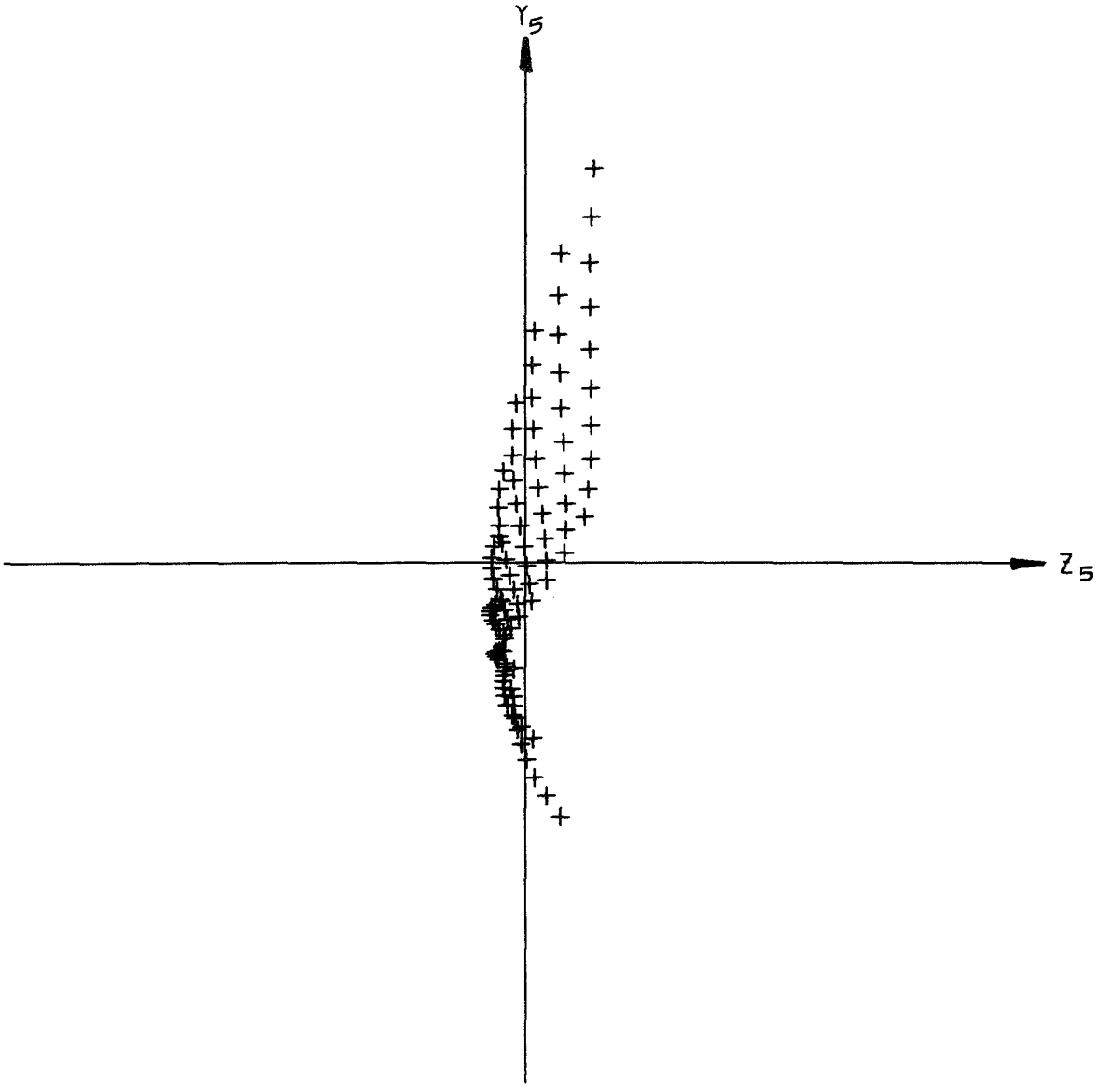

		MAX	MIN	
Z HALF AXIS LENGTH 0.050	Z =	0.007	-0.003	SURFACE NO.
Y HALF AXIS LENGTH 0.050	Y =	0.038	-0.024	5

Figure 11. Spectral Image for E4 Starting Point
W = 0.8953 λ = 4.2633

NIMS MONOCHROMATOR F/3.5 10 INCH FL. 26 DEGREE GRATING 12-18-69

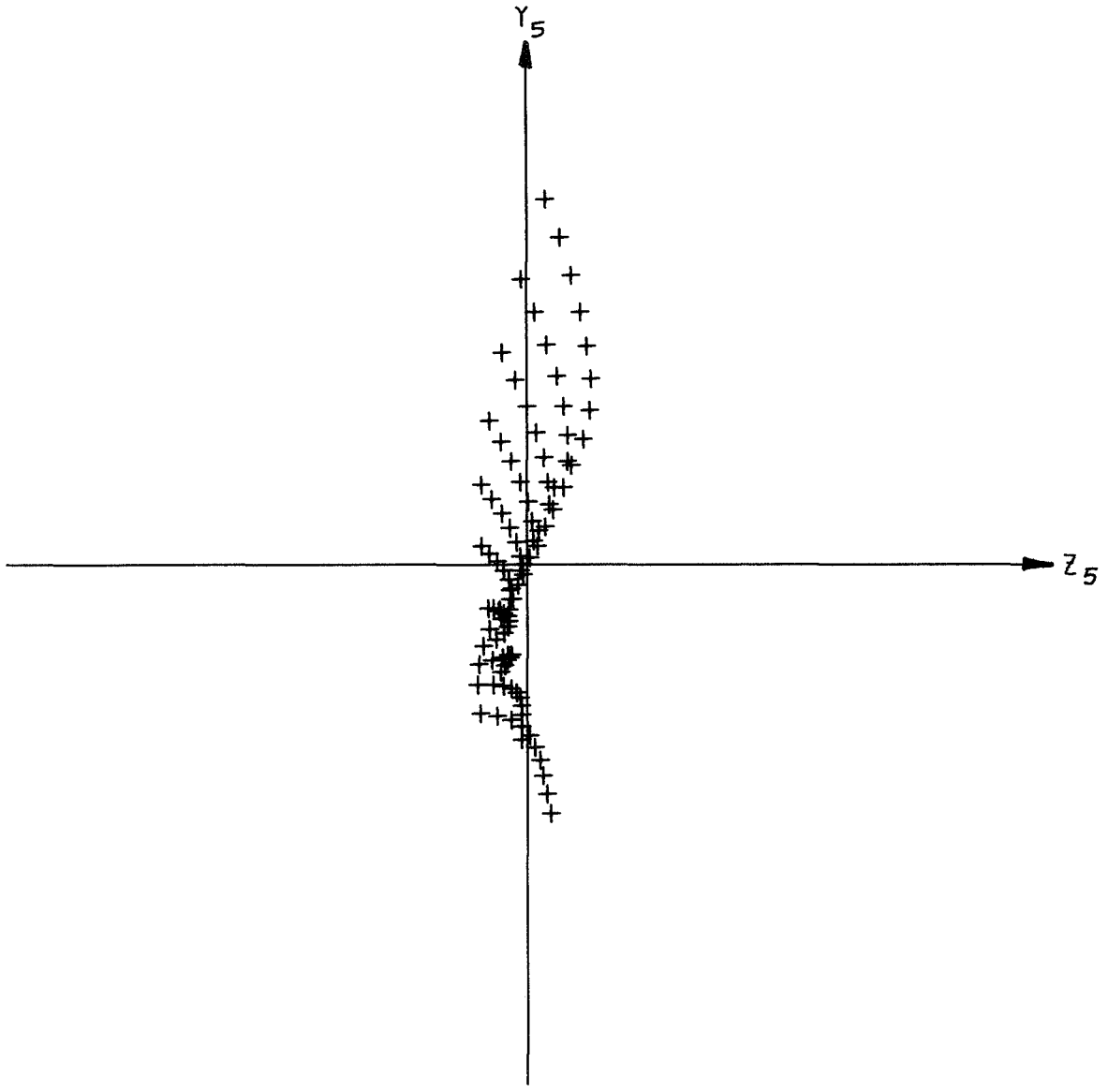

		MAX	MIN	
Z HALF AXIS LENGTH 0.050	Z =	0.006	-0.005	SURFACE NO.
Y HALF AXIS LENGTH 0.050	Y =	0.035	-0.024	5

Figure 12. Spectral Image for E4 Starting Point
W = 0.9163 λ = 4.3633

NIMS MONOCHROMATOR F/3.5 10 INCH FL. 26 DEGREE GRATING 12-18-69

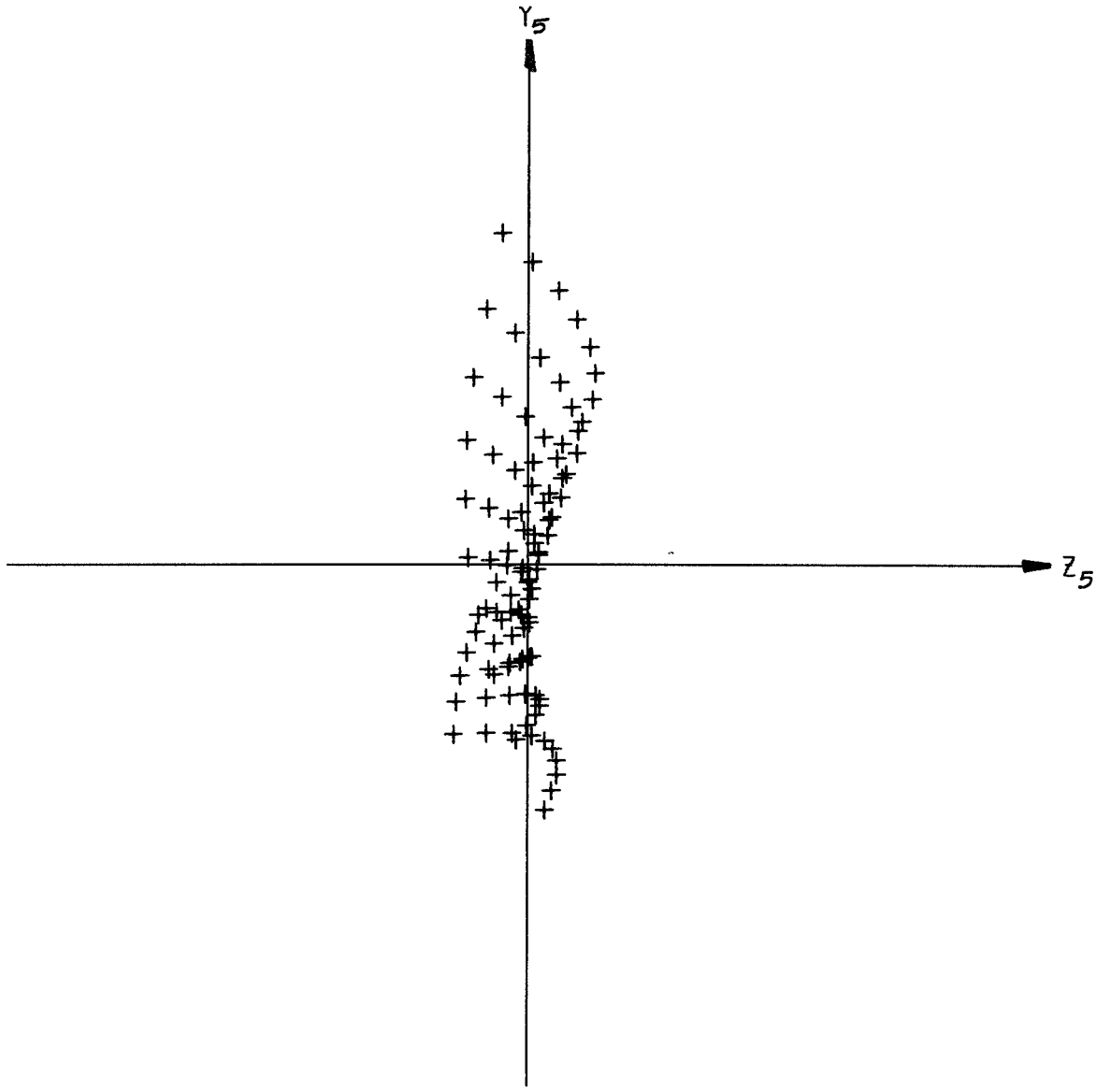

		MAX	MIN	
Z HALF AXIS LENGTH 0.050	Z =	0.006	-0.007	SURFACE NO.
Y HALF AXIS LENGTH 0.050	Y =	0.032	-0.024	5

Figure 13. Spectral Image for E4 Starting Point
W = 0.9373 λ = 4.4633

NIMS MONOCHROMATOR F/3.5 10 INCH FL. 26 DEGREE GRATING 12-18-69

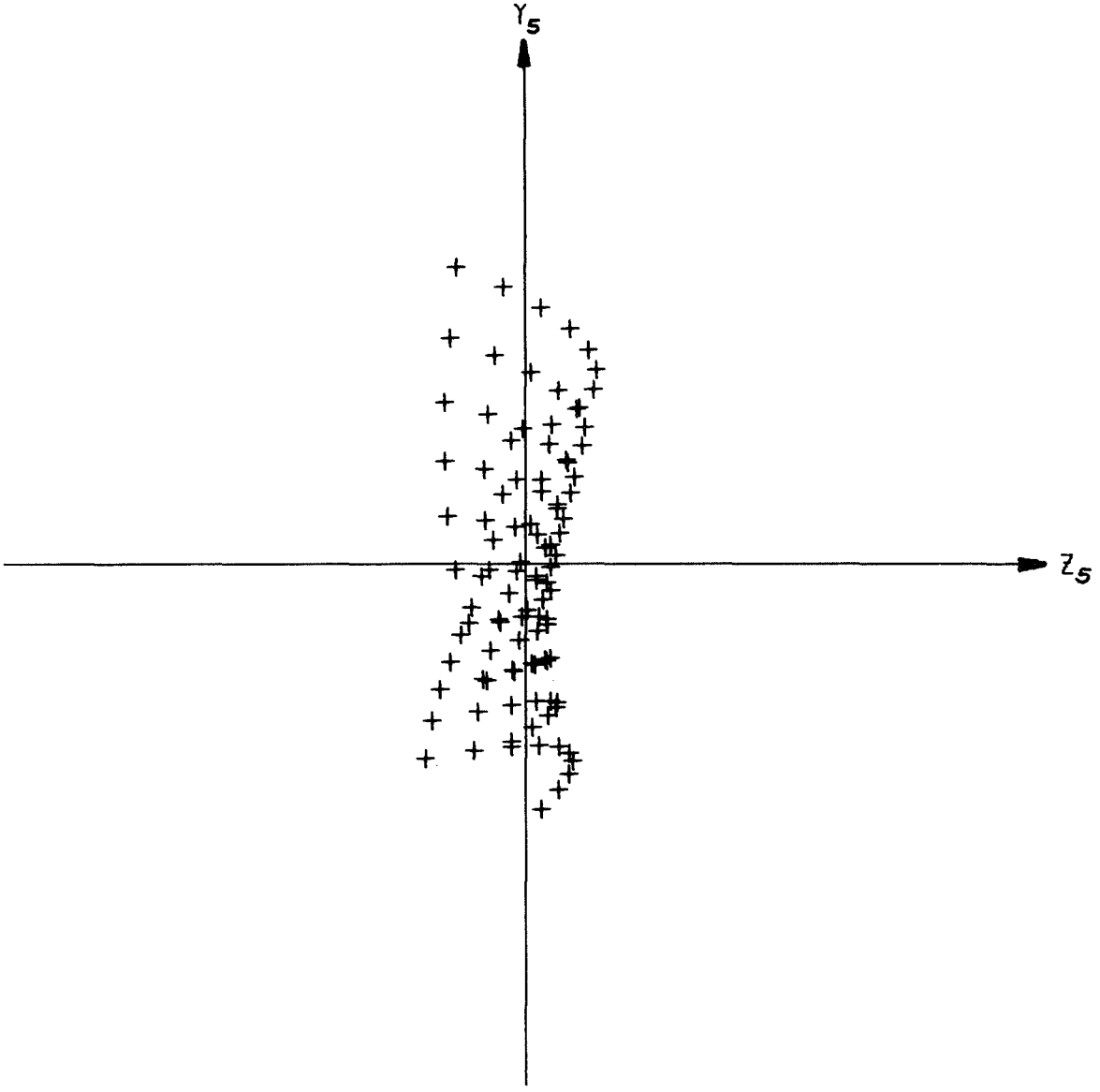

			MAX	MIN	
Z HALF AXIS LENGTH	0.050	Z =	0.007	-0.010	SURFACE NO.
Y HALF AXIS LENGTH	0.050	Y =	0.028	-0.023	5

Figure 14. Spectral Image for E4 Starting Point
W = 0.9583 λ = 4.5633

NIMS MONOCHROMATOR F/3.5 10 INCH FL. 26 DEGREE GRATING 12-18-69

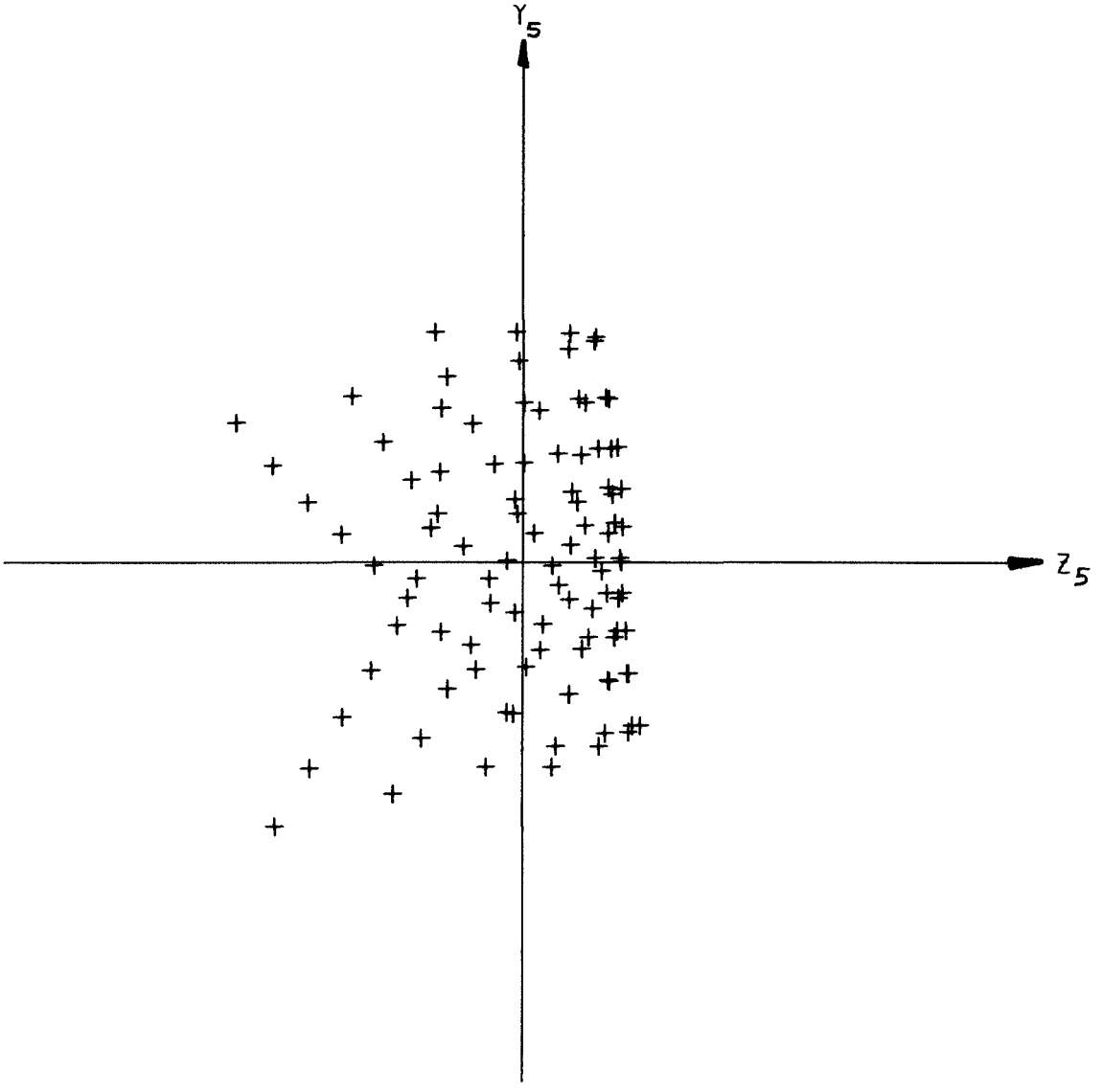

		MAX	MIN	
Z HALF AXIS LENGTH 0.050	Z =	0.011	-0.028	SURFACE NO.
Y HALF AXIS LENGTH 0.050	Y =	0.022	-0.025	5

Figure 15. Spectral Image for E4 Starting Point
W = 1.0633 λ = 5.0633

NIMS MONOCHROMATOR F/3.5 10 INCH FL. 26 DEGREE GRATING 12-18-69

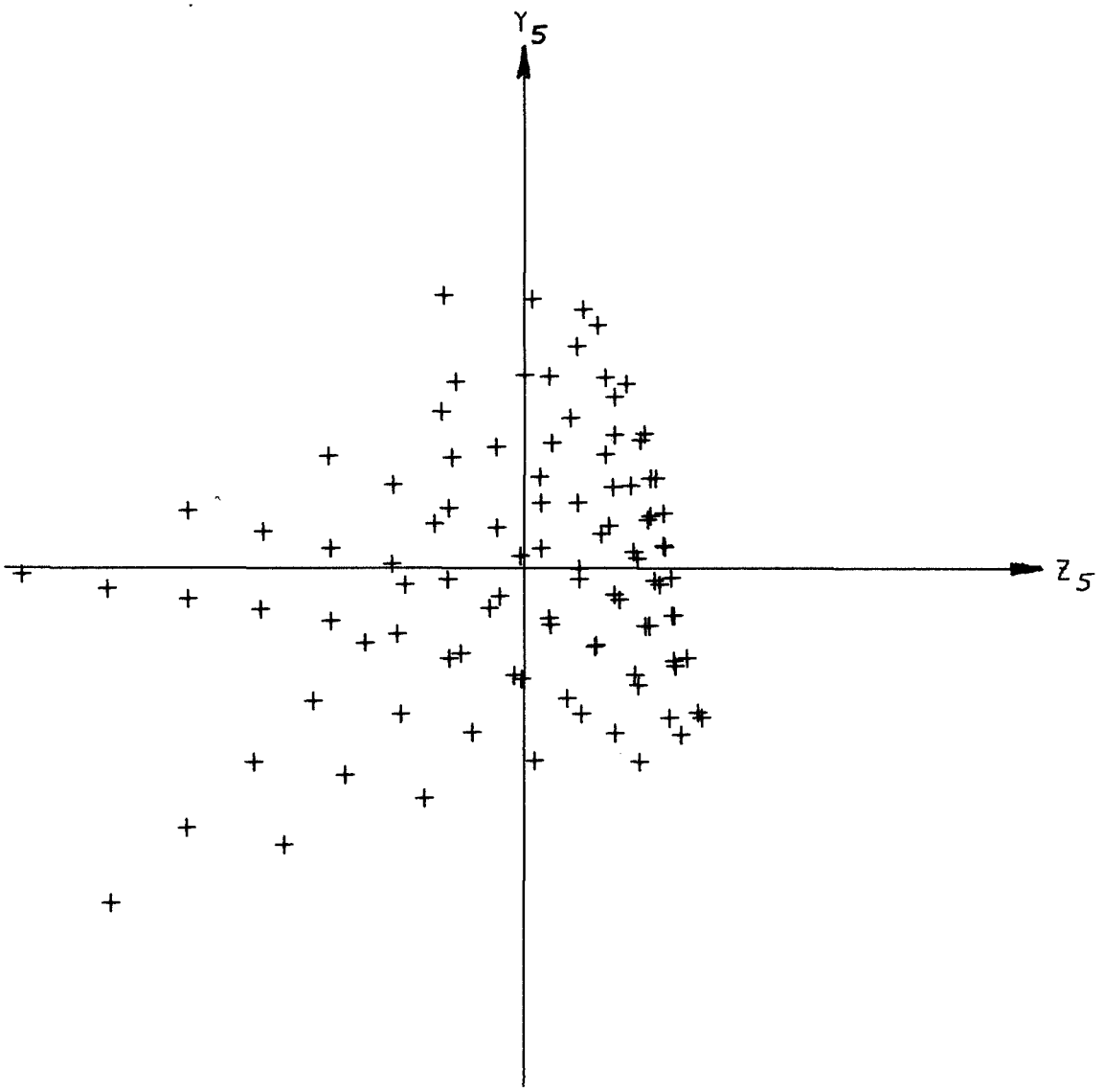

		MAX	MIN	
Z HALF AXIS LENGTH 0.050	Z =	0.017	-0.048	SURFACE NO.
Y HALF AXIS LENGTH 0.050	Y =	0.026	-0.032	5

Figure 16. Spectral Image for E4 Starting Point
W = 1.1683 λ = 5.5633

NIMS MONOCHROMATOR F/3.5 10 INCH FL. 26 DEGREE GRATING 12-18-69

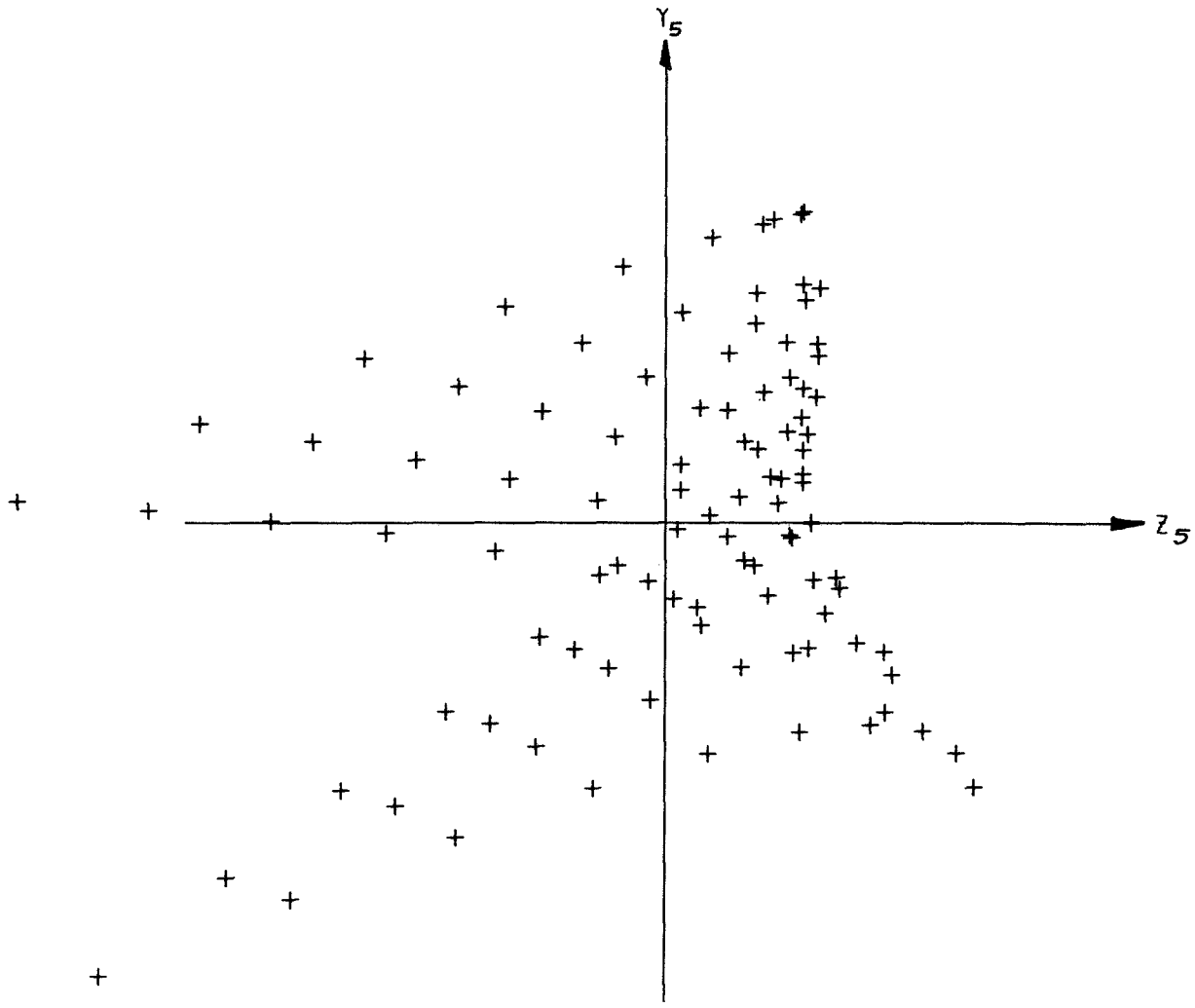

		MAX	MIN	
Z HALF AXIS LENGTH 0.050	Z =	0.032	-0.068	SURFACE NO.
Y HALF AXIS LENGTH 0.050	Y =	0.032	-0.047	5

Figure 17. Spectral Image for E4 Starting Point
W = 1.2733 λ = 6.0633

farthest from the collimating mirror axis, and thus produces slightly larger aberrations than any other entrance slit starting point. The Y-Z axes shown in Figures 9 through 17 are, of course, the Y_5-Z_5 axes of the monochromator. However, for the ray trace for each figure, it was necessary to move the origin of the (X_5, Y_5, Z_5) axis system to the centroid Y_5 and the centroid Z_5 coordinates shown in Table 34 for each of the nine W values. This means that for all nine spot diagrams, the origin of the axis system shown is at the true centroid of its 100-ray spot diagram.

All nine spot diagrams use the same scale of .050 inch per half axis.

7. COLLIMATING MIRROR

The collimating mirror is a paraboloid with a 10-inch focal length. Its apex must be accurately positioned at the origin of the ($X_{1,4}$, $Y_{1,4}$, $Z_{1,4}$) axis system, and its focal point must lie precisely on the $X_{1,4}$ axis.

The areas of the collimating mirror that actually reflect rays are shown in Figure 18. This is a plot of data taken from boundary-defining ray traces. The plot shows the optically used areas of the collimating mirror as projected on the $Y_{1,4}$-$Z_{1,4}$ plane. Each of the rectangular shapes in Figure 18 is formed by drawing straight lines between four ray-traced corner points. Each set of four corner points is the intersection between the collimating mirror and those rays which also intersected the four corners of the grating ruled areas.

Such intersection rectangles can be constructed for any combination of entrance slit starting point and W_1 or W_2 values. However, only those combinations have been plotted which actually contribute to a collimating mirror boundary condition. The four rectangular areas which lie below the origin of the ($X_{1,4}$, $Y_{1,4}$, $Z_{1,4}$) axis system in Figure 18 show the first reflections from the collimating mirror for those rays arriving directly from the entrance slits. The entrance slit starting points that have been used are B1, B4, E1, and E4 which represent the four outer corners of the two entrance slits. The W values are not involved at the first collimating mirror reflection.

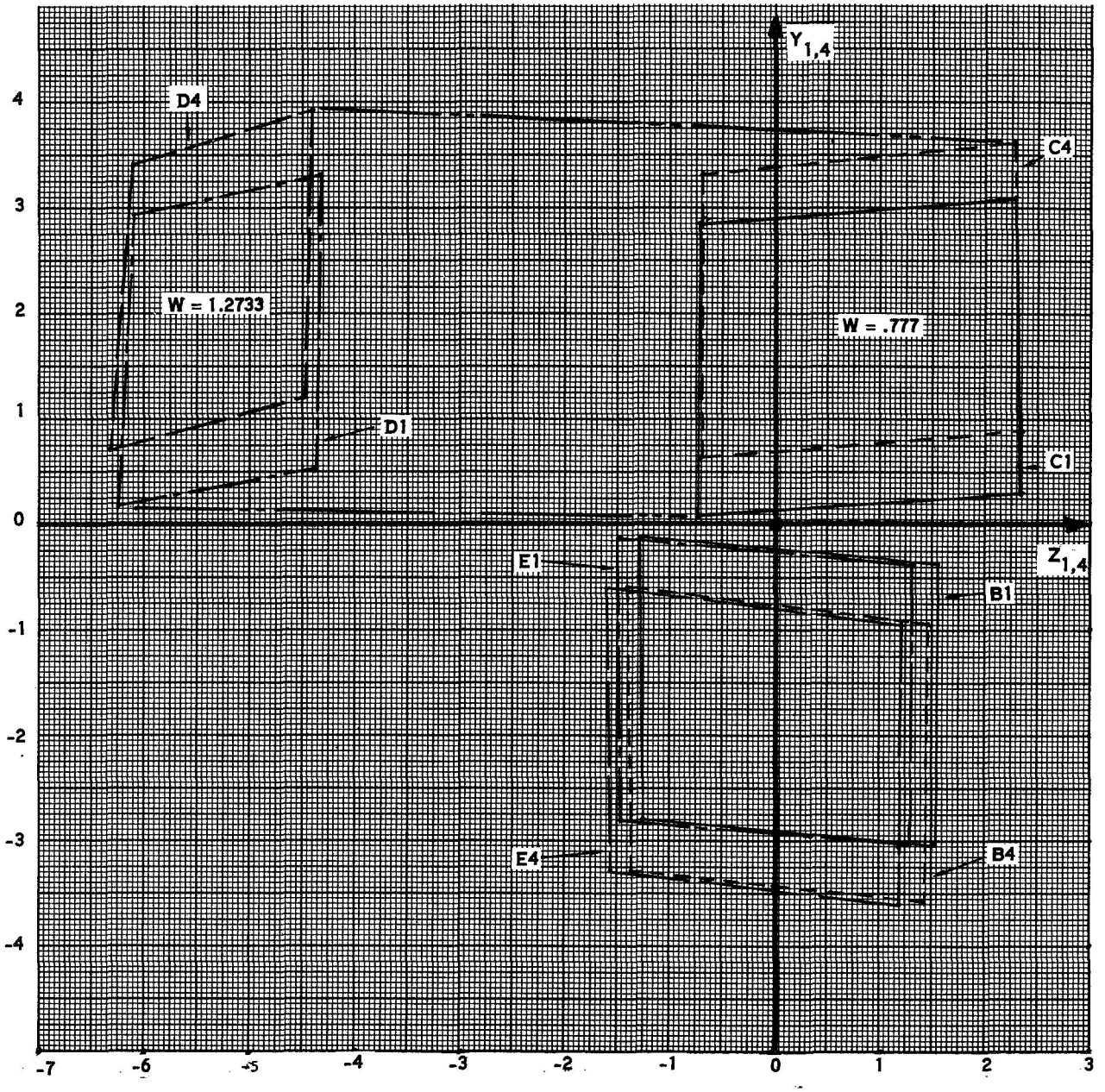

Figure 18. Optically Used Areas on Collimating Mirror Surface

The four rectangles which are shown above the origin of the $(X_{1,4}, Y_{1,4}, Z_{1,4})$ axis system in Figure 18 represent the second reflection from the collimating mirror, and are formed by rays that have been diffracted to the collimating mirror from the grating. The right-hand rectangles in Figure 18 have entrance slit starting points C1 and C4 used with a W value of .777. The left-hand rectangles have entrance slit starting points D1 and D4 and a W value of 1.2733. These four rectangles are shown connected by fantom lines, since the area so enclosed represents the optically used area.

SECTION 4

DETECTOR FOREOPTICS

The foreoptics for each detector is used to transfer radiant flux from the monochromator spectral image surface to the detector. The foreoptics should have the following characteristics:

1. The front optical element of each detector foreoptical system must have a rectangular cross-section, as viewed along its optical axis, which matches the spectral images of both the main entrance slit and the second entrance slit for their respective central wavelengths.

2. The detector will be emersed in either the front element of a single lens or the second element of a double lens detector foreoptical system.

3. The detector foreoptics must image the grating ruled area on the detector with as good image quality as possible. Having the detector area match the grating image precisely, so the detector receives no direct rays from outside the grating ruled area, is the best monochromator stray-light-control technique available.

Since the grating is to be imaged on each detector by its foreoptics, the ray-trace procedure consisted of actually ray-tracing diffracted rays from the center and the four corners of the grating to the collimating mirror which, in turn, reflects them to the spectral image surface where they are traced through the foreoptics to the detector. This ray trace procedure was repeated for nine W values with equivalent wavelengths: 3.7, 4.0, 4.2, 4.3, 4.4, 4.5, 5.0, 5.5, and 6.0 μ.

Figure 19 shows the axis systems that are used for the detector foreoptics ray trace, and Table 36 defines these axis systems. A single lens foreoptics is shown in Figure 19 and described in Table 36, since it has been selected for the final foreoptics design. Both singlet and doublet lenses were ray-traced. However, a germanium emersed singlet gives good image quality on the detector, and it is much easier to mount in the foreoptical arrays with high-positioning accuracy.

Five ray starting points, each using 25-ray families, are located on the diffraction grating surface. These locations include the center and the four corners of the grating ruled area, so the origin of the (X_o', Y_o', Z_o') axis system is located at the grating center. The grating ruled surface is on the Y_o'-Z_o' plane and the grating rulings are parallel to the Y_o'-axis. Table 37 defines the coordinates of the five starting points on the grating, G1, G2, G3, G4, and G5.

Each family of 25 rays from the five starting points on the grating must intersect and fill the rectangular aperture stop for the detector foreoptics which is in the (X_3', Y_3', Z_3') axis system in the same uniform 5 x 5 point array. This makes the rectangular edges of the front lens surface of each detector lens the true aperture stop of its detector foreoptical system.

Table 38 gives the dimensional parameters for the detector foreoptics ray trace axis systems shown in Figure 19, and Table 2 defines these parameters. The final radius of curvature for the front surface of each detector lens is .6 inch.

1. APERTURE STOPS FOR DETECTOR FOREOPTICS

In the preceding paragraphs, the ray-trace axis systems were defined and the procedures for ray-tracing the detector foreoptics for nine different W values were outlined. A major problem still to be solved before the ray traces could commence was the accurate determination of the proper aperture stop size and its physical location relative to the remainder of the monochromator for each detector optical system. This was solved by the following procedure:

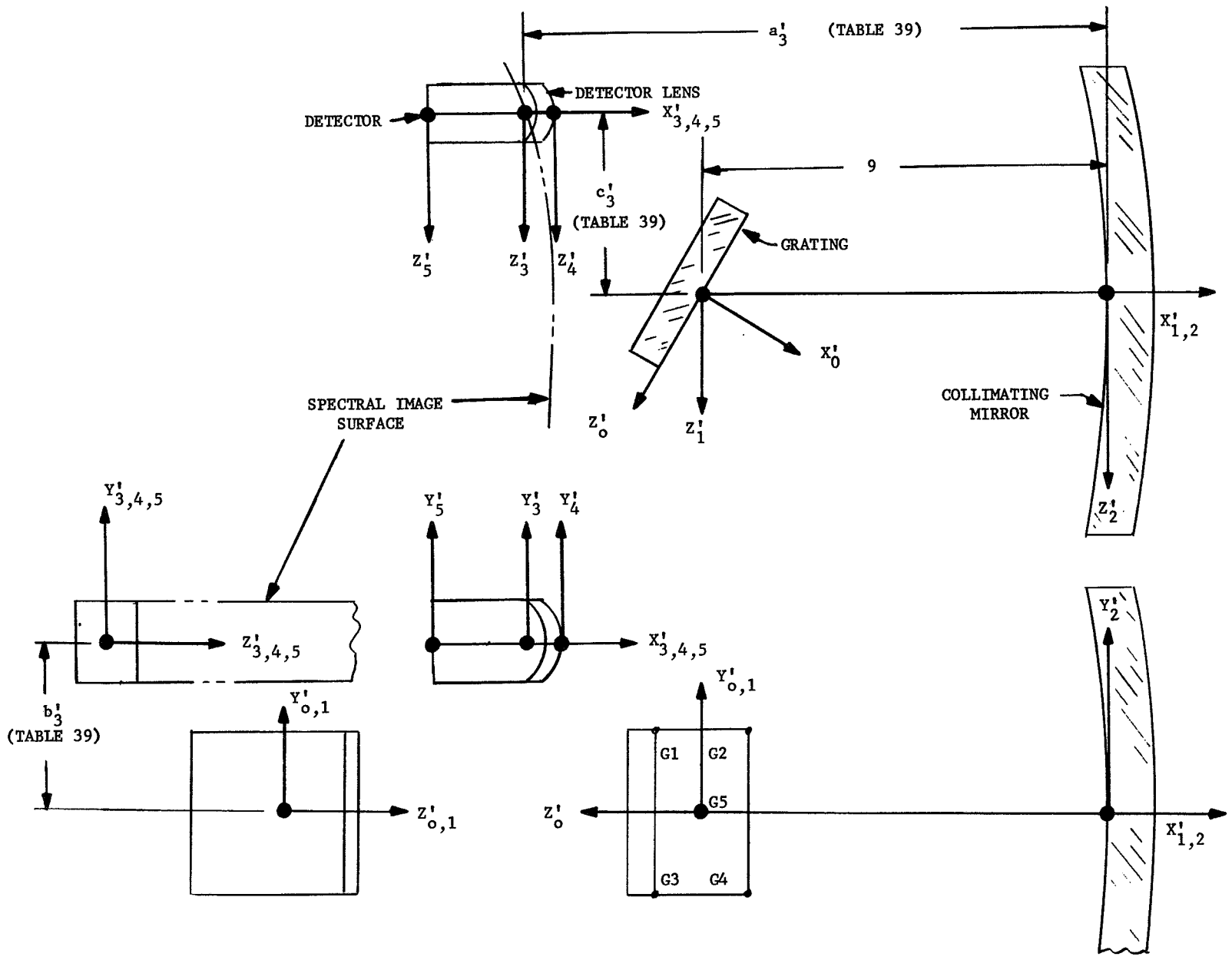

Figure 19. Three-View Drawing of Axis Systems for Ray Trace of Detector Foreoptics

Table 36. Definitions for the Axis Systems Used to Ray-Trace the Detector Foreoptics.

(X'_o, Y'_o, Z'_o)	DIFFRACTION GRATING--The grating ruled surface is on the Y'_o-Z'_o plane, and the rulings are parallel to the Y'_o-axis.
(X'_1, Y'_1, Z'_1)	MATHEMATICAL AXIS SYSTEM--This axis system has the same origin as the (X'_o, Y'_o, Z'_o) axis system, and is used as a mathematical aid.
(X'_2, Y'_2, Z'_2)	PARABOLOID COLLIMATING MIRROR--The apex of the paraboloid collimating mirror is tangential to the Y'_2-Z'_2 plane at the origin of the (X'_2, Y'_2, Z'_2) axis system. The focus of this paraboloid collimating mirror is located on the negative X'_2-axis.
(X'_3, Y'_3, Z'_3)	APERTURE STOP FOR EACH DETECTOR FOREOPTICS SYSTEM--The X'_3-axis is the optical center line for the detector foreoptical system. The X'_3-axis for every detector foreoptical system is parallel to the X'_2-axis which is the collimating mirror axis. The a'_3 input value for each of the nine W values ray traces is approximately equal to the average of the a_5 values for B1, B4, C1, and C4 from Tables 19, 22, 23, and 26, respectively, for the same W values. The b'_3 and c'_3 input values used for each of the nine W values are approximately equal to the Y_5 and Z_5 coordinates which represent the center for the four points B1, B4, C1, and C4, using the same above tables. (However, the actual input values for b'_3 and c'_3 are taken from Figures 20 through 28). The definitions for a'_3, b'_3, and c'_3 are the same as those given in Table 2 for a_n, b_n, and c_n, respectively.
(X'_4, Y'_4, Z'_4)	FRONT SURFACE OF THE SINGLE DETECTOR LENS--The origin of this axis system is on the X'_3-axis and at the apex of the spherical front lens surface. The center of curvature of the front lens surface lies on the negative X'_4 axis.
(X'_5, Y'_5, Z'_5)	SECOND SURFACE OF THE SINGLE DETECTOR LENS--The second surface is a plane surface and the detector is emersed in optical contact with it. For each family of rays from a single starting point on the grating, the origin of the (X'_5, Y'_5, Z'_5) axis system is linearly transformed along the X'_4 axis by the computer until a best focus is obtained on the Y'_5-Z'_5 plane.

Table 37. Five Ray Starting Points on Grating Ruled Surface that are used to Ray-Trace Detector Foreoptics

Starting Points	X'_o	Y'_o	Z'_o
G1	0	1.38	-1.59
G2	0	1.38	1.59
G3	0	-1.38	-1.59
G4	0	-1.38	1.59
G5	0	0	0

Table 38. Dimensional Parameters for the Axis System used to Ray-Trace the Detector Foreoptics

Axis Subscripts	a'	b'	c'	α'	β'	γ'
1	0	0	0	-26°	0	0
2	9.0	0	0	0	0	0
3	See Table 39	See Table 39	See Table 39	0	0	0
4	See Table 39	0	0	0	0	0
5	Determined by Automatic Focus	0	0	0	0	0

a. The spectral images of the main entrance slit formed on the spectral image surface are plotted in Figures 20 through 28 for each of the nine W values, respectively. All data for these figures is taken from the monochromator spectral image characteristics, Tables 19 through 26, for starting points B1, B2, B3, B4, C1, C2, C3, and C4. The centroid Y_5 and centroid Z_5 image locations for each of the above eight starting points is shown by the heavy dots in Figures 20 through 28. The solid lines connecting the dots detail the shape of the main entrance slit image for each of the nine W values. If one compares the spectral image produced by the second entrance slit by plotting the centroid Y_5 and centroid Z_5 values for D1, D2, D3, D4, E1, E2, E3, and E4 starting points from Tables 27 through 34, respectively, it is found they also match the spectral images for the main slit within .002 inch for all wavelengths except 6.0 μ, where the mismatch is only .004 inch between E4 and C4. This is an unexpectedly good match for the spectral images of these two entrance slits.

Figure 29 is a composite plot of the spectral images for all nine W values. It shows the plots from Figures 20 through 28 normalized about the starting point C2 vicinity for all values.

b. Figures 20 through 28 suggest that it may be desirable to use different size aperture stops for the detector foreoptics in different wavelength regions. Following this suggestion, the experimenters decided to use three different aperture stop sizes, which are defined thus:

1. One aperture stop will match the 4.3 μ spectral image as near as practical, and that aperture stop size will be used for all foreoptics from 3.7 μ to 4.65 μ.

2. A second aperture stop will match the 5.0 μ spectral image as near as practical and that aperture stop size will be used for all foreoptics from 4.65 μ to 5.5 μ.

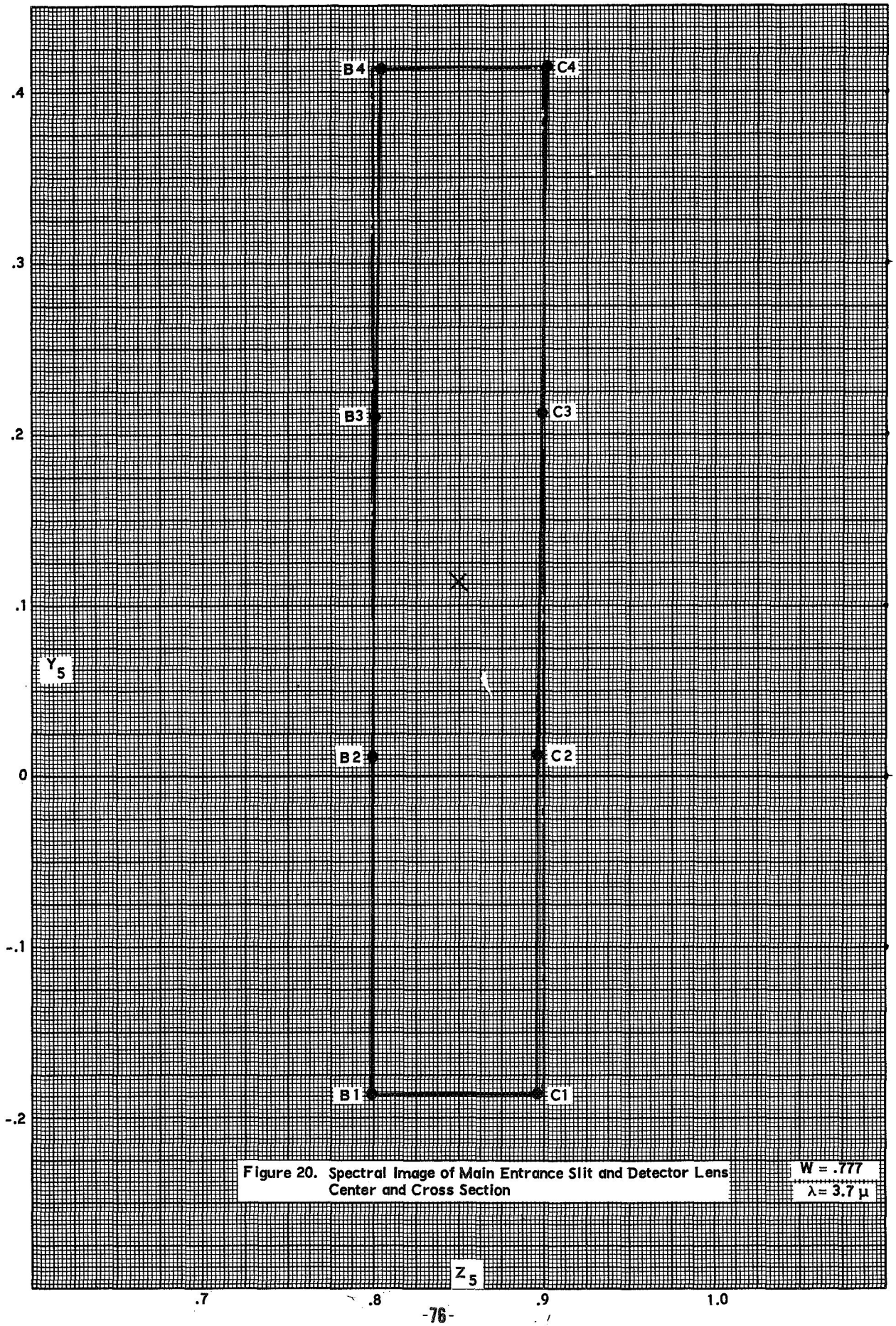

Figure 20. Spectral Image of Main Entrance Slit and Detector Lens Center and Cross Section

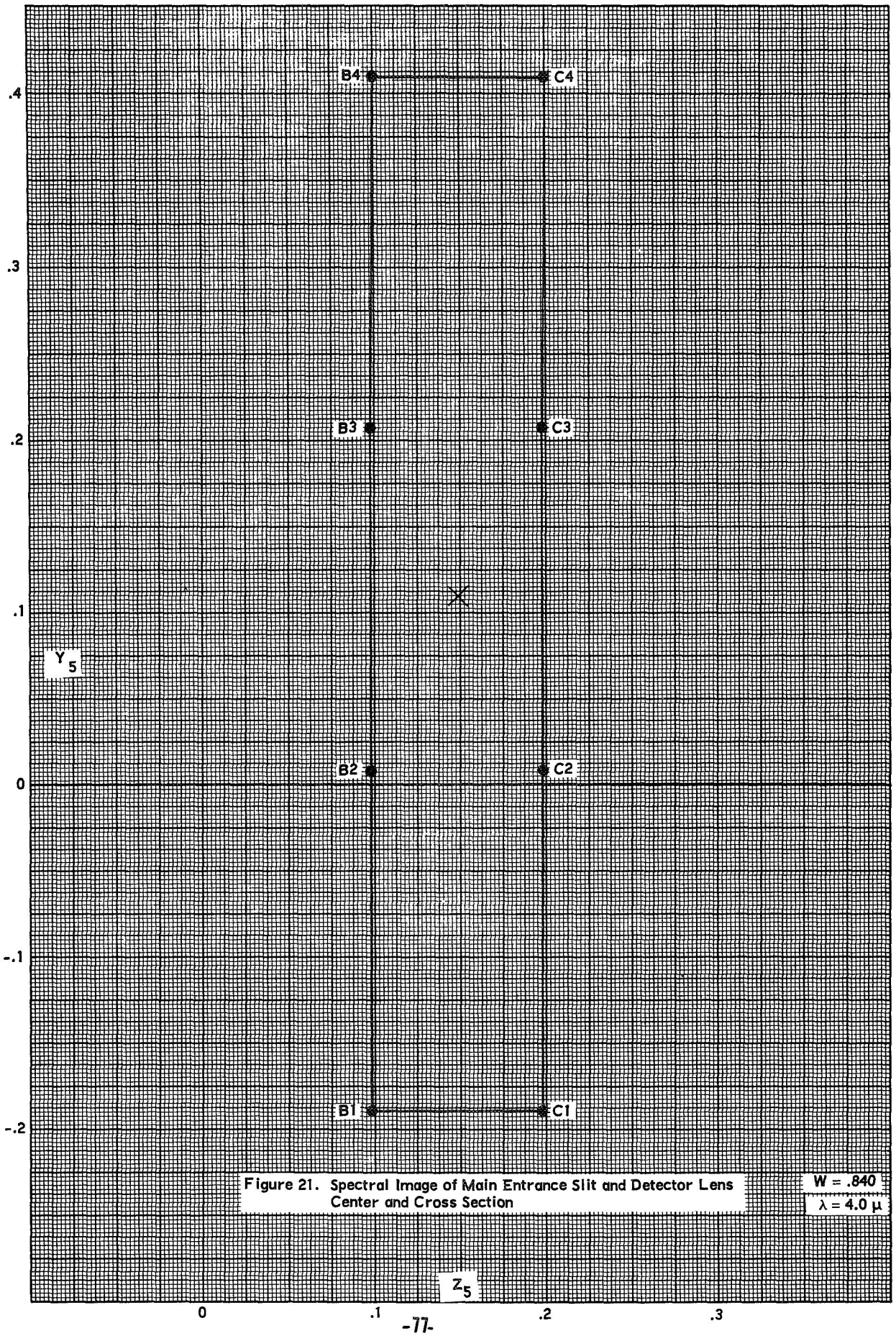

Figure 21. Spectral Image of Main Entrance Slit and Detector Lens Center and Cross Section

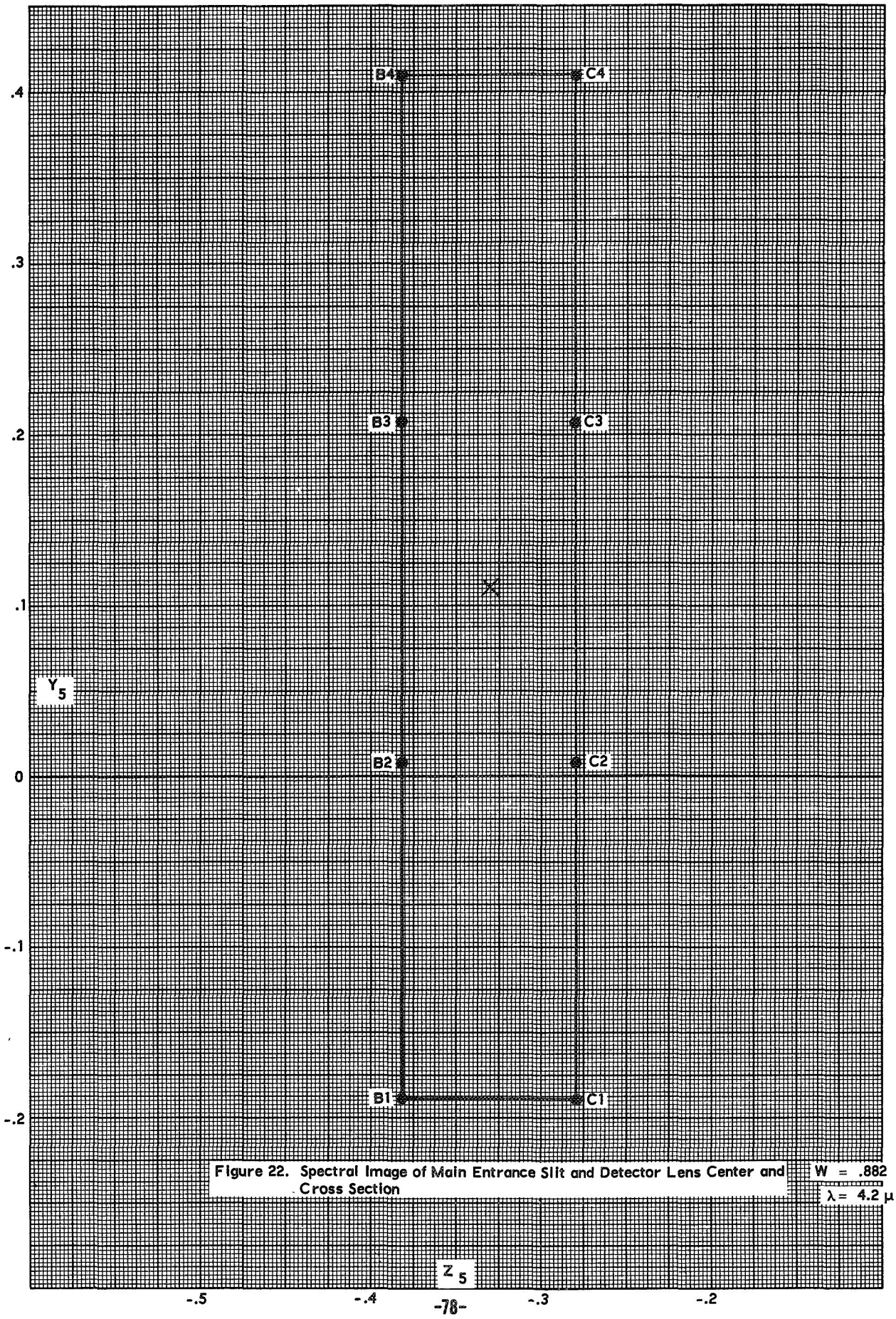

Figure 22. Spectral Image of Main Entrance Slit and Detector Lens Center and Cross Section

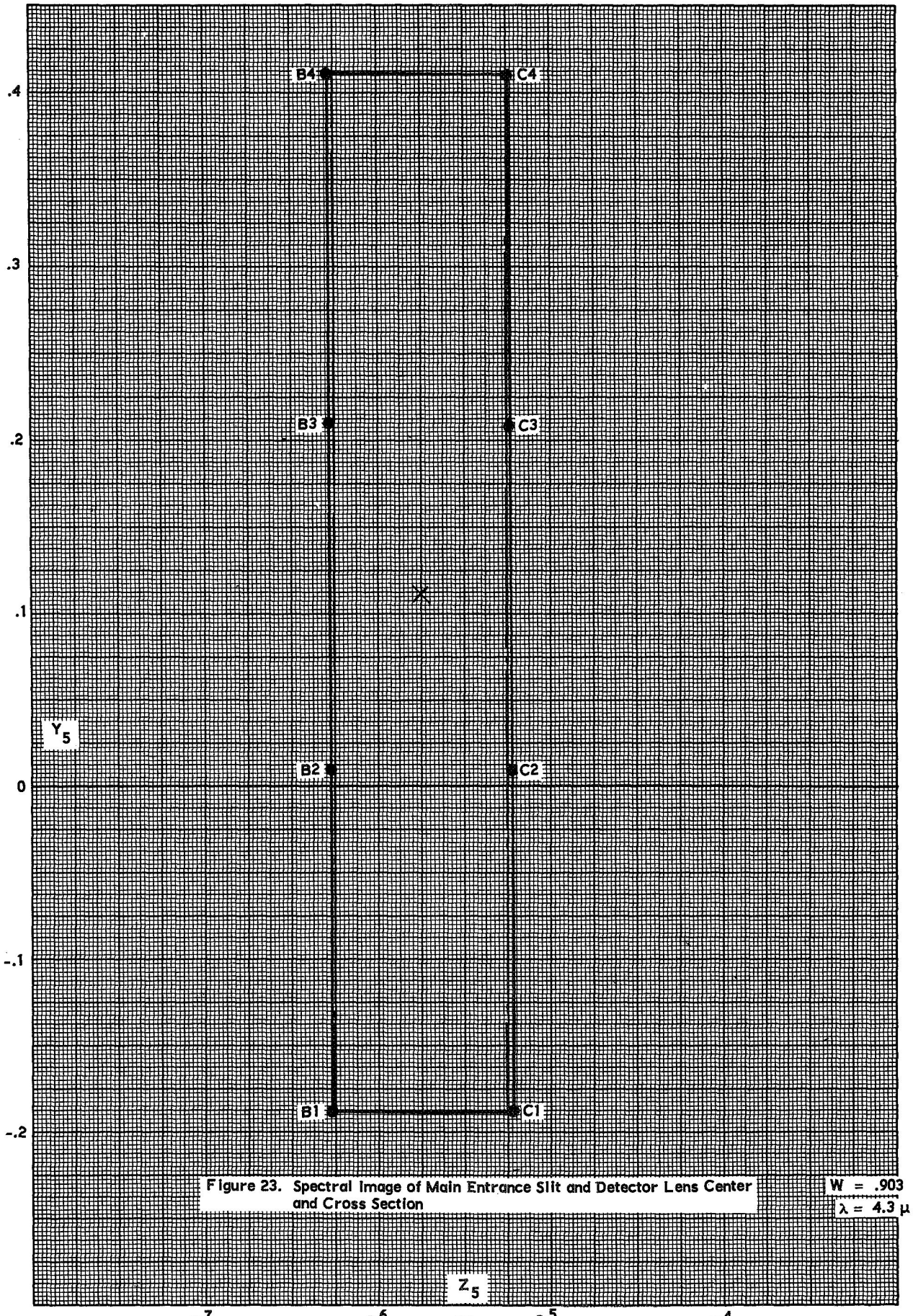

Figure 23. Spectral Image of Main Entrance Slit and Detector Lens Center and Cross Section

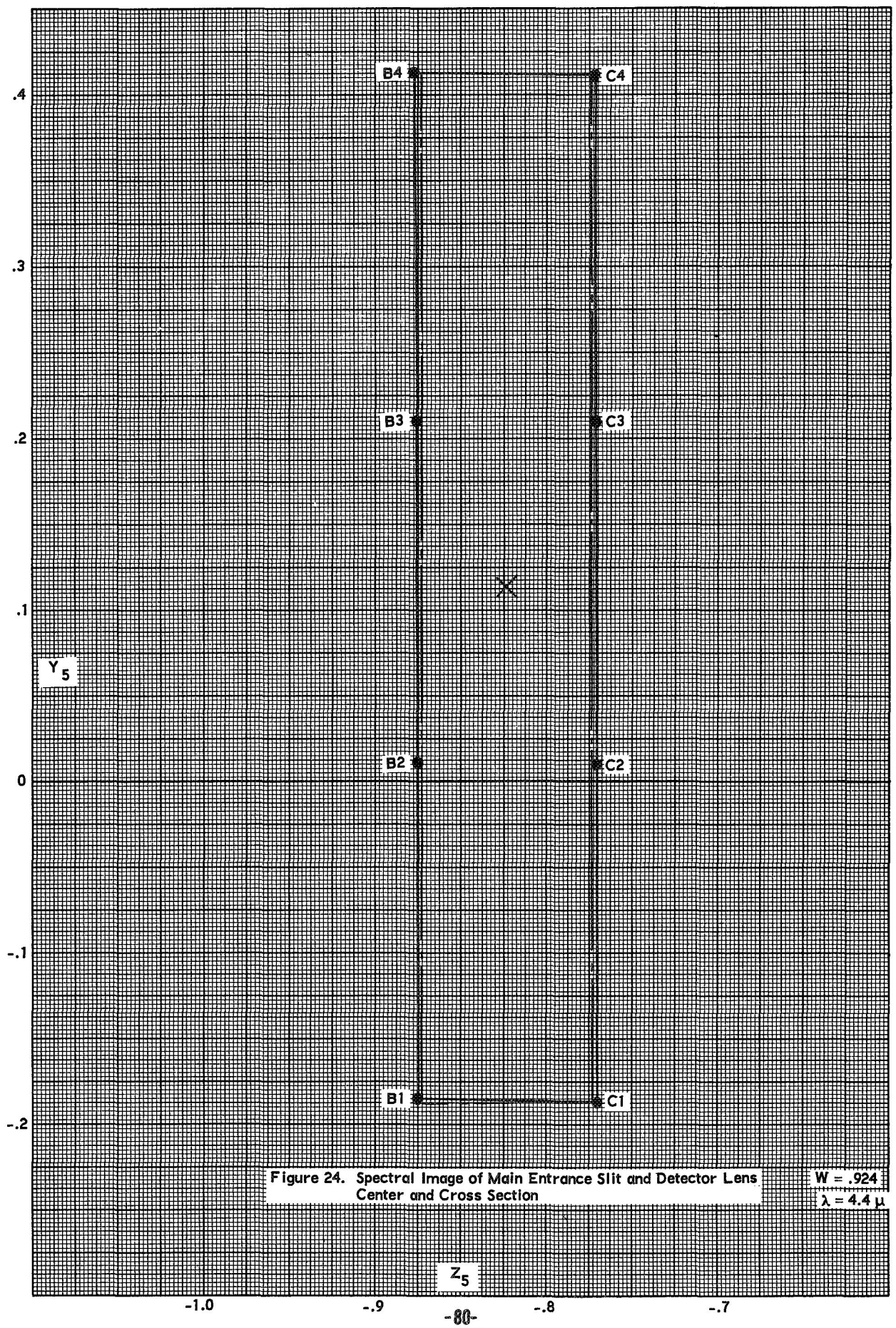

Figure 24. Spectral Image of Main Entrance Slit and Detector Lens Center and Cross Section

W = .924
$\lambda = 4.4\ \mu$

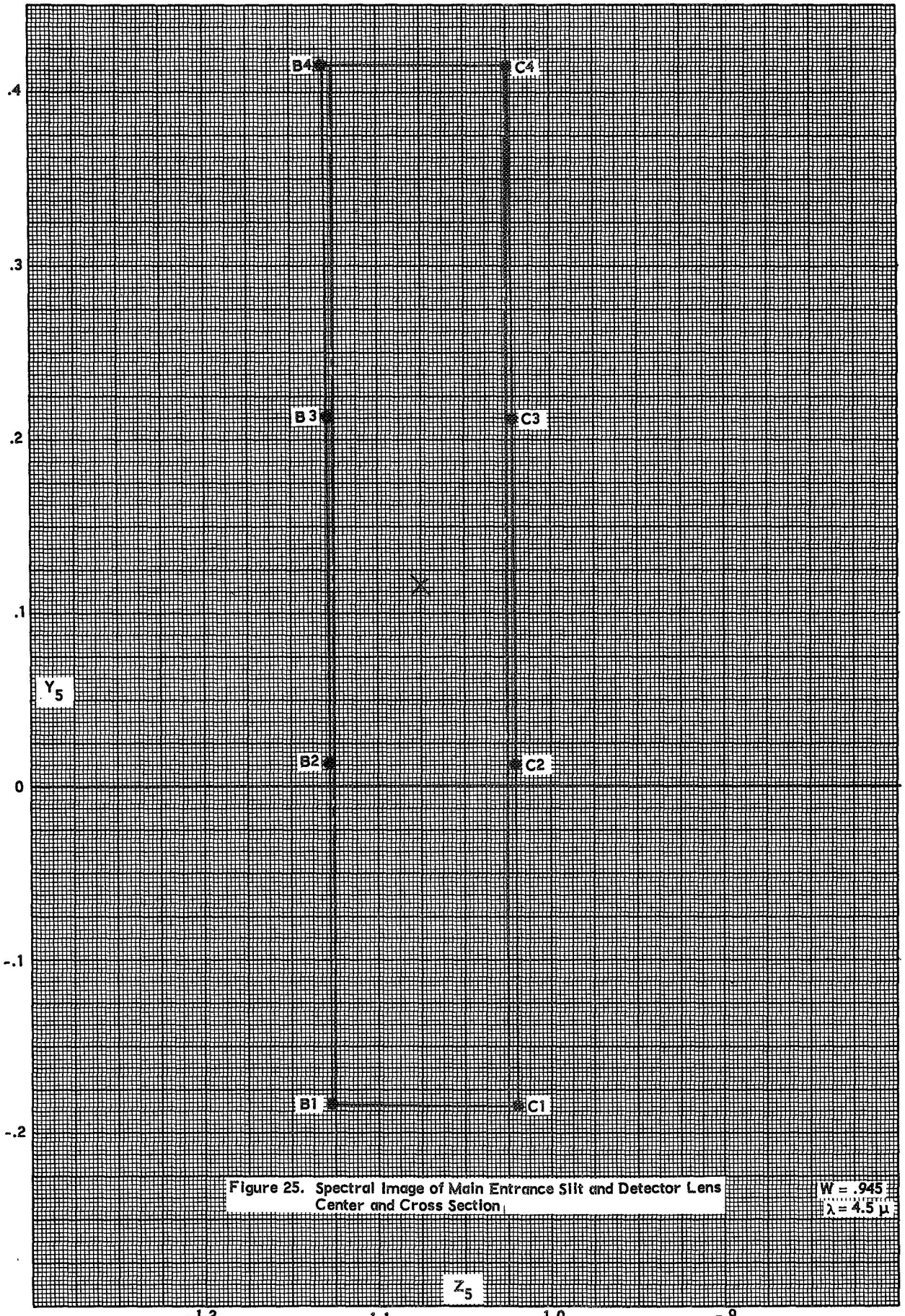

Figure 25. Spectral Image of Main Entrance Slit and Detector Lens Center and Cross Section

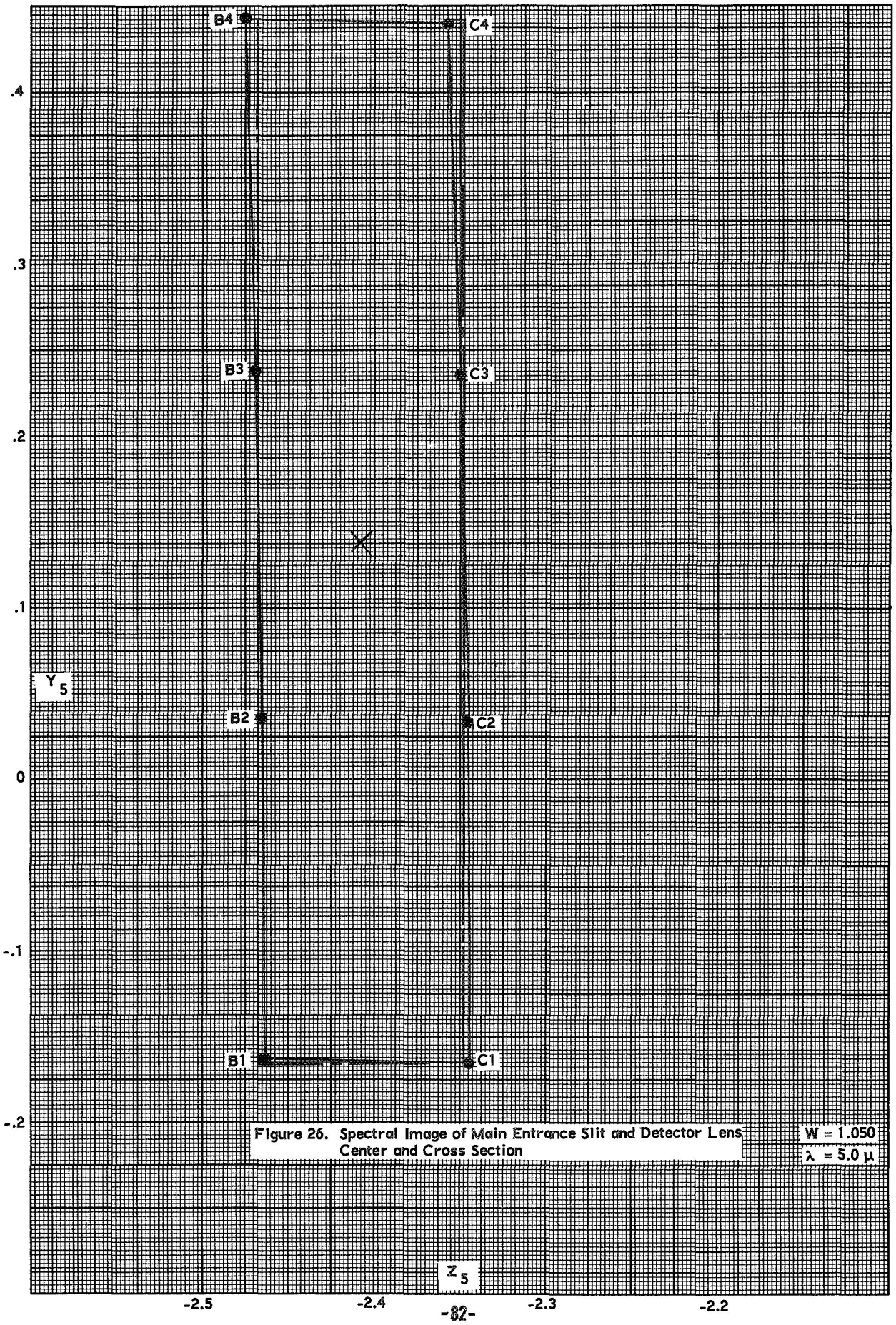

Figure 26. Spectral Image of Main Entrance Slit and Detector Lens Center and Cross Section

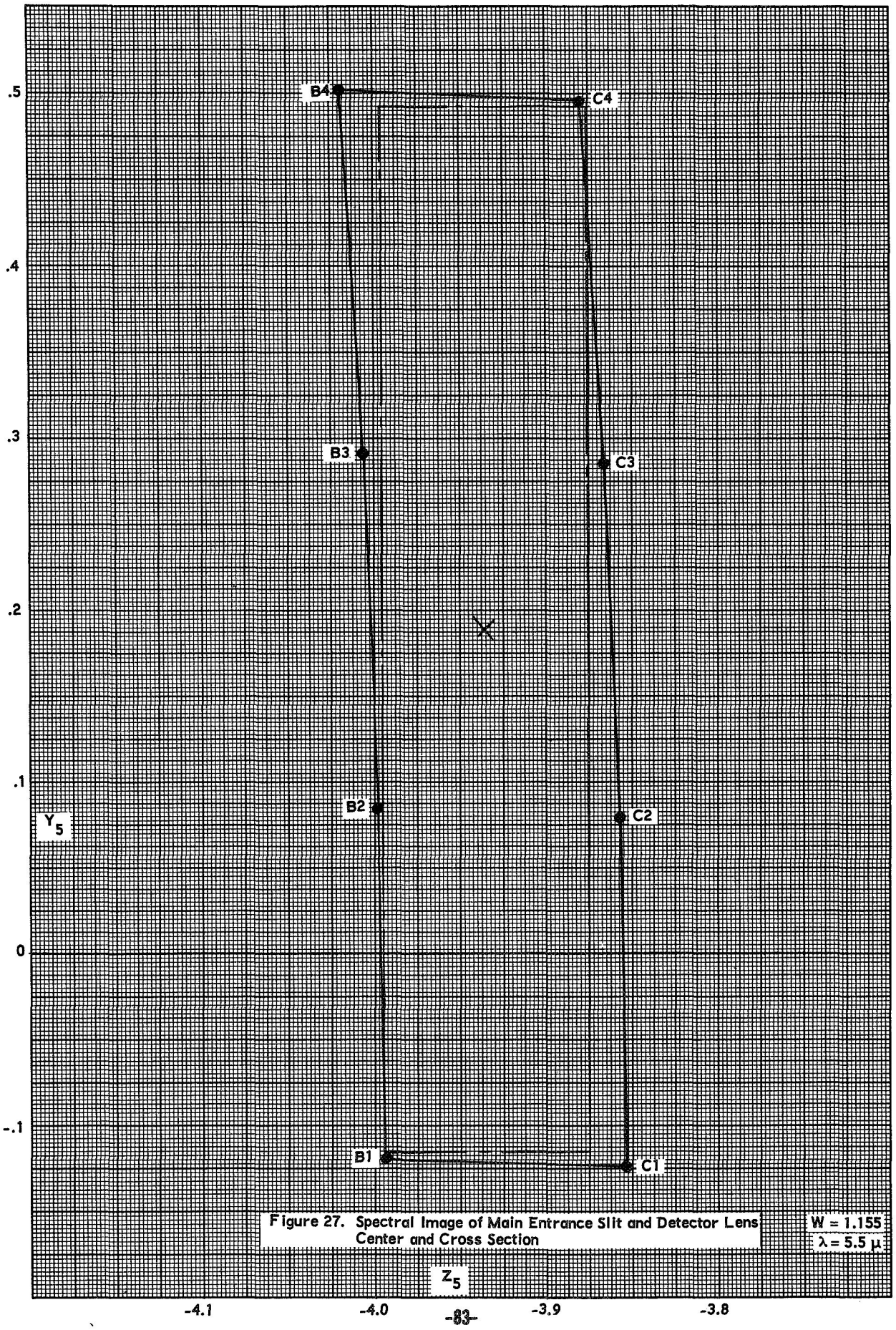

Figure 27. Spectral Image of Main Entrance Slit and Detector Lens Center and Cross Section

W = 1.155
λ = 5.5 μ

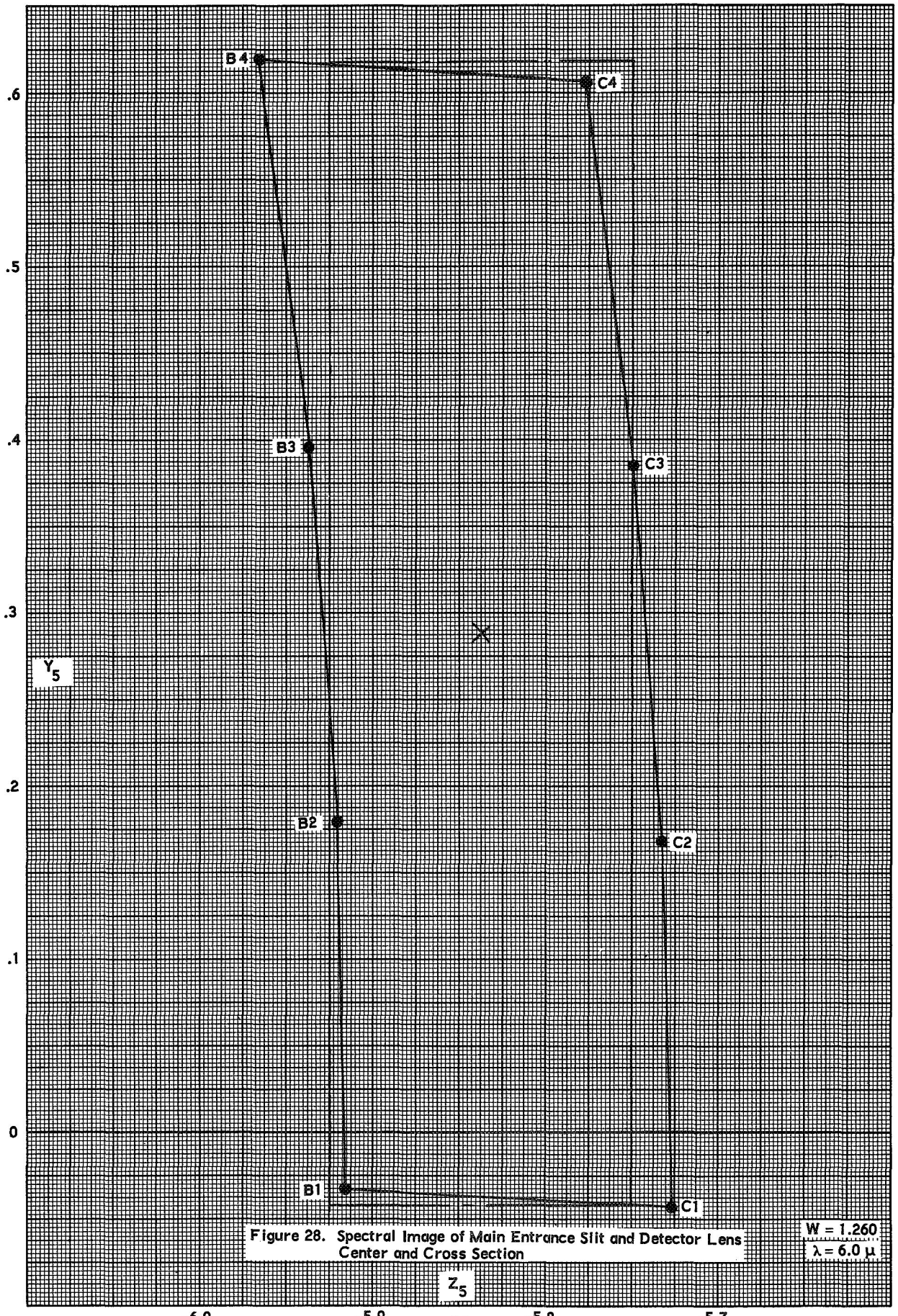

Figure 28. Spectral Image of Main Entrance Slit and Detector Lens Center and Cross Section

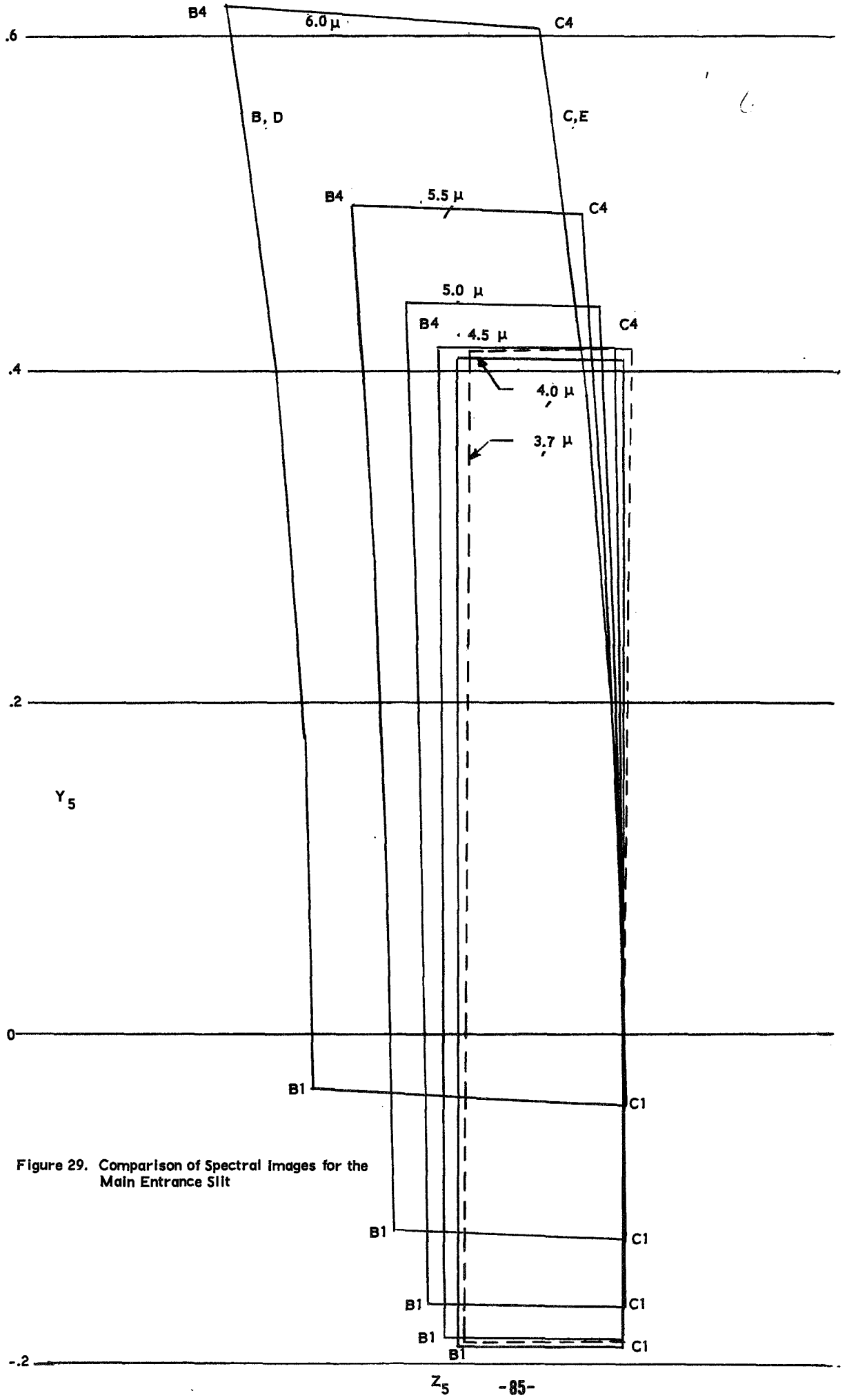

Figure 29. Comparison of Spectral Images for the Main Entrance Slit

3. A third aperture stop will match the 6.0 μ spectral image as near as practical and that aperture stop size will be used for all foreoptics from 5.5 μ to 6.0 μ.

Three aperture stop templates were developed which gave a best-fit for the 4.3 μ, 5,0 μ, and 6.0 μ spectral images shown in Figures 23, 26, and 28, respectively. These three templates are shown in Figure 30. They are rectangular and have the following overall dimensions:

Width	Height	
.1 in.	x .6 in.	for 3.7, 4.0, 4.2, 4.3, 4.4, and 4.5 μ
.12 in.	x .607 in.	for 5.0 and 5.5 μ
.175 in.	x .660 in.	for 6.0 μ

These three aperture stop templates were positioned over the graphs of the appropriate spectral images in Figures 20 through 28, and the best match found. In all cases, the template long edges were kept parallel with the Y_5-axis. The dash-dot lines on Figures 20 through 28 show the final rectangular template locations relative to the spectral images.

c. The X mark is at the true center of each template, and it was directly transferred to the matched spectral image. These X marks on Figures 20 through 28 then give the best Y_3' and Z_3' coordinates for the optical center lines of the nine detector foreoptical systems to be ray-traced.

The procedures that have just been outlined for determining the aperture stops of the detector foreoptics were used to develop Table 39, which accurately defines the best locations of the nine foreoptical lens systems to be ray-traced. The b_3' values are equal to the Y_5 coordinates of the X mark in Figures 20 through 28, plus 2.0 inches. The 2.0-inch amount is the b_5 dimensional parameter from the monochromator ray trace. The c_3' values are equal to the Z_5 coordinates from Figures 20 through 28. The a_3' values are roughly equal to the average of the a_5 values for starting points B1, B4, C1, and C4 listed

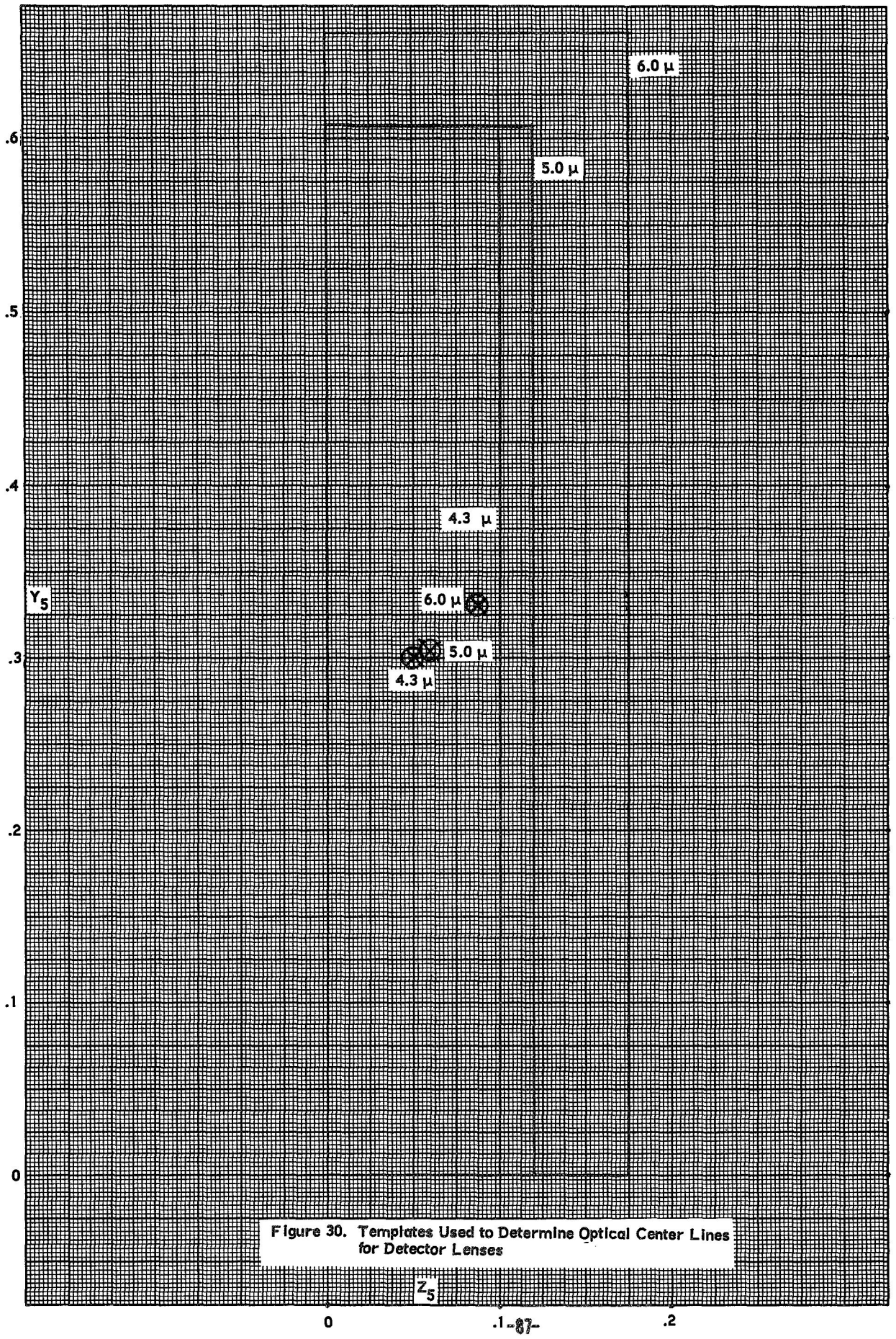

Figure 30. Templates Used to Determine Optical Center Lines for Detector Lenses

W	λ 210 L/MM Grating	Location of Center of Detector Foreoptics Aperture Stop Relative to the (X_2', Y_2', Z_2') Axis System			Aperture Stop Size	a_4'	Front Lens Location	Four Corner Points of Detection Foreoptic Aperture Stop								Index of Refraction of Germanium Lens
								1		2		3		4		
		a_3'	b_3'	c_3'	Width x Height		$a_3' - a_4'$	Y_3'	Z_3'	Y_3'	Z_3'	Y_3'	Z_3'	Y_3'	Z_3'	
.777	3.7	-10.439	2.114	.849	.1 x .6	.083	-10.356	.3	.05	.3	-.05	-.3	.05	-.3	-.05	4.0290
.840	4.0	-10.429	2.110	.148	.1 x .6	.083	-10.346	.3	.05	.3	-.05	-.3	.05	-.3	-.05	4.0250
.882	4.2	-10.442	2.111	- .331	.1 x .6	.083	-10.359	.3	.05	.3	-.05	-.3	.05	-.3	-.05	4.0225
.903	4.3	-10.454	2.111	- .575	.1 x .6	.083	-10.371	.3	.05	.3	-.05	-.3	.05	-.3	-.05	4.0215
.924	4.4	-10.473	2.113	- .824	.1 x .6	.083	-10.390	.3	.05	.3	-.05	-.3	.05	-.3	-.05	4.0205
.945	4.5	-10.497	2.116	-1.075	.1 x .6	.083	-10.414	.3	.05	.3	-.05	-.3	.05	-.3	-.05	4.0198
1.050	5.0	-10.714	2.138	-2.408	.12 x .607	.086	-10.631	.303	.06	.303	-.06	-.303	.06	-.303	-.06	4.0160
1.155	5.5	-11.166	2.189	-3.936	.12 x .607	.086	-11.083	.303	.06	.303	-.06	-.303	.06	-.303	-.06	4.0130
1.260	6.0	-12.130	2.288	-5.837	.175 x .660	.107	-12.047	.330	.088	.330	-.088	-.330	.088	-.330	-.088	4.0110

Table 39. Location of Aperture Stops Relative to (X_2', Y_2', Z_2') Axis System, Aperture Stop Size, and Index of Refraction of Detector Lens.

in Tables 19, 22, 23, and 26, respectively. The a_4' values represent the axial distance along the X_3'-axis between the apex of the front lens at the origin of the (X_4', Y_4', Z_4') axis system and the four rectangular corner points of the front lens surface which lies in the Y_3'-Z_3' plane. The a_4' distances were obtained by a ray-trace procedure, assuming a .6-inch radius spherical front lens surface.

Figure 31 shows a plan view of the locations of the nine ray-traced detector lenses relative to the spectral image surface. This plot shows, also, the spectral lines created by the spectral images of points B1, B2, C1, and C2. It also shows the detector lens reference line upon which the apexes of the front lens surface of all detector lenses should lie. The a_5' coordinates of this detector lens reference line are given in Table 39 in the column headed a_3'-a_4'.

2. DETECTOR LOCATION

In ray tracing each family of 25 rays from one of the five starting points on the grating, the computer automatically moves the Y_5'-Z_5' plane which supports the detector along the X_4' axis until a best focus is found. The criterian for a best-focus in this case is when the sum of the least square $(Y_5'^2 + Z_5'^2)$ about the combined Y_5', Z_5' centroid is a minimum for all 25 rays. This gives an image which is approximately the minimum circle of confusion.

The upper half of Tables 40 through 48 describe the characteristics of the five images on each of the nine different detectors analyzed. Each of these Tables has the same format, but represents a different W value and resultant spectral image surface location. The a_5' column gives the required thickness of the lens for a best focus for each of the five starting points on the grating G1, G2, G3, G4, and G5. Studying the a_5' values for all five starting points and for all nine W values, it is seen that each of the five image points requires different lens thicknesses. However, the lens thickness does not differ more than .004 inch for the G1, G2, G3, and G4 starting points at all W values. The G5 (center point) requires a longer lens than the other four points. However, its image is well inside the detector boundaries and its focus is of no importance.

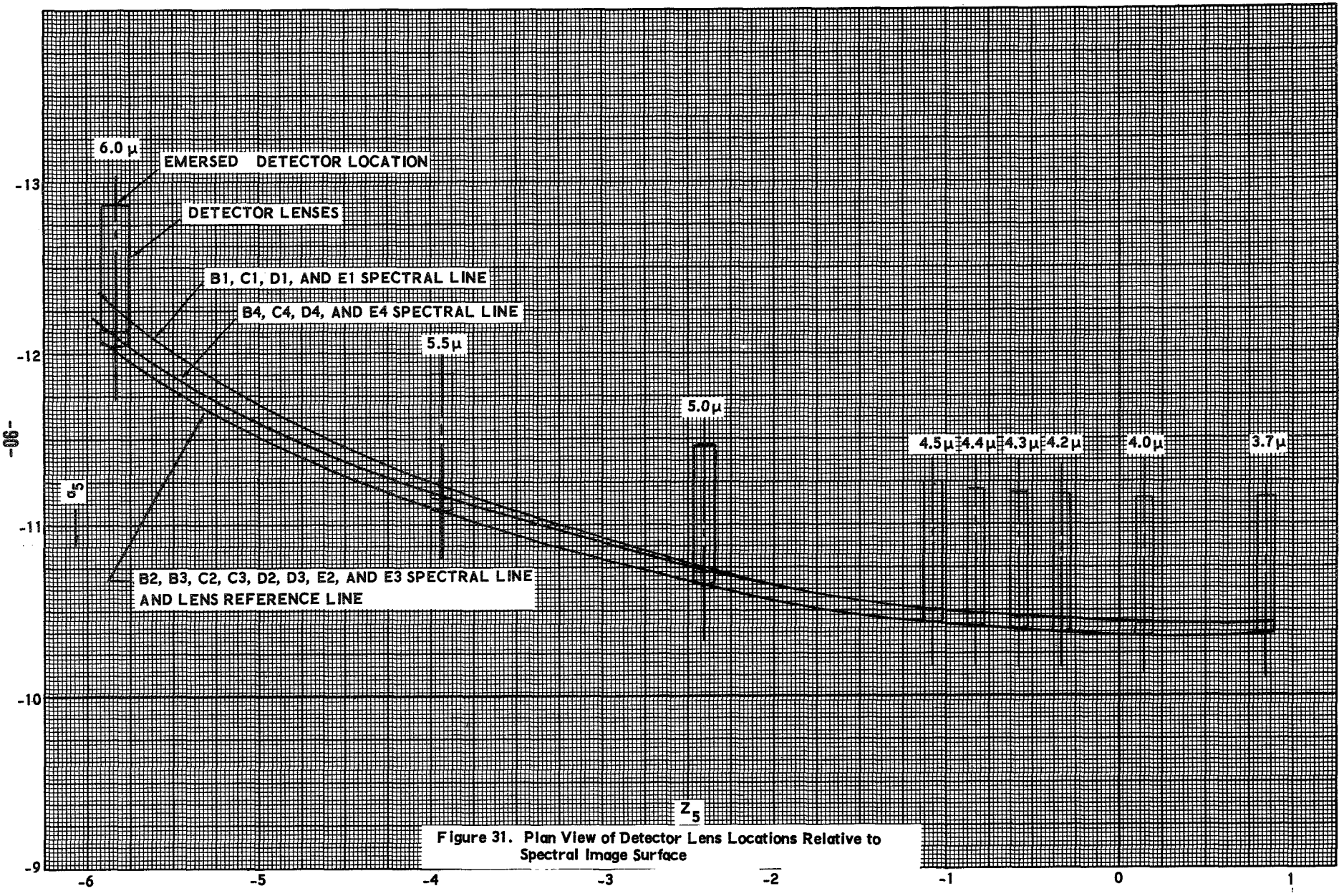

Figure 31. Plan View of Detector Lens Locations Relative to Spectral Image Surface

Table 40. Diffraction Grating Image Characteristics on Emersed Detector, $W = .777$, $\lambda = 3.7\ \mu$ for 210 L/MM Grating

Starting Points on Grating	a_5' Automatic Focus	Centroid Y_5'	$\Delta Y_5'$	80% $\Delta Y_5'$	Centroid Z_5'	$\Delta Z_5'$	80% $\Delta Z_5'$
G1	-.7890	-.0229	.0030	.0021	-.0260	.0015	.0008
G2	-.7907	-.0180	.0029	.0020	.0301	.0016	.0009
G3	-.7871	.0270	.0033	.0023	-.0262	.0017	.0009
G4	-.7869	.0318	.0038	.0028	.0294	.0021	.0011
G5	-.7936	.0039	.0017	.0016	.0016	.0007	.0004

Average a_5' for G1, G2, G3, and G4 = -.7884

Figure 32 is a composite spot diagram for this Table.

Nominal value for a_5' used in composite spot diagram = -.789.

Table 41. Diffraction Grating Image Characteristics on Emersed Detector, $W = .840$, $\lambda = 4.0\ \mu$ for 210 L/MM Grating

Starting Points on Grating	a_5' Automatic Focus	Centroid Y_5'	$\Delta Y_5'$	80% $\Delta Y_5'$	Centroid Z_5'	$\Delta Z_5'$	80% $\Delta Z_5'$
G1	-.7890	-.0231	.0031	.0022	-.0269	.0015	.0008
G2	-.7914	-.0179	.0029	.0019	.0277	.0015	.0008
G3	-.7872	.0269	.0033	.0023	-.0269	.0018	.0010
G4	-.7875	.0320	.0038	.0028	.0273	.0020	.0011
G5	-.7938	.0039	.0017	.0016	.0003	.0007	.0004

Average a_5' for G1, G2, G3, G4 = -.7888

Figure 33 is a composite spot diagram for this Table.

Nominal value for a_5' used in composite spot diagram = -.789

Table 42. Diffraction Grating Image Characteristics on Emersed Detector, $W = .882$, $\lambda = 4.2\ \mu$ for 210 L/MM Grating

Starting Points on Grating	a_5' Automatic Focus	Centroid Y_5'	$\Delta Y_5'$	80% $\Delta Y_5'$	Centroid Z_5'	$\Delta Z_5'$	80% $\Delta Z_5'$
G1	-.7890	-.0232	.0031	.0022	-.0275	.0016	.0008
G2	-.7919	-.0179	.0029	.0019	.0260	.0015	.0008
G3	-.7873	.0268	.0033	.0023	-.0272	.0018	.0010
G4	-.7880	.0322	.0038	.0028	.0257	.0019	.0011
G5	-.7940	.0039	.0017	.0016	-.0006	.0007	.0004

Average a_5' for G1, G2, G3, and G4 = -.7891

Figure 34 is a composite spot diagram for this Table.

Nominal value for a_5' used in composite spot diagram = -.789.

Table 43. Diffraction Grating Image Characteristics on Emersed Detector, $W = .903$, $\lambda = 4.3\ \mu$ for 210 L/MM Grating

Starting Points on Grating	a_5' Automatic Focus	Centroid Y_5'	$\Delta Y_5'$	80% $\Delta Y_5'$	Centroid Z_5'	$\Delta Z_5'$	80% $\Delta Z_5'$
G1	-.7890	-.0232	.0031	.0022	-.0277	.0016	.0008
G2	-.7922	-.0179	.0028	.0019	.0251	.0014	.0008
G3	-.7873	.0267	.0033	.0023	-.0274	.0018	.0010
G4	-.7882	.0322	.0038	.0028	.0249	.0019	.0011
G5	-.7940	.0039	.0017	.0016	-.0011	.0007	.0004

Average a_5' for G1, G2, G3, and G4 = -.7892

Figure 35 is a composite spot diagram for this Table.

Nominal value for a_5' used in composite spot diagram = -.789.

Table 44. Diffraction Grating Image Characteristics on Emersed Detector, $W = .924$, $\lambda = 4.4\ \mu$ for 210 L/MM Grating

Starting Points on Grating	a_5' Automatic Focus	Centroid Y_5'	$\Delta Y_5'$	80% $\Delta Y_5'$	Centroid Z_5'	$\Delta Z_5'$	80% $\Delta Z_5'$
G1	-.7890	-.0233	.0031	.0022	-.0279	.0016	.0008
G2	-.7924	-.0178	.0028	.0019	.0241	.0014	.0008
G3	-.7874	.0266	.0033	.0023	-.0275	.0018	.0010
G4	-.7884	.0323	.0038	.0028	.0241	.0018	.0010
G5	-.7941	.0039	.0017	.0016	-.0016	.0007	.0004

Average a_5' for G1, G2, G3, and G4 = -.7893

Figure 36 is a composite spot diagram for this Table.

Nominal value for a_5' used in composite spot diagram = -.789.

Table 45. Diffraction Grating Image Characteristics on Emersed Detector, $W = .945$, $\lambda = 4.5\ \mu$ for 210 L/MM Grating

Starting Points on Grating	a_5' Automatic Focus	Centroid Y_5'	$\Delta Y_5'$	80% $\Delta Y_5'$	Centroid Z_5'	$\Delta Z_5'$	80% $\Delta Z_5'$
G1	-.7890	-.0233	.0031	.0022	-.0282	.0016	.0008
G2	-.7926	-.0178	.0028	.0019	.0231	.0013	.0008
G3	-.7874	.0265	.0033	.0023	-.0276	.0018	.0010
G4	-.7885	.0323	.0038	.0028	.0232	.0018	.0010
G5	-.7941	.0039	.0017	.0015	-.0020	.0007	.0004

Average a_5' for G1, G2, G3, and G4 = -.7894

Figure 37 is a composite spot diagram for this Table.

Nominal value for a_5' used in composite spot diagram = -.789.

Table 46. Diffraction Grating Image Characteristics on Emersed Detector, $W = 1.050$, $\lambda = 5.0\ \mu$ for 210 L/MM Grating

Starting Points on Grating	a_5' Automatic Focus	Centroid Y_5'	$\Delta Y_5'$	80% $\Delta Y_5'$	Centroid Z_5'	$\Delta Z_5'$	80% $\Delta Z_5'$
G1	-.7888	-.0233	.0033	.0023	-.0288	.0018	.0008
G2	-.7935	-.0174	.0028	.0019	.0177	.0013	.0007
G3	-.7875	.0259	.0034	.0024	-.0276	.0021	.0011
G4	-.7894	.0323	.0038	.0028	.0183	.0017	.0009
G5	-.7941	.0039	.0017	.0017	-.0045	.0009	.0005

Average a_5' for G1, G2, G3, and G4 = -.7898

Figure 38 is a composite spot diagram for this Table.

Nominal value for a_5' used in composite spot diagram = -.790.

Table 47. Diffraction Grating Image Characteristics on Emersed Detector, $W = 1.155$, $\lambda = 5.5\ \mu$ for 210 L/MM Grating

Starting Points on Grating	a_5' Automatic Focus	Centroid Y_5'	$\Delta Y_5'$	80% $\Delta Y_5'$	Centroid Z_5'	$\Delta Z_5'$	80% $\Delta Z_5'$
G1	-.7889	-.0232	.0033	.0023	-.0287	.0018	.0008
G2	-.7944	-.0167	.0027	.0019	.0113	.0011	.0007
G3	-.7879	.0250	.0034	.0023	-.0267	.0021	.0011
G4	-.7902	.0320	.0037	.0027	.0124	.0013	.0010
G5	-.7942	.0038	.0017	.0012	-.0070	.0009	.0006

Average a_5' for G1, G2, G3, and G4 = -.7904

Figure 39 is a composite spot diagram for this Table.

Nominal value for a_5' used in composite spot diagram = -.790.

Table 48. Diffraction Grating Image Characteristics on Emersed Detector, $W = 1.260$, $\lambda = 6.0\ \mu$ for 210 L/MM Grating

Starting Points on Grating	a_5' Automatic Focus	Centroid Y_5'	$\Delta Y_5'$	80% $\Delta Y_5'$	Centroid Z_5'	$\Delta Z_5'$	80% $\Delta Z_5'$
G1	-.7880	-.0224	.0043	.0031	-.0273	.0026	.0011
G2	-.7935	-.0154	.0033	.0025	.0036	.0016	.0010
G3	-.7873	.02320	.0043	.0030	-.0244	.0027	.0014
G4	-.7897	.0307	.0046	.0032	.0053	.0020	.0015
G5	-.7927	.0036	.0024	.0021	-.0095	.0015	.0010

Average a_5' for G1, G2, G3, and G4 = -.7896

Figure 40 is a composite spot diagram for this Table.

Nominal value for a_5' used in composite spot diagram = -.790.

In designing the lens thickness, the back surface of each detector lens could be given a slanting surface which matches the required lens thickness at the respective G1, G2, G3, and G4 images on the detector. However, the more practical solution is to use a back surface which is perpendicular to the optical axis of the detector lens with a lens thickness equal to the average of G1, G2, G3, and G4 values.

A second ray trace was then performed for the same nine W values. Instead of using the automatic focus for the (X_5', Y_5', Z_5') axis system, a_5' was set equal to .789 inch for six W values and equal to .790 for the other three W values, as shown in Tables 40 through 48. The lens thicknesses represent a fairly good average value for the a_5' value for each detector lens.

Figures 32 through 40 are composite spot diagrams for the five image points on the Y_5'-Z_5' plane for fixed a_5' values for all nine W values. Each point image consists of 25 rays. All plots have the same scale factor which is .030 inch for the Y_5' and Z_5' half-axis lengths. These plots readily show that the detectors for the 6.0 μ end of the spectral image surface should be narrower than those used at the 3.7 μ end. The detector areas should match these grating images which are represented by the corner images to maximize radiant sensitivity and minimize stray light.

Figures 41 through 45 are expanded scale plots of G1, G2, G3, G4, and G5 for the 4.3 μ detector. For each of these, the origin of the (X_5', Y_5', Z_5') axis system was moved to correspond to centroid Y_5' and centroid Z_5' coordinates listed in Table 43 for 4.3 μ. These images are thus expanded about their true centroids. All five of these plots have the same scale, .0025 inch for the Y_5' and Z_5' half-axis length. These images look strange until it is realized that the aperture stop for the detector lens is .1-inch wide by .6-inch tall for 4.3 μ, which is a very narrow rectangle on which to spread a 5 x 5 array of points. In width, five points fall within .1 inch. However, in height, five points spread over .6 inch. So the spread of the array is six times greater vertically than horizontally.

SINGLE DETECTOR LENS--NIMS, .1X.6 SLIT, 26 DEGREE GRATING OFFSET, .777 2-9-70

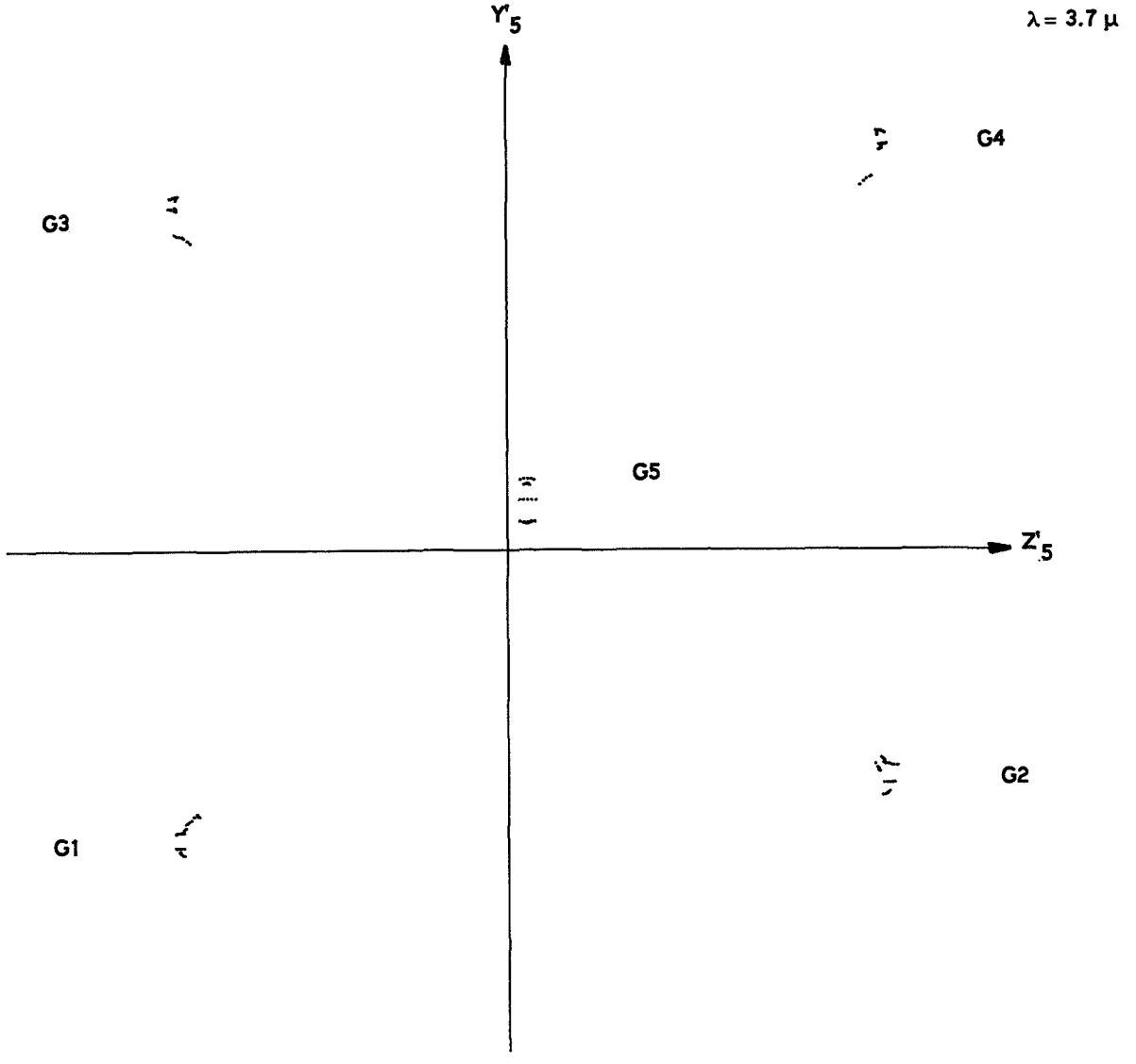

					MAX	MIN	
Z	HALF AXIS LENGTH	0.040	Z	=	0.031	-0.027	SURFACE NO.
Y	HALF AXIS LENGTH	0.040	Y	=	0.033	-0.024	5

Figure 32. 25-Ray Spot Images of the Center and Four Corners of the Diffraction Grating Formed on the Detector

(λ=3.7 μ)

SINGLE DETECTOR LENS--NIMS, .1X.6 SLIT, 26 DEGREE GRATING OFFSET, .840 2-9-70

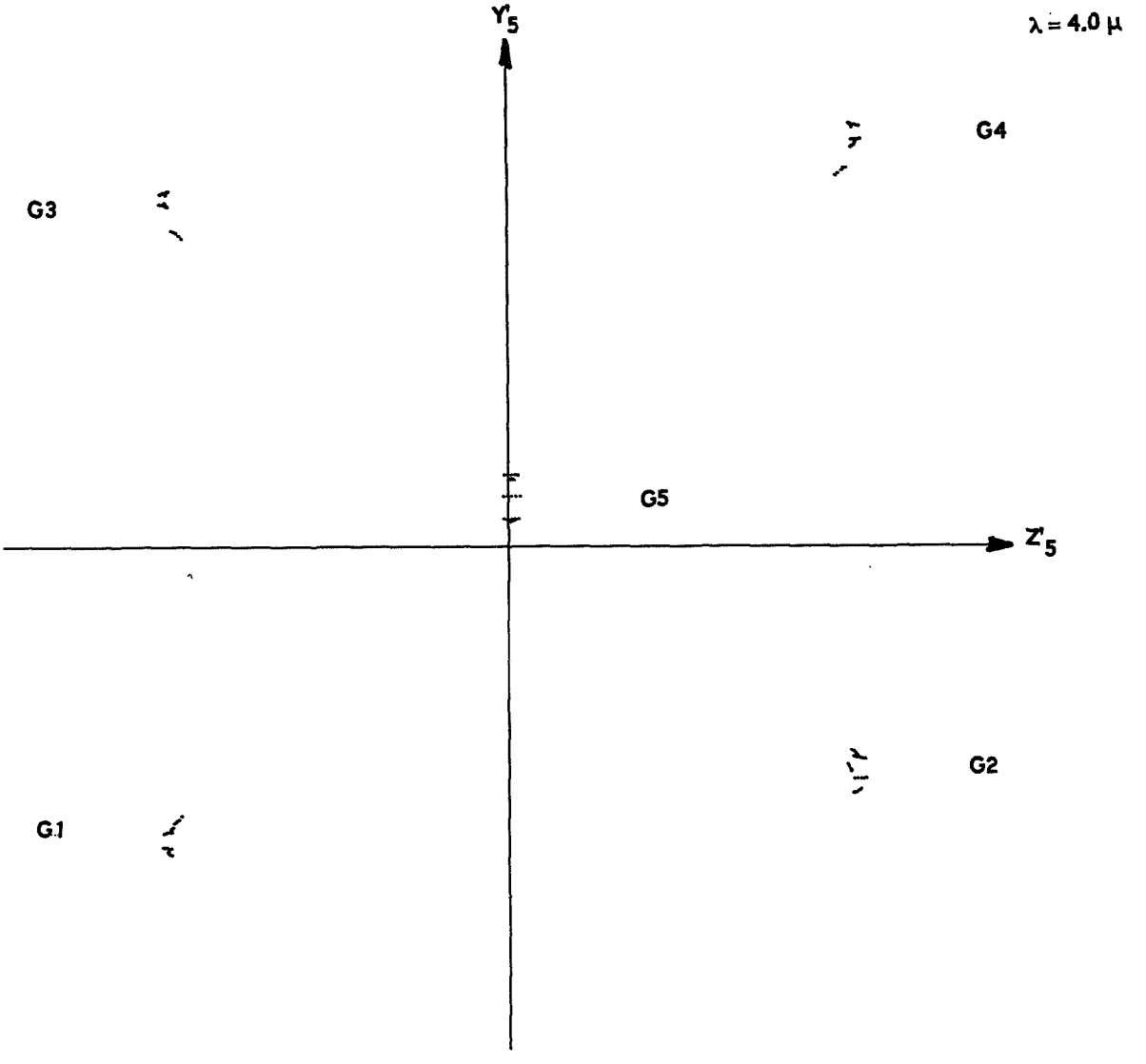

					MAX	MIN	
Z	HALF AXIS LENGTH	0.040	Z	=	0.028	-0.028	SURFACE NO.
Y	HALF AXIS LENGTH	0.040	Y	=	0.034	-0.025	5

Figure 33. 25-Ray Spot Images of the Center and Four Corners of the Diffraction Grating Formed on the Detector

(λ=4.0 μ)

SINGLE DETECTOR LENS--NIMS, .1X.6 SLIT, 26 DEGREE GRATING OFFSET, .882 2-9-70

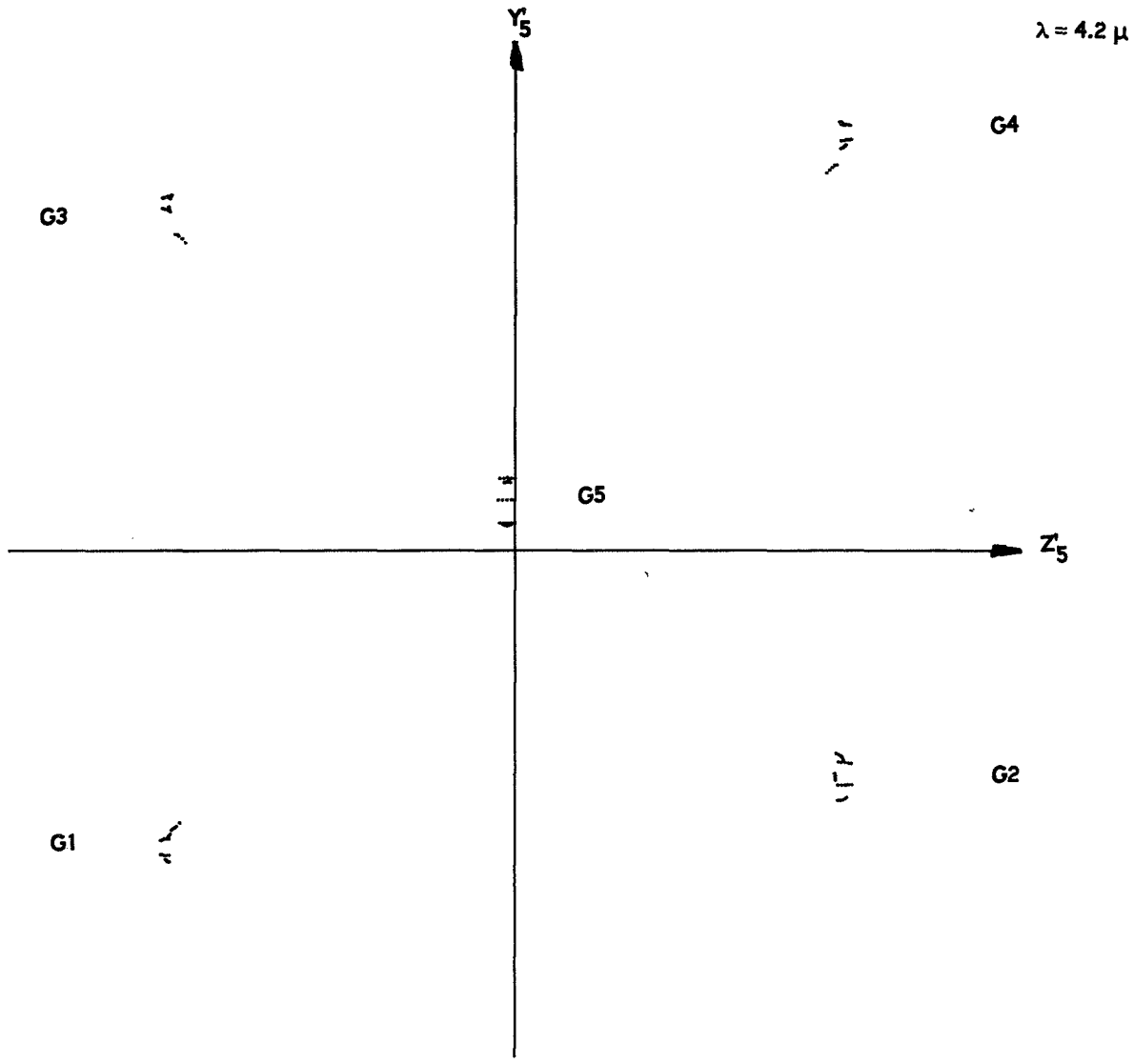

					MAX	MIN	
Z	HALF AXIS LENGTH	0.040	Z	=	0.027	-0.028	SURFACE NO.
Y	HALF AXIS LENGTH	0.040	Y	=	0.034	-0.025	5

Figure 34. 25-Ray Spot Images of the Center and Four Corners of the Diffraction Grating Formed on the Detector

(λ=4.2 μ)

SINGLE DETECTOR LENS--NIMS, .1X.6 SLIT, 26 DEGREE GRATING OFFSET, .903 2-9-70

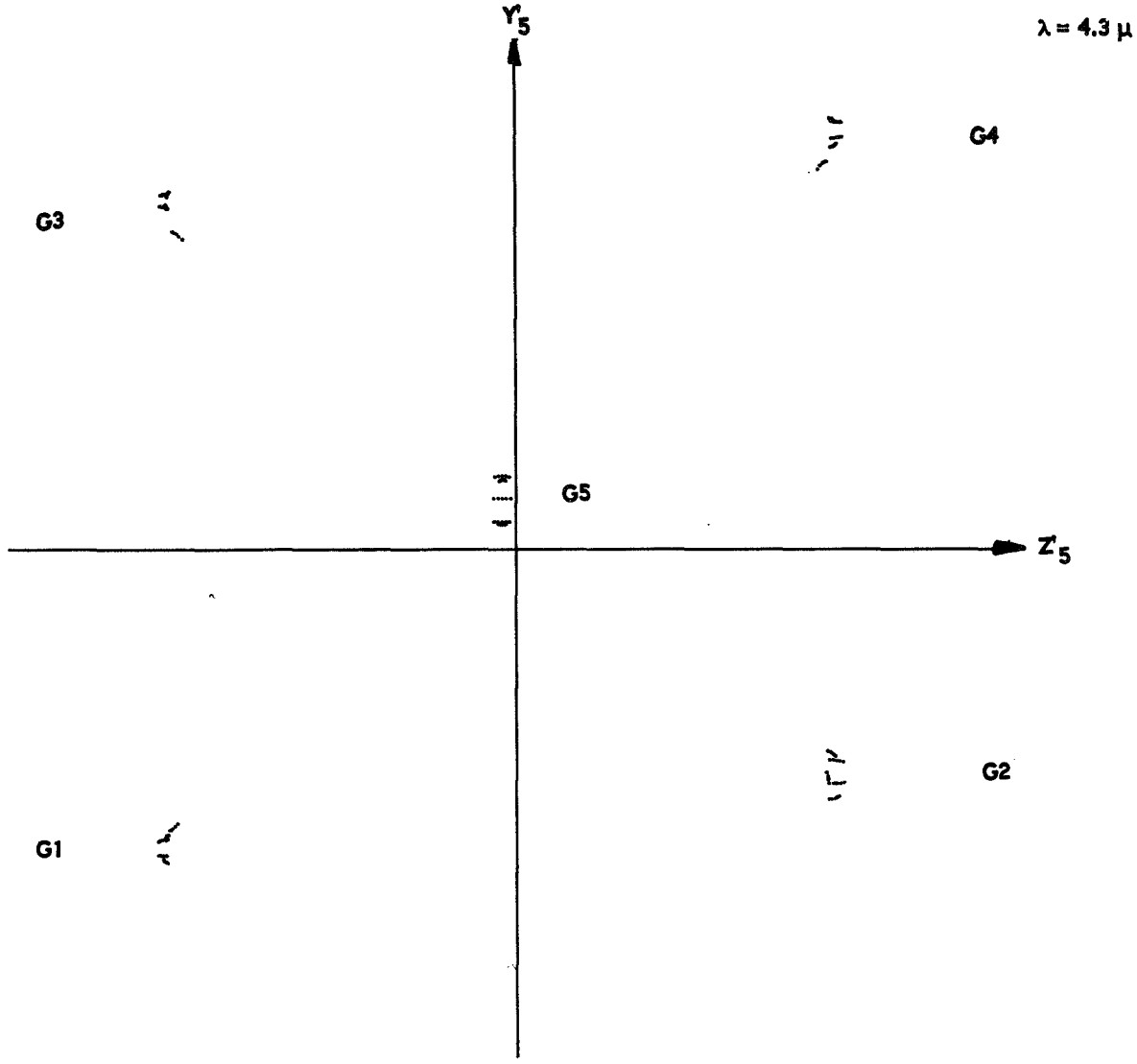

					MAX	MIN	
Z	HALF AXIS LENGTH	0.040	Z	=	0.026	-0.028	SURFACE NO.
Y	HALF AXIS LENGTH	0.040	Y	=	0.034	-0.025	5

Figure 35. 25-Ray Spot Images of the Center and Four Corners of the Diffractior Grating Formed on the Detector

(λ=4.3 μ)

SINGLE DETECTOR LENS--NIMS, .1X.6 SLIT, 26 DEGREE GRATING OFFSET, .924 2-9-70

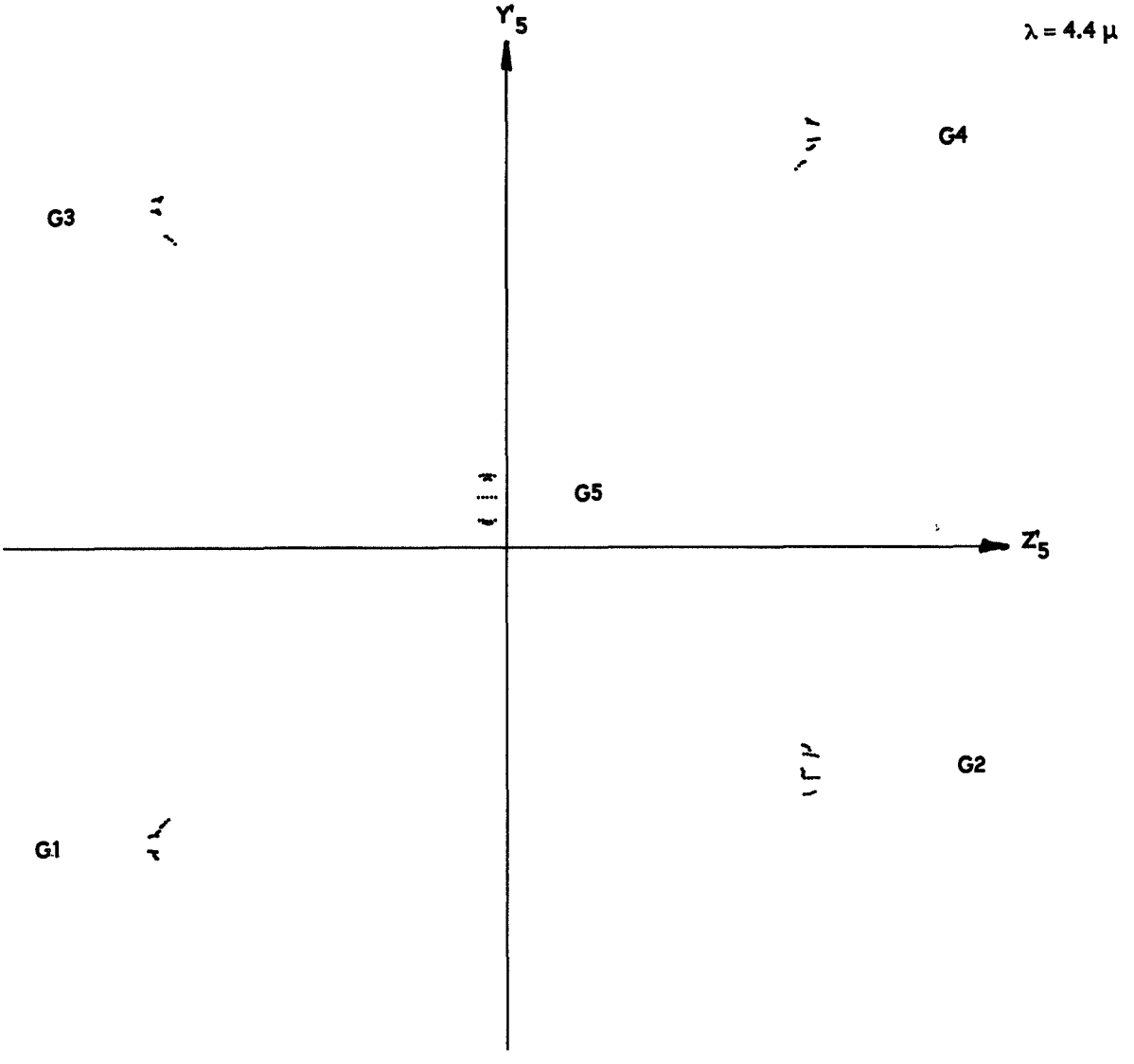

					MAX	MIN	
Z	HALF AXIS LENGTH	0.040	Z	=	0.025	-0.029	SURFACE NO.
Y	HALF AXIS LENGTH	0.040	Y	=	0.034	-0.025	5

Figure 36. 25-Ray Spot Images of the Center and Four Corners of the Diffraction Grating Formed on the Detector

(λ=4.4 μ)

SINGLE DETECTOR LENS--NIMS, .1X.6 SLIT, 26 DEGREE GRATING OFFSET, .945 2-9-70

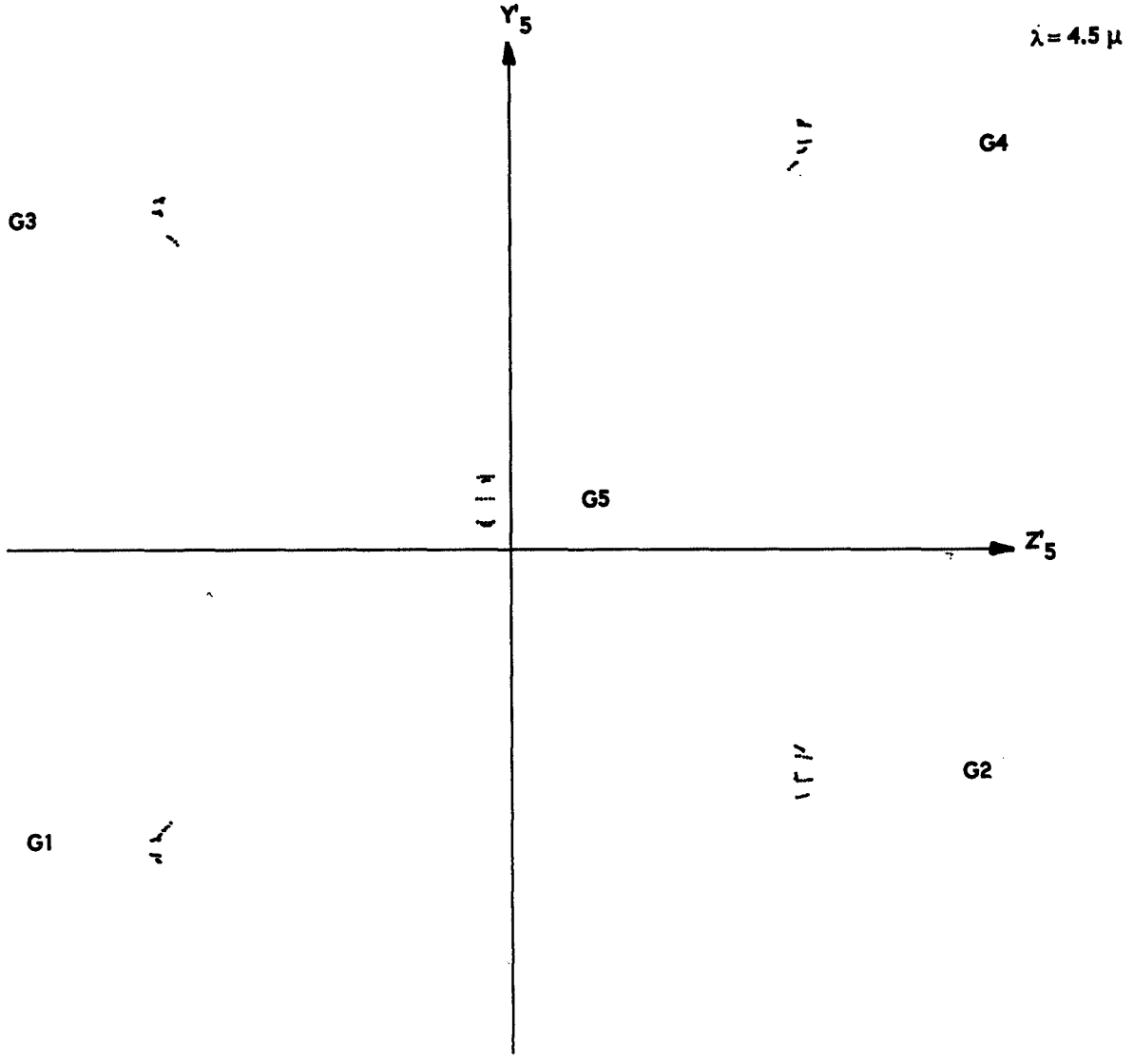

					MAX	MIN	
Z	HALF AXIS LENGTH	0.040	Z	=	0.024	-0.029	SURFACE NO.
Y	HALF AXIS LENGTH	0.040	Y	=	0.034	-0.025	5

Figure 37. 25-Ray Spot Images of the Center and Four Corners of the Diffraction Grating Formed on the Detector

(λ=4.5 μ)

SINGLE DETECTOR LENS--NIMS, .1X.6 SLIT, 26 DEGREE GRATING OFFSET, 1.050 2-9-70

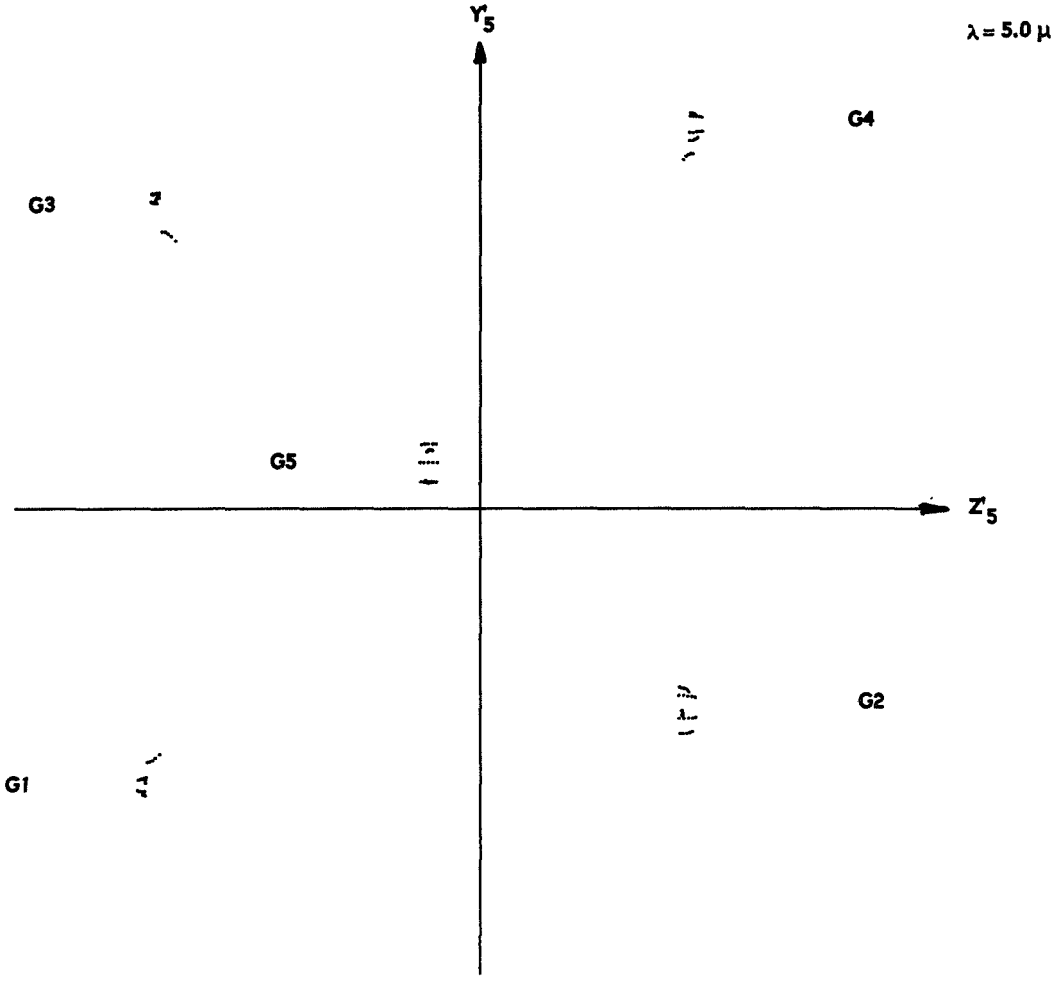

					MAX	MIN	
Z	HALF AXIS LENGTH	0.040	Z	=	0.019	-0.029	SURFACE NO.
Y	HALF AXIS LENGTH	0.040	Y	=	0.034	-0.025	5

Figure 38. 25-Ray Spot Images of the Center and Four Corners of the Diffraction Grating Formed on the Detector

(λ=5.0 μ)

SINGLE DETECTOR LENS--NIMS, .1X.6 SLIT, 26 DEGREE GRATING OFFSET, 1.155 2-9-70

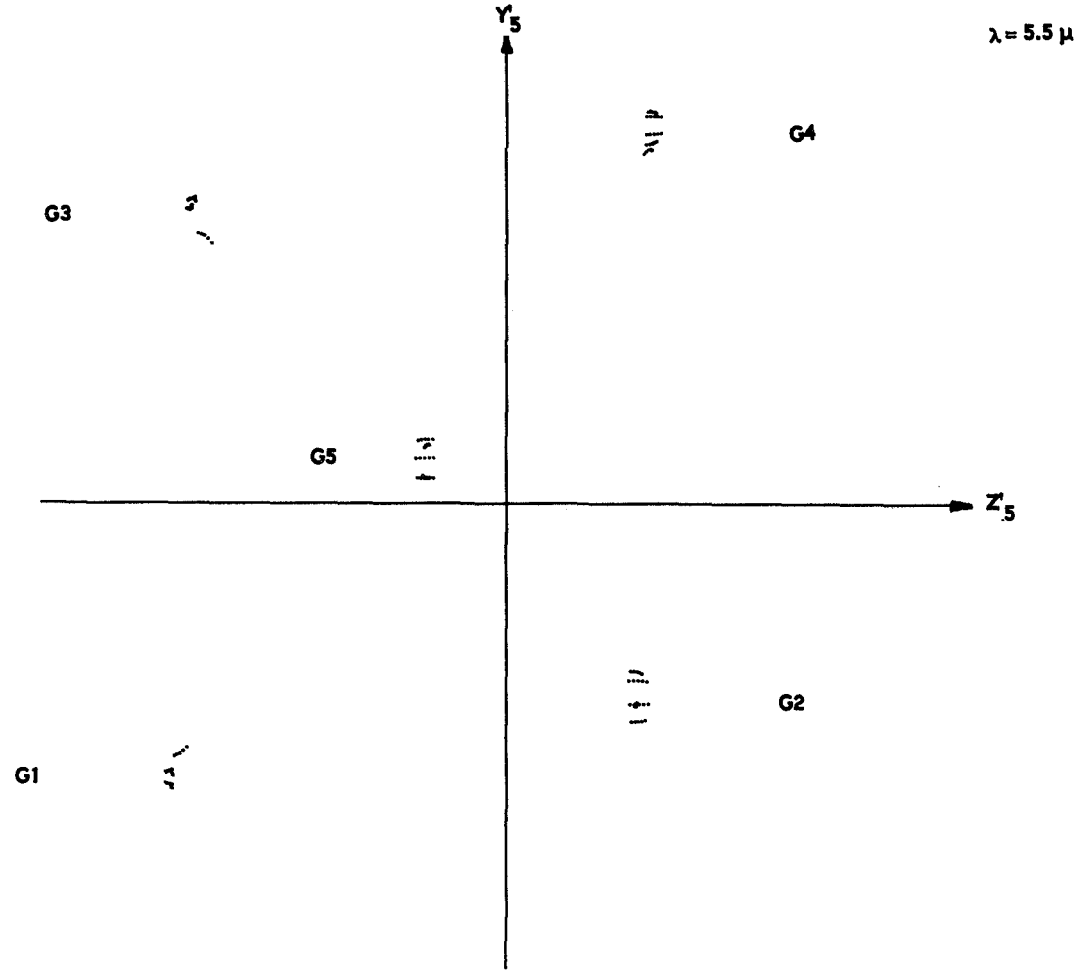

					MAX	MIN	
Z	HALF AXIS LENGTH	0.040	Z	=	0.013	-0.029	SURFACE NO.
Y	HALF AXIS LENGTH	0.040	Y	=	0.034	-0.025	5

Figure 39. 25-Ray Spot Images of the Center and Four Corners of the Diffraction Grating Formed on the Detector

(λ=5.5 μ)

SINGLE DETECTOR LENS--NIMS, .1X.6 SLIT, 26 DEGREE GRATING OFFSET, 1.260 2-9-70

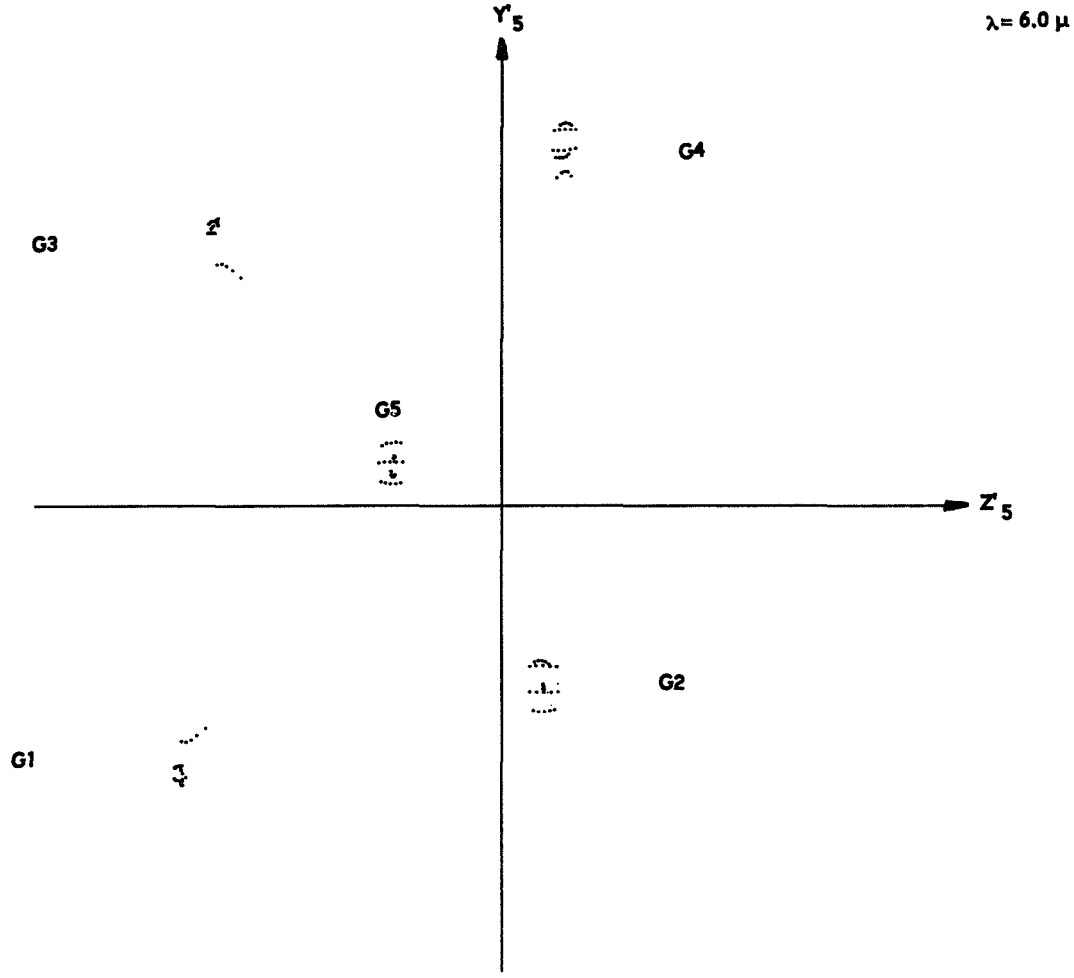

					MAX	MIN	
Z	HALF AXIS LENGTH	0.040	Z	=	0.006	-0.028	SURFACE NO.
Y	HALF AXIS LENGTH	0.040	Y	=	0.033	-0.024	5

Figure 40. 25-Ray Spot Images of the Center and Four Corners of the Diffraction Grating Formed on the Detector

(λ=6.0 μ)

SINGLE DETECTOR LENS--NIMS, .1X.6 SLIT, 26 DEGREE GRATING OFFSET, .903 2-9-70

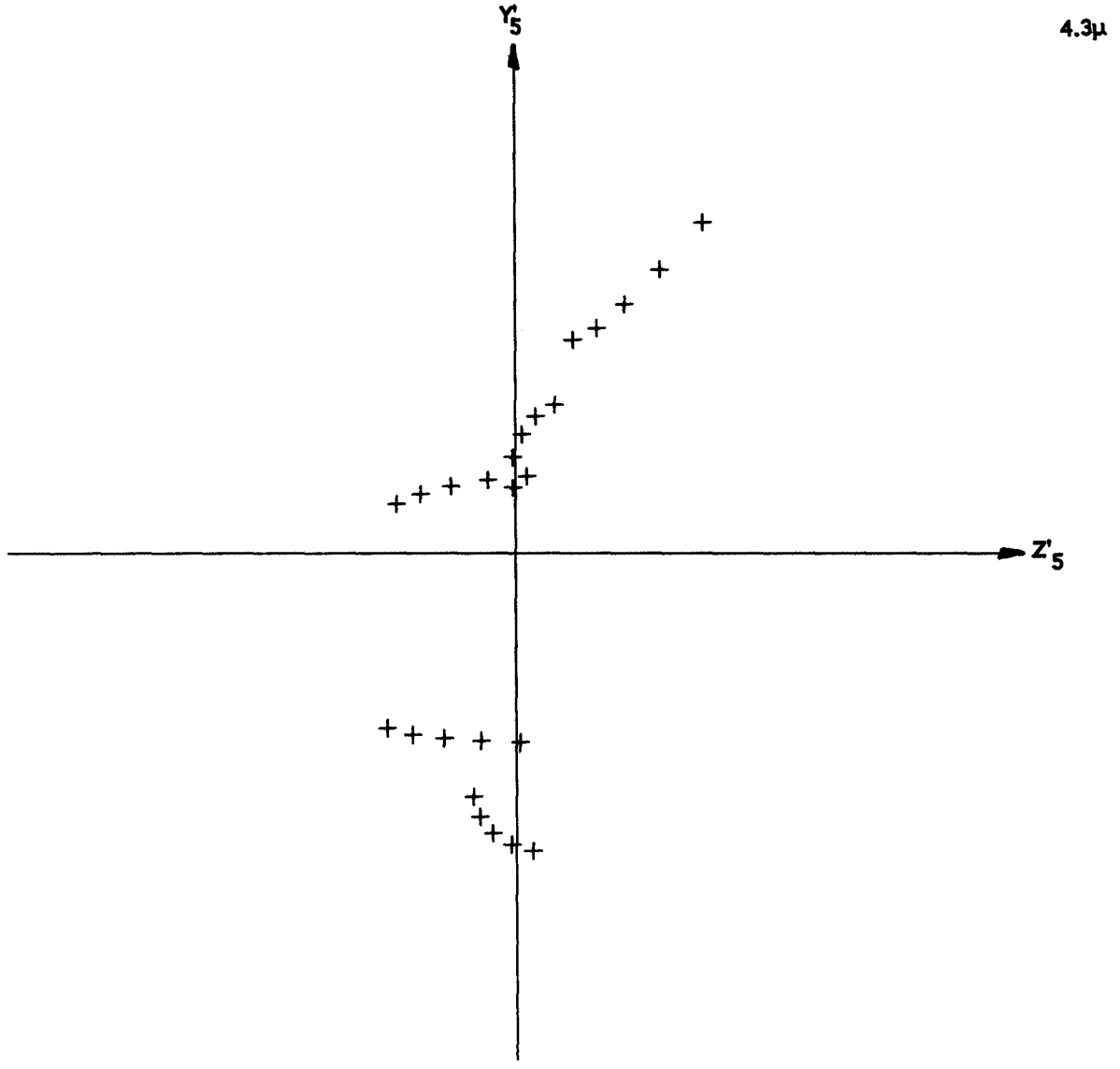

					MAX	MIN	
Z	HALF AXIS LENGTH	0.0025	Z	=	0.001	-0.001	SURFACE NO.
Y	HALF AXIS LENGTH	0.0025	Y	=	0.002	-0.001	5

Figure 41. Expanded 25-Ray Spot Image for G1 Starting Point on Diffraction Grating

SINGLE DETECTOR LENS--NIMS, .1X.6 SLIT, 26 DEGREE GRATING OFFSET, .903 2-9-70

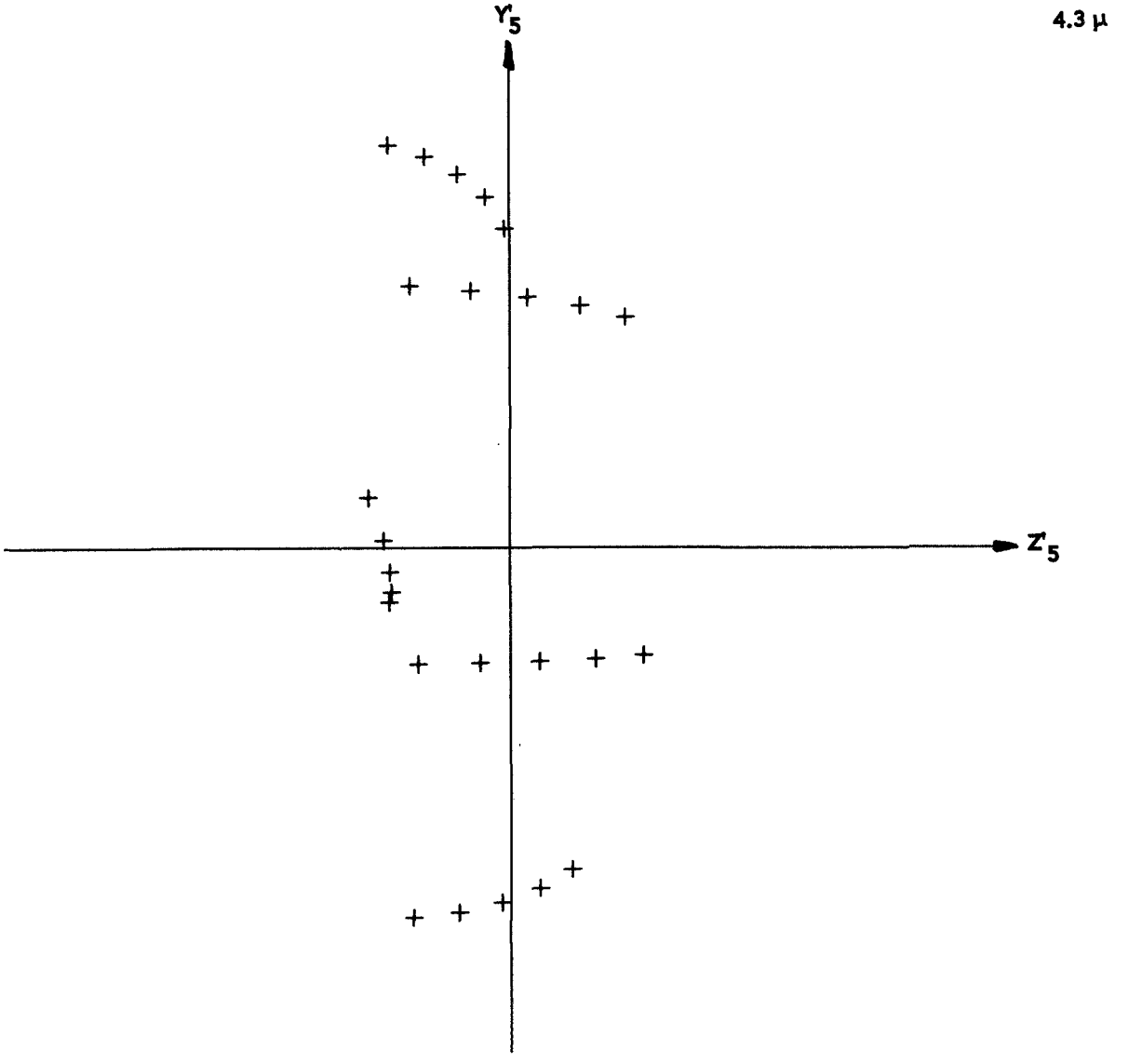

					MAX	MIN	
Z	HALF AXIS LENGTH	0.0025	Z	=	0.001	-0.001	SURFACE NO.
Y	HALF AXIS LENGTH	0.0025	Y	=	0.002	-0.002	5

Figure 42. Expanded 25-Ray Image for G2 Starting Point on Diffraction Grating

SINGLE DETECTOR LENS--NIMS, .1X.6 SLIT, 26 DEGREE GRATING OFFSET, .903 2-9-70

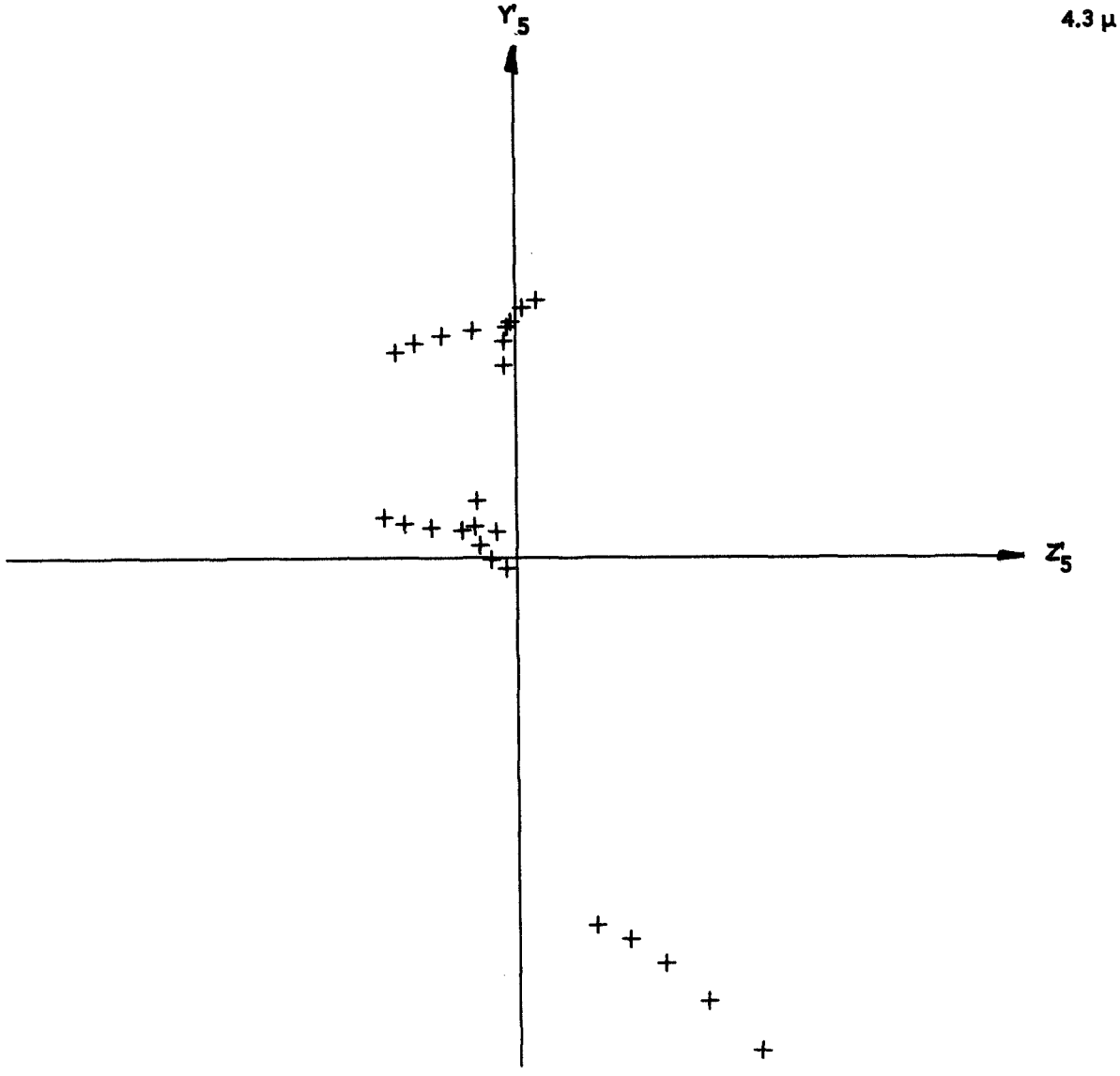

					MAX	MIN	
Z	HALF AXIS LENGTH	0.0025	Z	=	0.001	-0.001	SURFACE NO.
Y	HALF AXIS LENGTH	0.0025	Y	=	0.001	-0.002	5

Figure 43. Expanded 25-Ray Spot Image for G3 Starting Point on Diffraction Grating

SINGLE DETECTOR LENS--NIMS, .1X.6 SLIT, 26 DEGREE GRATING OFFSET, .903 2-9-70

4.3 μ

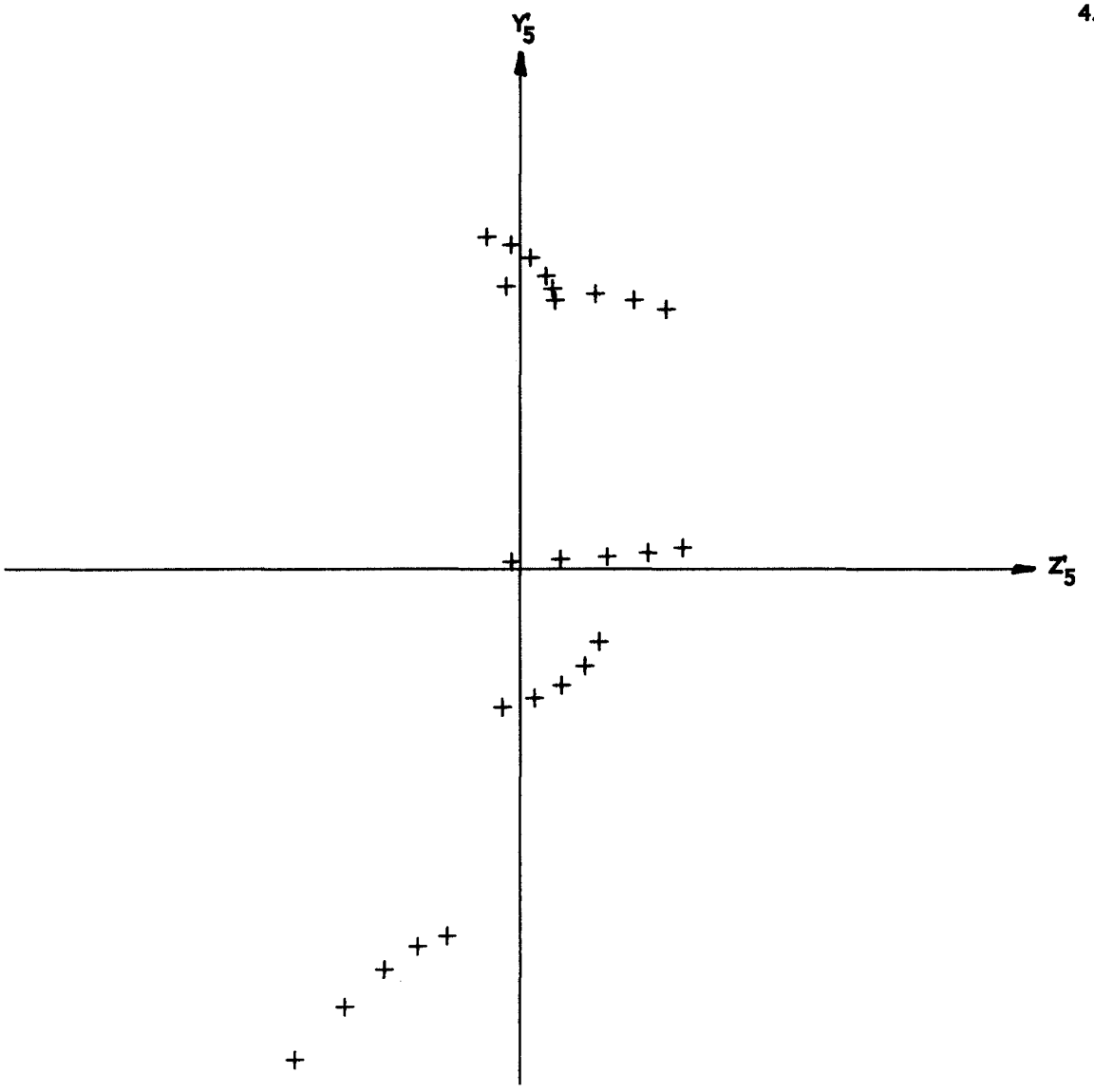

					MAX	MIN	
Z	HALF AXIS LENGTH	0.0025	Z	=	0.001	-0.001	SURFACE NO.
Y	HALF AXIS LENGTH	0.0025	Y	=	0.002	-0.002	5

Figure 44. Expanded 25-Ray Image for G4 Starting Point on Diffraction Grating

SINGLE DETECTOR LENS--NIMS, .1X.6 SLIT, 26 DEGREE GRATING OFFSET, .903 2-9-70

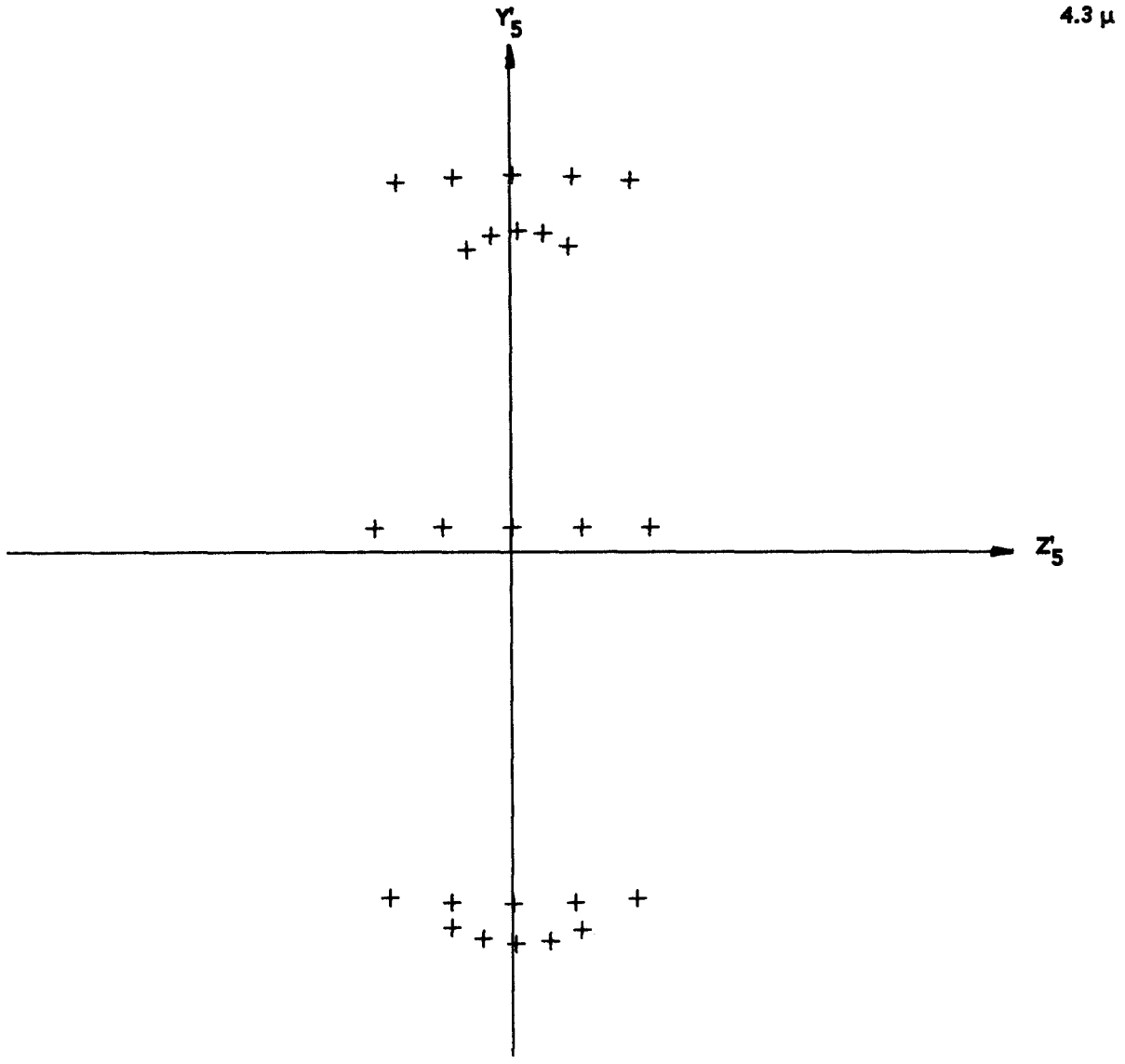

					MAX	MIN	
Z	HALF AXIS LENGTH	0.0025	Z	=	0.001	-0.001	SURFACE NO.
Y	HALF AXIS LENGTH	0.0025	Y	=	0.002	-0.002	5

Figure 45. Expanded 25-Ray Spot Image for G5 Starting Point on Diffraction Grating

SECTION 5

TELESCOPE AND SCAN MIRROR

The proposed Nimbus experiment requires a reflective-type telescope of approximately 10-inch focal length which uses a minimum number of mirror surfaces. The telescope is located before the entrance slits, and it images the earth on the two entrance slits. Conversely, the telescope projects the two entrance-slit images onto the earth. These slit images on the earth must have their long dimensions as nearly perpendicular to the Nimbus orbital path as possible. A scan mirror is to be located in front of the telescope which scans the earth at right angles to the Nimbus orbit through an angular range of ±22°. The scan mirror must also be able to rotate to an angular location which gives the telescope a view of space.

The overall length of the monochromator from the entrance slit to the collimating mirror is 10 inches. Another inch should be allowed for the collimating mirror thickness and the protective cover. This means that only 4 inches of usable spectrometer length exists in front of the entrance slit if the overall spectrometer is to be no longer than 15 inches. This also means the 10-inch focal length telescope must be optically folded by an auxillary mirror.

The two entrance slits are tilted roughly 15° from the positive Y_o-axis along both the positive X_o-axis and the positive Z_o-axis (Figure 8). For a single paraboloid telescope to produce a best possible image for these two tilted entrance slits, it is necessary for the optical axis of the paraboloid mirror to both pass through or near the origin of the (X_o, Y_o, Z_o) axis system, and be perpendicular to the best fitting plane for the two entrance slits. This means the optical axis of the parabolic mirror deviates 15° from the positive X_o-axis toward both the negative Y_o-axis and the negative Z_o-axis.

This type of telescope, however, does not work for this spectrometer, since an auxillary mirror located in front of the entrance slit must reflect the monochromator input optical axis toward the positive Z_o and negative Y_o side of the entrance slits. This is the proper location for an ideal 15° x 15° offset paraboloid. The ray cross-sections which are accepted by the monochromator are roughly 3.5 inches square at the parabolic telescope mirror 10 inches from the entrance slit, and there would be no room on the positive Z_o side of the monochromator. Further, a 15° offset is not nearly enough to prevent vignetting of the rays traveling between the paraboloid telescope mirror and the auxillary mirror by the entrance slits.

Since the best telescope imaging system does not work, it then becomes necessary to find the most practical telescope system. The axis system for the telescope design that has been found most practical after considerable investigation is shown in Figure 46 and defined in Table 49, and its dimensional parameters are defined in Table 50.

Figure 46 gives only a plan view, since all the X"-axes are in the same plane with the exception of the X''_o axis. To prevent vignetting of rays traveling between the paraboloid telescope mirror and the auxillary mirror by the entrance slits and the grating, it was necessary to offset the paraboloid telescope optical axis 37° from the monochromator entrance axis. Further, this offset is on the poorest side of the entrance slit for image quality. However, the angular aberrations for the 37° offset telescope are only slightly larger than for the more ideal 15° x 15° offset telescope.

The same 100-ray families from the same sixteen starting points on the two entrance slits that were used to ray-trace the monochromator were again used to ray-trace the telescope by multiplying all ray direction cosines by -1.0. This directs all the rays toward the telescope rather than the monochromator.

The entrance slit images have not been ray-traced to the earth, but rather the ray trace gives the angular orientation of each ray relative to the (X''_8, Y''_8, Z''_8)

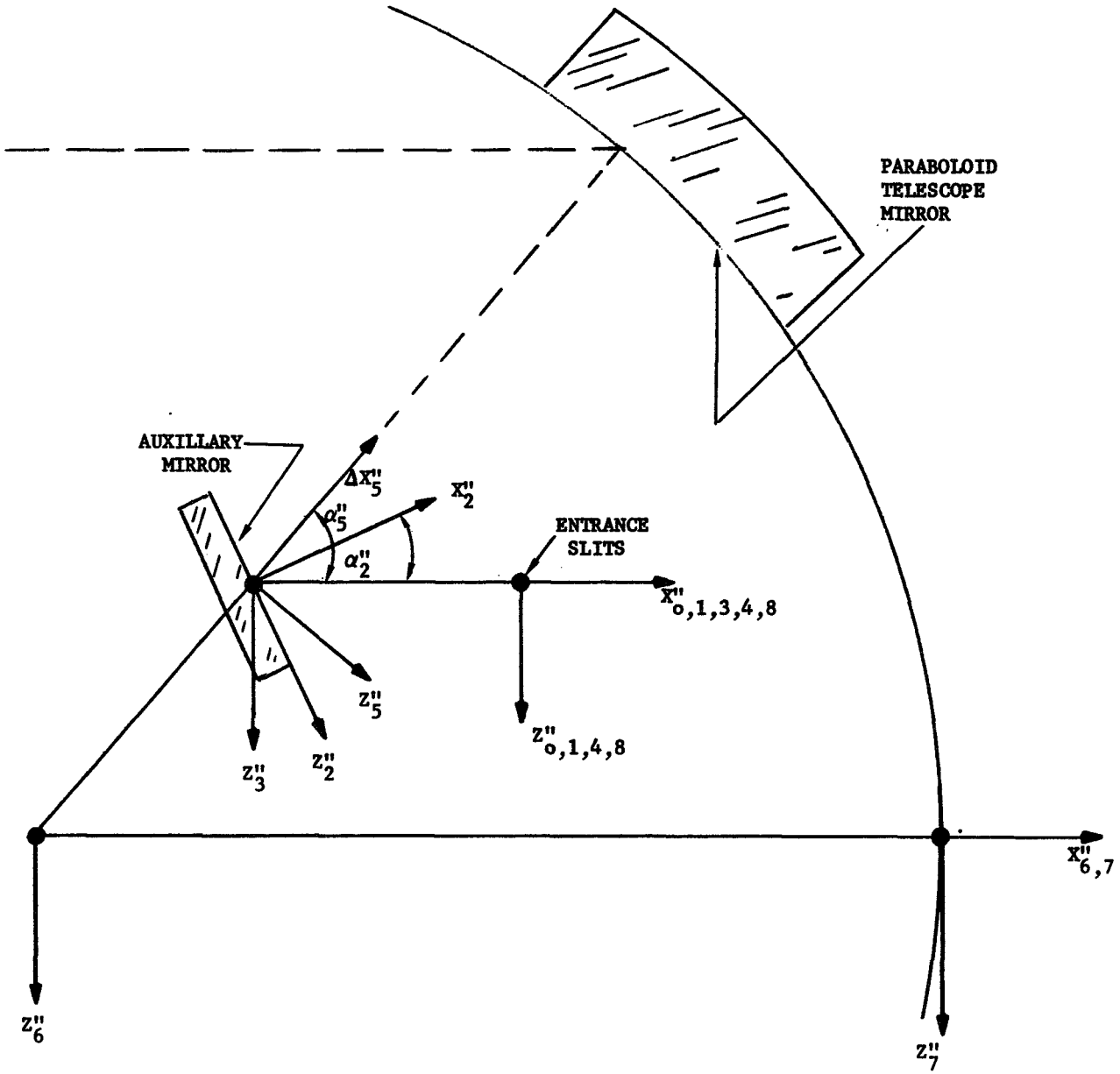

Figure 46. Plan View of Axes Used for Ray Trace of Telescope System

Table 49. Definitions for the Axis System Used to Ray-Trace the Telescope System

(X''_o, Y''_o, Z''_o)	This axis system is identical to the (X_o, Y_o, Z_o) axis system for the monochromator, in which the two entrance slits are defined.
(X''_1, Y''_1, Z''_1)	The origin of this axis system is located at $Y''_o = -.1$ inch. This sets the remainder of the telescope axis systems at the height of the true vertical center of the two entrance slits.
(X''_2, Y''_2, Z''_2)	The origin of this axis system is on the negative X''_1-axis, and the reflective auxillary mirror surface is in the Y''_2-Z''_2 plane. The X''_2-axis has been rotated through the angle α''_2 from the X''_1 axis in the X''_2-Z''_2 plane.
(X''_3, Y''_3, Z''_3)	The origin of this axis system is the same as the (X''_2, Y''_2, Z''_2) axis system, and it is used as a mathematical aid.
(X''_4, Y''_4, Z''_4)	This axis system is identical to the (X''_1, Y''_1, Z''_1) axis system, and the Y''_4-Z''_4 plane is used to show where those rays traveling between the paraboloid telescope mirror and the auxillary mirror pass, relative to the two entrance slits.
(X''_5, Y''_5, Z''_5)	The origin of this axis system is the same as the (X''_2, Y''_2, Z''_2) axis system. However, $\alpha''_5 = 2\,\alpha''_2$. This axis system is a mathematical aid.
(X''_6, Y''_6, Z''_6)	The origin of this axis system is at the focus of the paraboloid telescope mirror, and the X''_6-axis is parallel to the X''_o-axis and the X''_1-axis.
(X''_7, Y''_7, Z''_7)	The origin of this axis system is at the apex of the paraboloid mirror, and the focus of the paraboloid is on the negative X''_7-axis.
(X''_8, Y''_8, Z''_8)	This axis system is identical to the (X''_1, Y''_1, Z''_1) axis system. It is used to show the locations of the rays from the earth traveling to the paraboloid telescope mirror, relative to the entrance slit.

Table 50. Dimensional Parameter for Telescope System

Axis Subscript	a"	b"	c"	α"	β"	γ"
1	0	-.1	0	0	0	0
2	- 3.0	0	0	-18.75°	0	0
3	0	0	0	18.75°	0	0
4	3.0	0	0	0	0	0
5	- 3.0	0	0	-37.0°	0	0
6	- 3.0	0	0	37.0°	0	0
7	10.0	0	0	0	0	0
8	- 4.604	0	-1.805	0	0	0

axis system by three direction cosines. Since all the earth rays are within 2° of the X''_8-axis, the Y''_8 component direction cosine, Eta, and the Z''_8 component direction cosine, Zeta, are substantially equal numerically to their respective angular offsets in radians.

Figure 47 is a composite spot diagram of the angular field image of the two entrance slits, as projected by the telescope system. These are sixteen groups of 100-ray spot images, which represent the sixteen starting points B1 through E4 on the two entrance slits. The length of the Eta and Zeta half-axes are each .030 radians. Table 51 lists the angular image characteristics for the outer eight images which represent starting points B1, B2, B3, B4, E1, E2, E3, and E4.

Figures 48 through 55 are expanded plots of angular field aberrations for starting points B1, B2, B3, B4, E1, E2, E3, and E4.

For each of these expanded plots, it was necessary to change α''_8 and β''_8 such that the X''_8-axis was parallel with the centroid Eta and centroid Zeta for the particular spot image. So the origin of these plot axes are the centroids of the patterns. The half-axis scales for Figures 48 through 55 are .0025 radian.

TELESCOPE PARABOLOID MIRROR AND AUXILLARY MIRROR

Optical schematics are shown in Drawings 1 and 2 for the Telescope Paraboloid and Auxillary Mirrors as they are physically related to the monochromator. Boundary rays for two entrance slit starting points, B1 and E4, are accurately shown as determined by computer ray traces. These boundary rays which are shown are the true boundary rays for the telescope and show the used areas of both of these mirrors.

Figure 56 also shows in greater detail the optically used area on the face of the paraboloid telescope mirror. The boundary areas represented by starting points B1, B4, E1, and E4 are shown projected on the Y''_7-Z''_7 plane. If the required paraboloid sector is taken from a full paraboloid mirror, then the diameter of that paraboloid mirror must be slightly greater than 14 inches.

NIM TELESCOPE - PARABOLOID 10 INCH FL. 37X00 DEGREE OFFSET 12-30-69

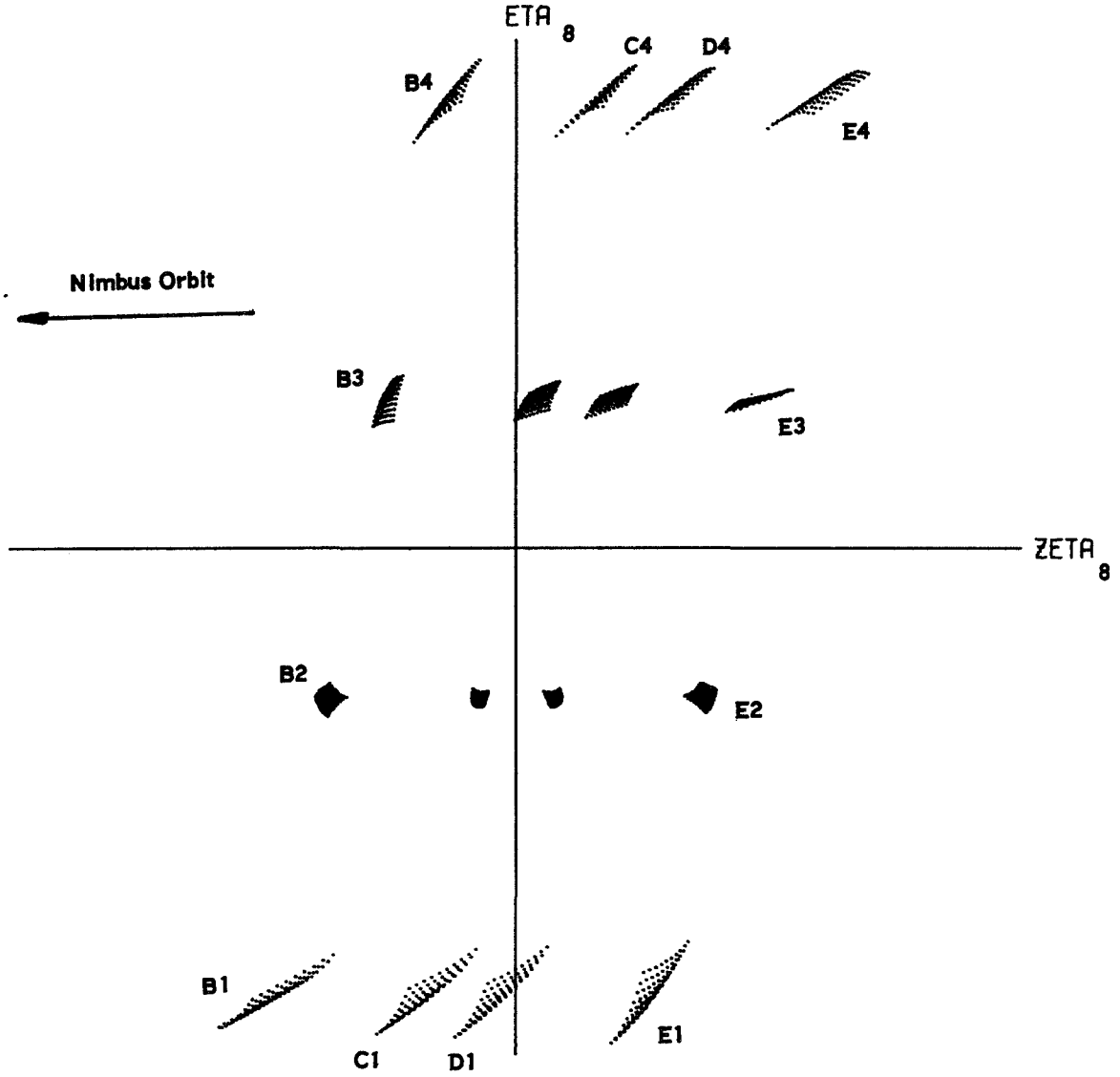

All Dimensions in Radians

					MAX	MIN	
ZETA	HALF AXIS LENGTH	0.030	ZETA	=	0.007	-0.008	SURFACE NO.
ETA	HALF AXIS LENGTH	0.030	ETA	=	0.028	-0.029	8

Figure 47. Telescope Angular Field-of-View--Sixteen 100-Ray Angular Images for the Sixteen Starting Points on the Two Entrance Slits.

Table 51. Angular Field Image Characteristics for the Paraboloid Telescope, and the α''_8 and β''_8 Angular Displacements Required to Match the Angular Centroids for the Starting Points Along the Outer Edges of the Two Entrance Slits.

Starting Points	Centroid ETA (Radian)	ΔETA (Radian)	80% ΔETA (Radian)	Centroid ZETA (Radian)	ΔZETA (Radian)	80% ΔZETA (Radian)	α''_8 (Degree)	β''_8 (Degree)
B1	-.026665	.0043	.0025	-.014502	.0068	.0042	-.8320°	-1.5277°
B2	-.009011	.0019	.0012	-.011164	.0018	.0010	-.6397°	- .5161°
B3	.008718	.0030	.0022	-.007655	.0017	.0012	-.4392°	.4995°
B4	.026540	.0049	.0029	-.00389	.0039	.0024	-.2300°	1.5206°
E1	-.026491	.0060	.0037	.007877	.0046	.0028	.4517°	-1.5178°
E2	-.008837	.0018	.0012	.011138	.0019	.0011	.6385°	- .5063°
E3	.008891	.0013	.0007	.01573	.0039	.0027	.8351°	.5092°
E4	.026709	.0034	.0022	.018182	.0060	.0036	1.0419°	1.5305°

NIM TELESCOPE - PARABOLOID 10 INCH FL. 37X00 DEGREE OFFSET 12-30-69

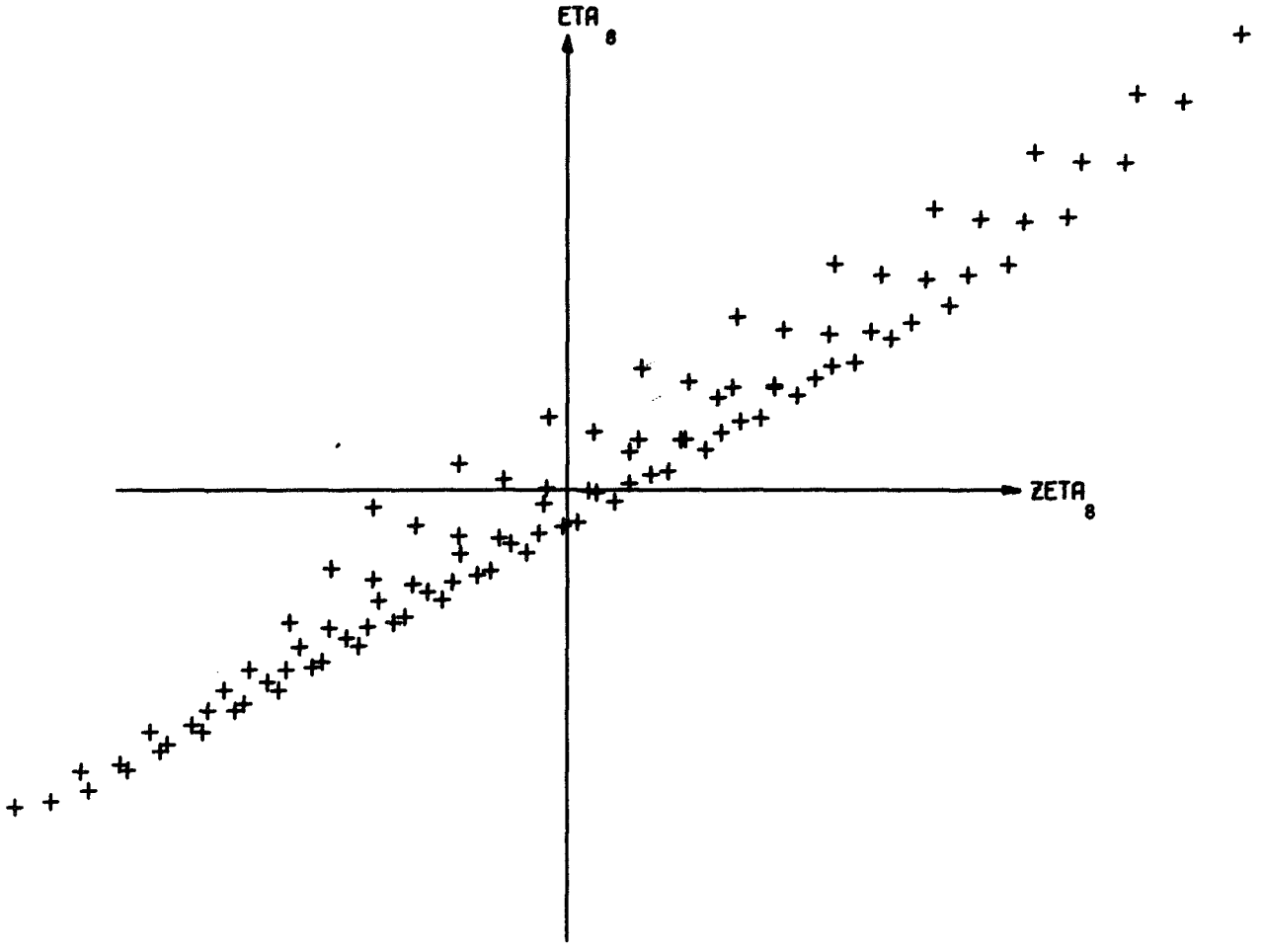

All Dimensions in Radians

				MAX	MIN	
ZETA	HALF AXIS LENGTH	0.002	ZETA =	0.004	-0.003	SURFACE NO.
ETA	HALF AXIS LENGTH	0.002	ETA =	0.003	-0.002	8

Figure 48. Telescope Angular Field-of-View--Expanded 100-Ray Angular Image for Starting Point B1 on the Main Entrance Slit.

NIM TELESCOPE - PARABOLOID 10 INCH FL. 37X00 DEGREE OFFSET 12-30-69

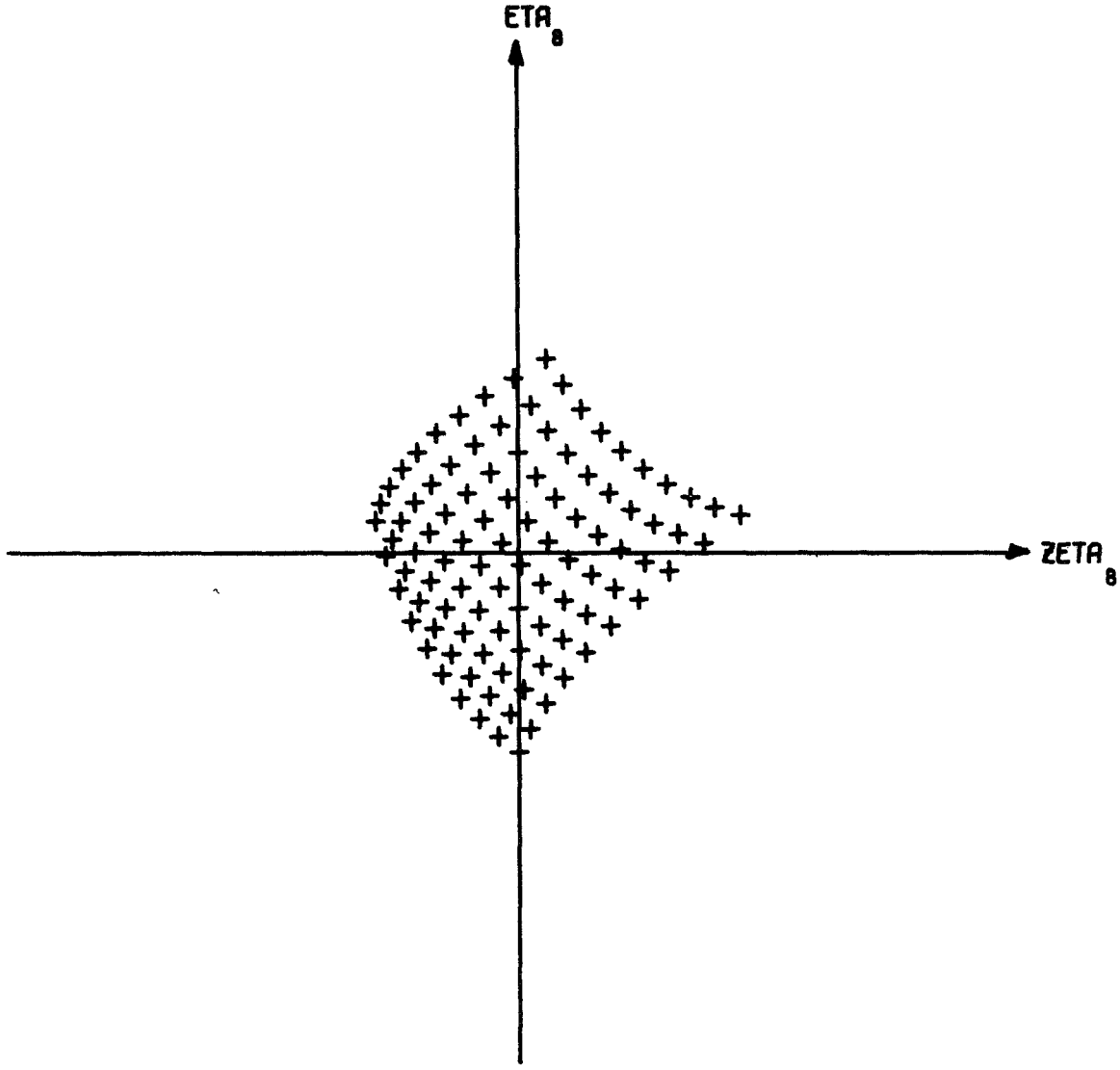

All Dimensions in Radians

				MAX	MIN	
ZETA	HALF AXIS LENGTH	0.002	ZETA =	0.001	-0.001	SURFACE NO.
ETA	HALF AXIS LENGTH	0.002	ETA =	0.001	-0.001	8

Figure 49. Telescope Angular Field-of-View--Expanded 100-Ray Angular Image for Starting Point B2 on the Main Entrance Slit.

NIM TELESCOPE - PARABOLOID 10 INCH FL. 37X00 DEGREE OFFSET 12-30-69

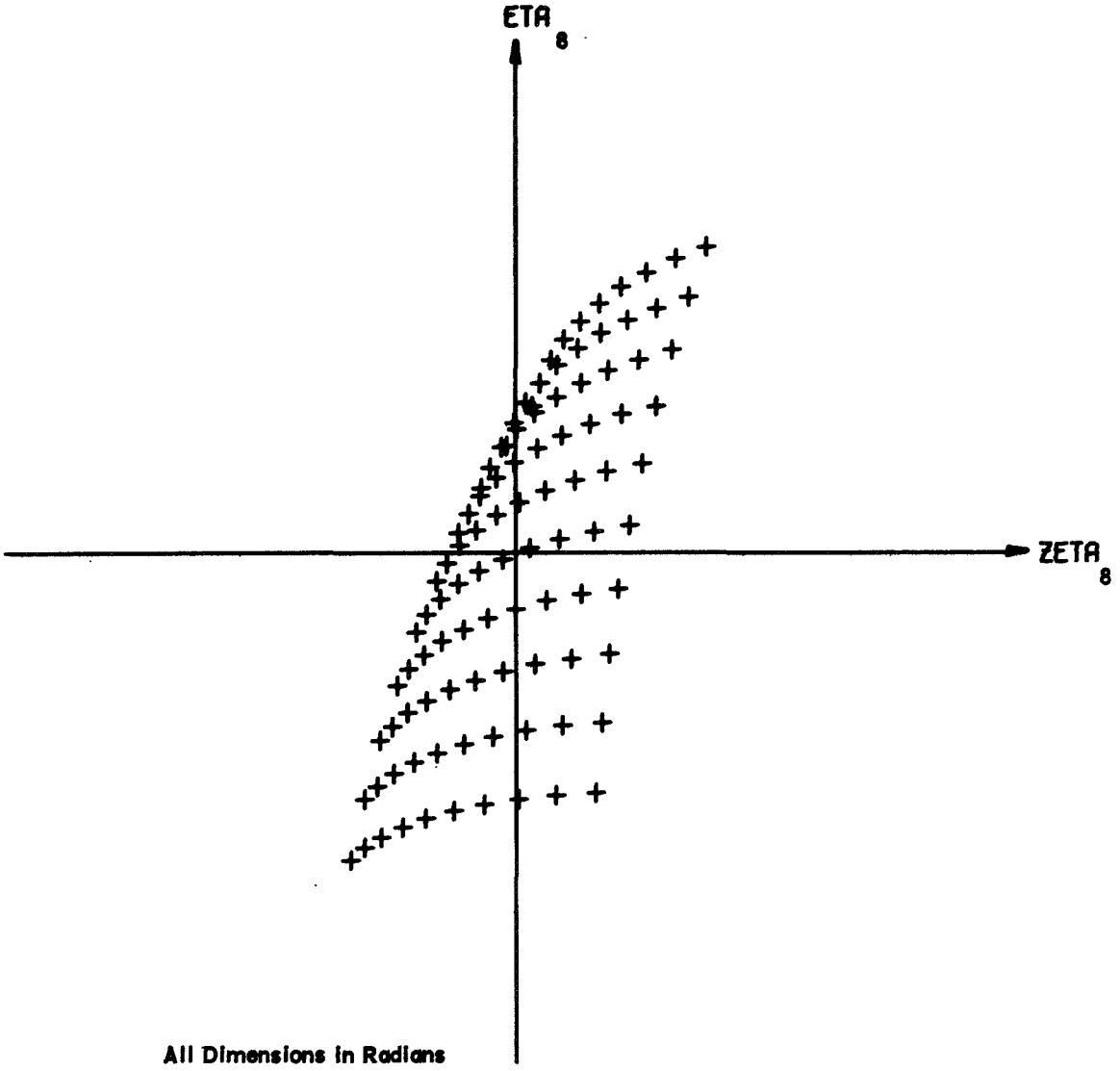

				MAX	MIN	
ZETA	HALF AXIS LENGTH	0.002	ZETA =	0.001	-0.001	SURFACE NO.
ETA	HALF AXIS LENGTH	0.002	ETA =	0.001	-0.002	8

Figure 50. Telescope Angular Field-of-View--Expanded 100-Ray Angular Image for Starting Point B3 on the Main Entrance Slit.

NIM TELESCOPE - PARABOLOID 10 INCH FL. 37X00 DEGREE OFFSET 12-30-69

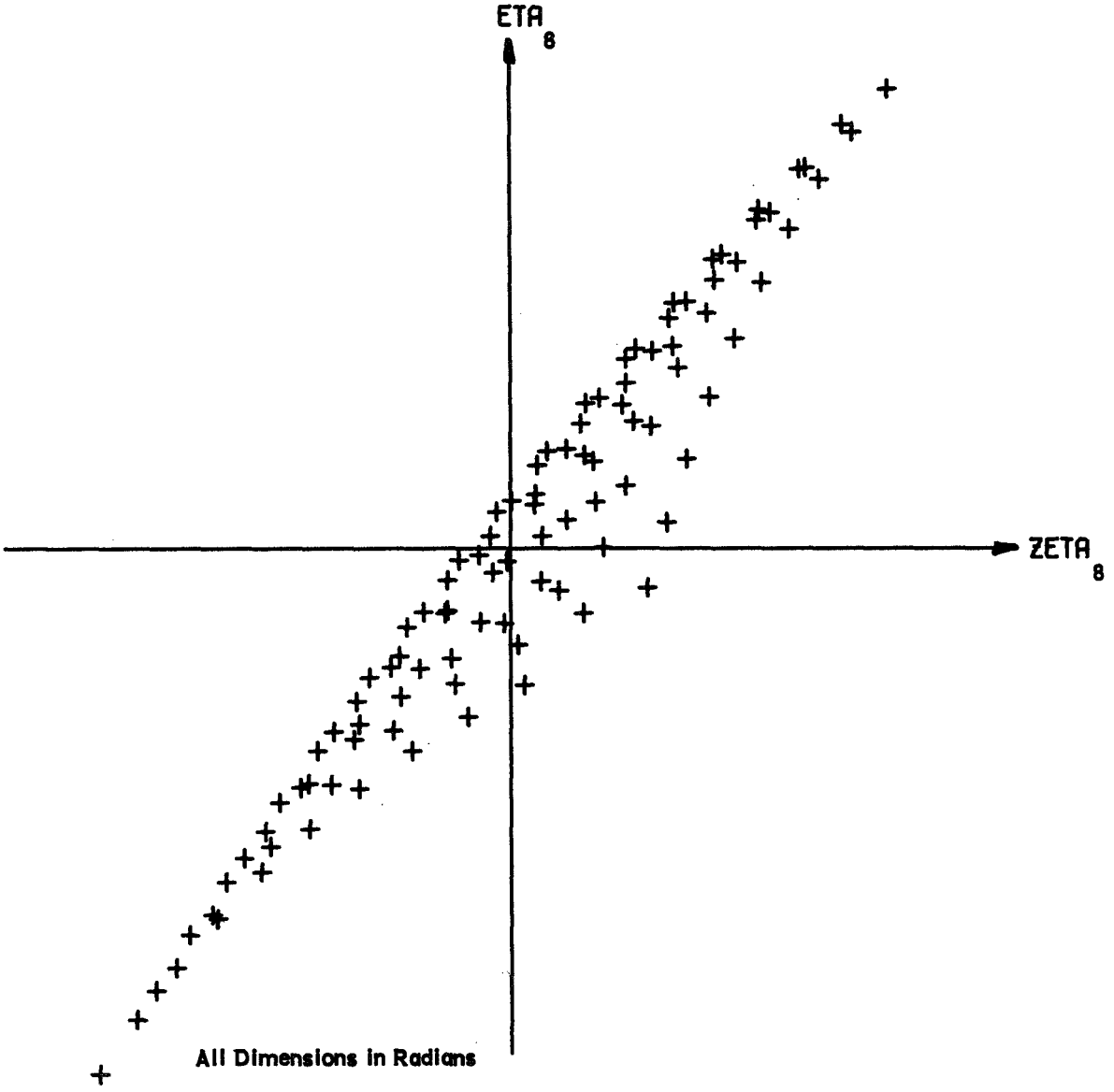

				MAX	MIN	
ZETA	HALF AXIS LENGTH	0.002	ZETA =	0.002	-0.002	SURFACE NO.
ETA	HALF AXIS LENGTH	0.002	ETA =	0.002	-0.003	8

Figure 51. Telescope Angular Field-of-View--Expanded 100-Ray Angular Image for Starting Point B4 on the Main Entrance Slit.

NIM TELESCOPE - PARABOLOID 10 INCH FL. 37X00 DEGREE OFFSET 12-30-69

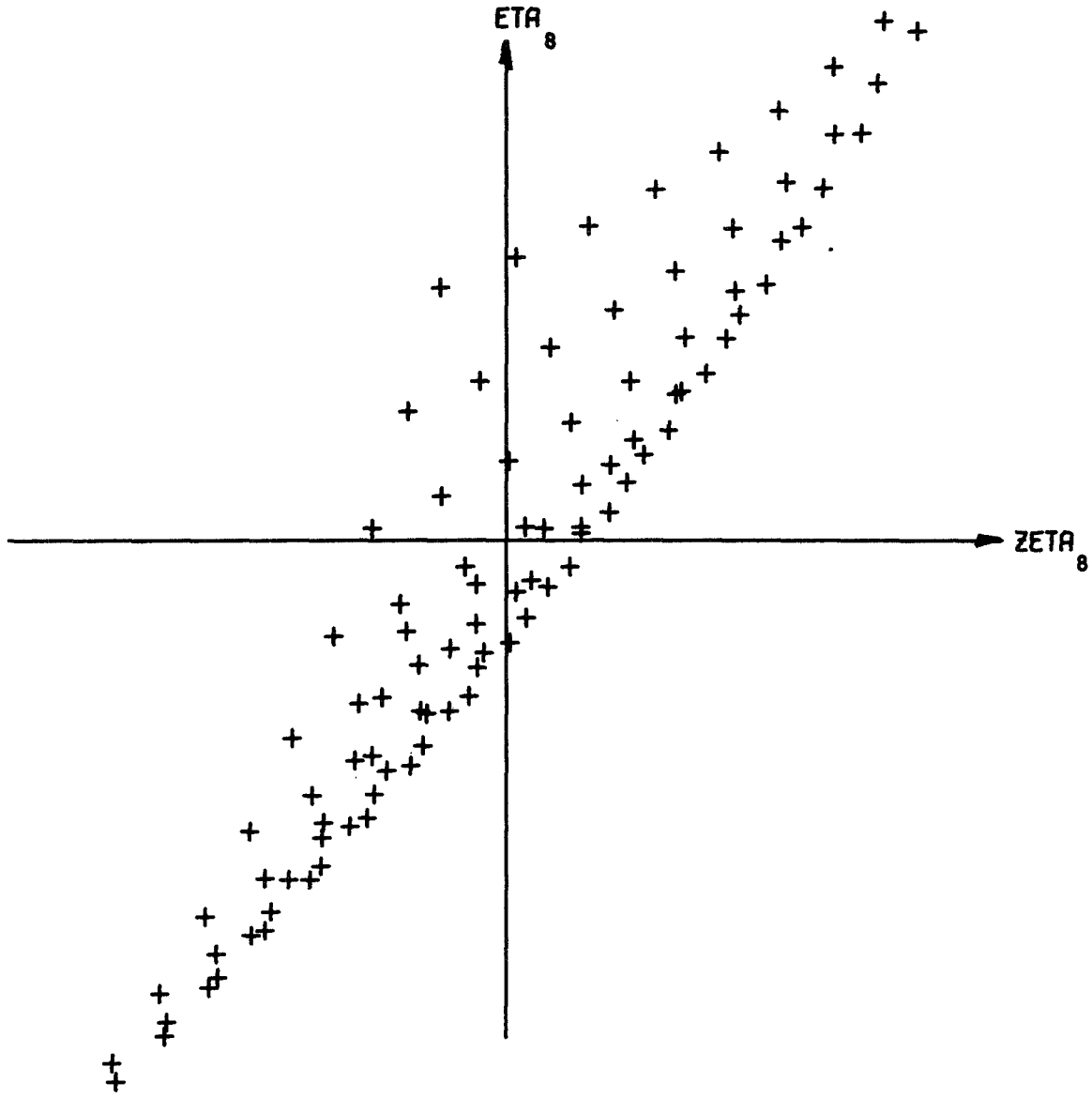

All Dimensions in Radians

				MAX	MIN	
ZETA	HALF AXIS LENGTH	0.002	ZETA =	0.002	-0.002	SURFACE NO.
ETA	HALF AXIS LENGTH	0.002	ETA =	0.003	-0.003	8

Figure 52. Telescope Angular Field-of-View--Expanded 100-Ray Angular Image for Starting Point E1 on the Second Entrance Slit.

NIM TELESCOPE - PARABOLOID 10 INCH FL. 37X00 DEGREE OFFSET 12-30-69

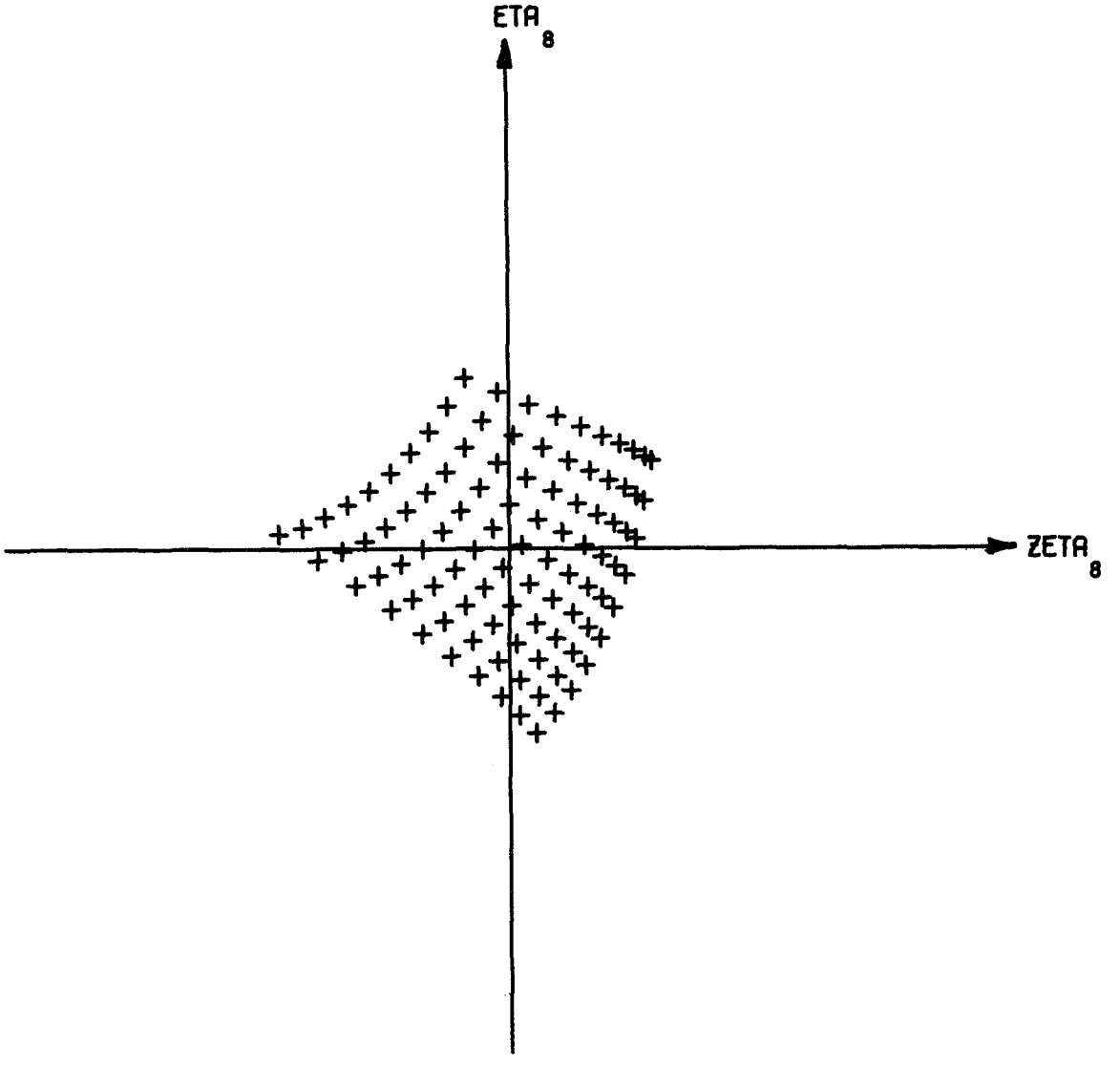

All Dimensions in Radians

				MAX	MIN	
ZETA	HALF AXIS LENGTH	0.002	ZETA =	0.001	-0.001	SURFACE NO.
ETA	HALF AXIS LENGTH	0.002	ETA =	0.001	-0.001	8

Figure 53. Telescope Angular Field-of-View--Expanded 100-Ray Angular Image for Starting Point E2 on the Second Entrance Slit.

NIM TELESCOPE - PARABOLOID 10 INCH FL. 37X00 DEGREE OFFSET 12-30-69

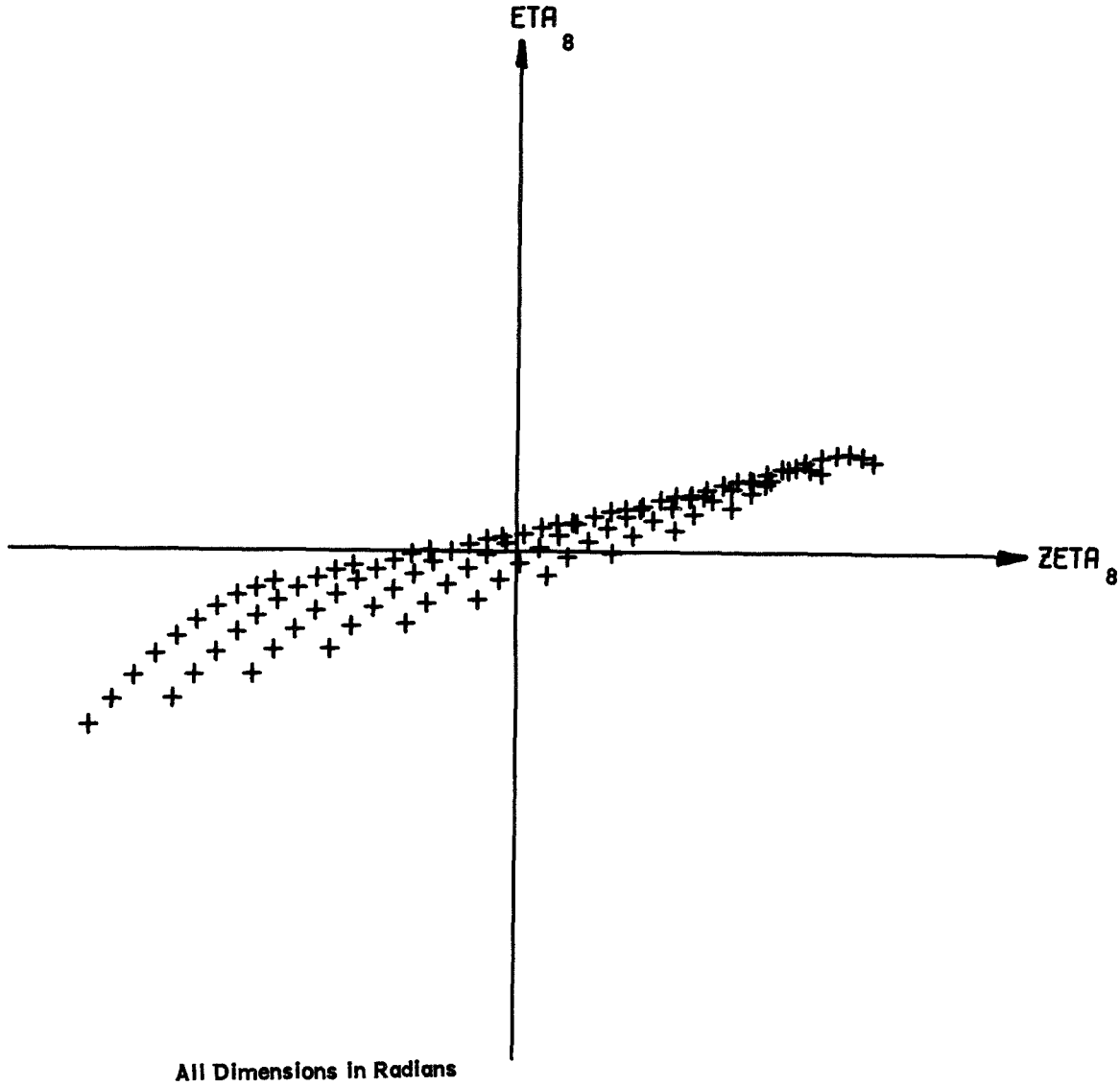

				MAX	MIN	
ZETA	HALF AXIS LENGTH	0.002	ZETA =	0.002	-0.002	SURFACE NO.
ETA	HALF AXIS LENGTH	0.002	ETA =	0.000	-0.001	8

Figure 54. Telescope Angular Field-of-View--Expanded 100-Ray Angular Image for Starting Point E3 on the Second Entrance Slit.

NIM TELESCOPE - PARABOLOID 10 INCH FL. 37X00 DEGREE OFFSET 12-30-69

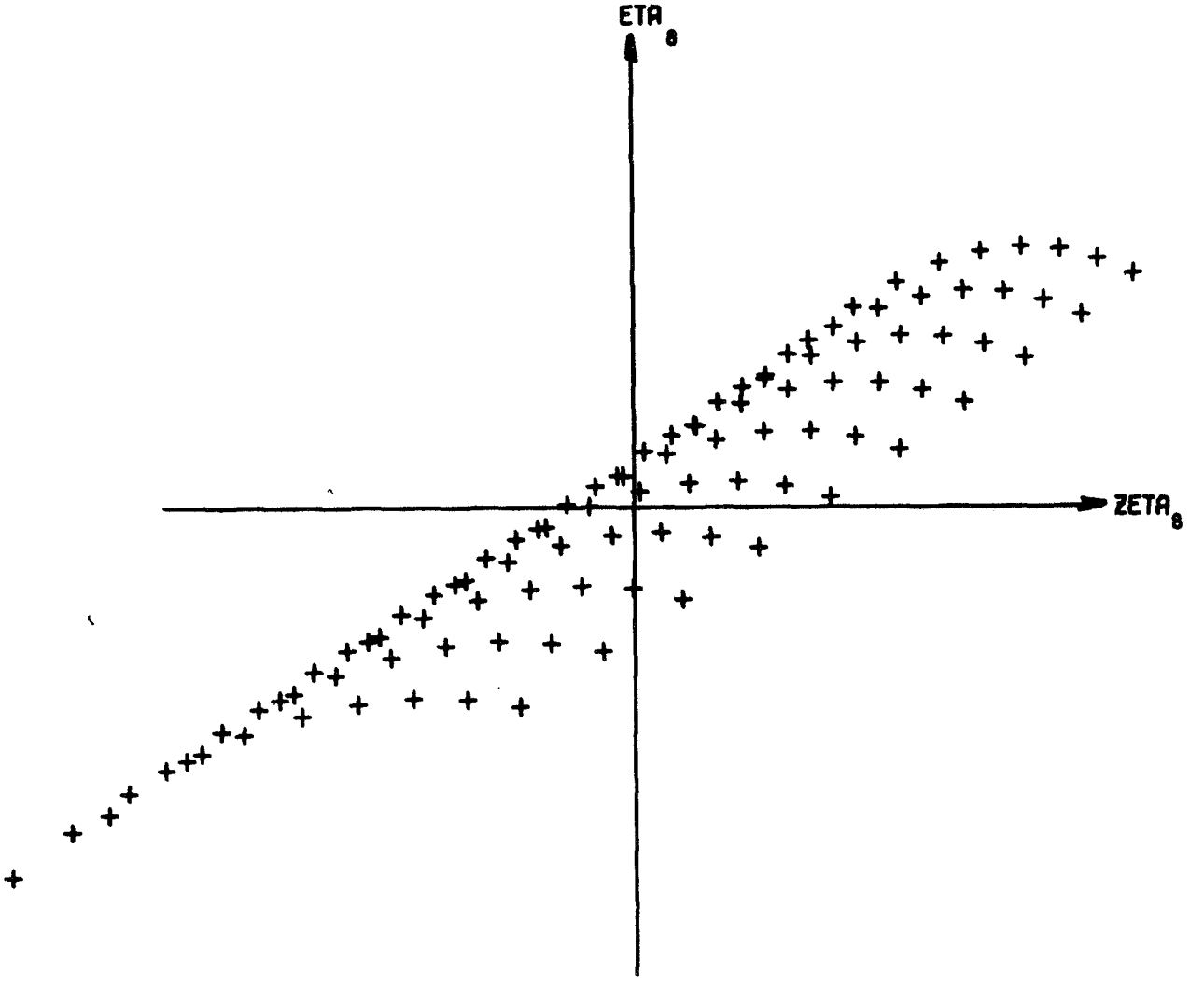

All Dimensions in Radians

				MAX	MIN	
ZETA	HALF AXIS LENGTH	0.002	ZETA =	0.003	-0.003	SURFACE NO.
ETA	HALF AXIS LENGTH	0.002	ETA =	0.001	-0.002	8

Figure 55. Telescope Angular Field-of-View--Expanded 100-Ray Angular Image for Starting Point E4 on the Second Entrance Slit.

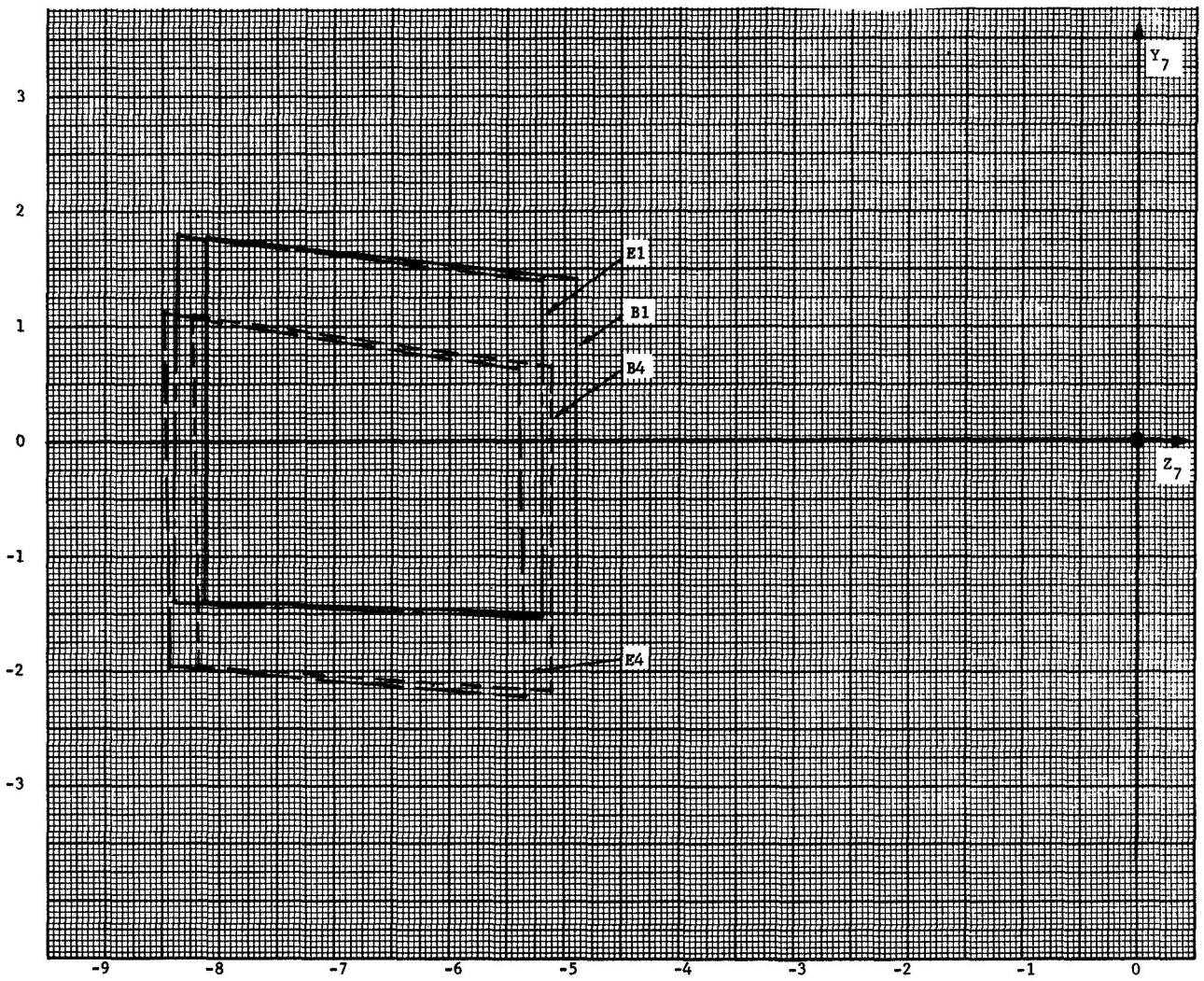

Figure 56. Optically Used Area on Paraboloid Telescope Mirror

SCAN MIRROR LOCATION

The scan mirror must be located in that volume of the spectrometer which is fully within the telescope's field-of-view. Further, the scan mirror must be located sufficiently far forward of the Y_8''-Z_8'' plane that it doesn't vignette the rays which travel between the telescope paraboloid mirror and the auxillary mirror. The boundaries for these latter rays are shown clearly in Drawing 1.

Figure 57 demonstrates, however, that there is only one practical location for the rotational axis for the scan mirror; and that location is as far forward of the telescope paraboloid mirror as is permitted by the spectrometer housing. Figure 57 shows the telescope paraboloid mirror and its field-of-view boundary ray projections on the Y_7''-Z_7'' plane. The rotational axis for the scan mirror is parallel to the Z_o''-axis and is located 4 inches forward of the Y_8''-Z_8'' plane, and above all of the field-of-view rays.

Figure 57 shows the boundary rays for four different spectrometer scan mirror angles, , of 14°, 34°, 45°, and 56°. These four scan mirror angles give respective spectrometer view angles, , of 28°, 68°, 90°, and 112°. The spectrometer view angle needs to be as small as 28° in order for the telescope to have a clear view of space, unaffected by the radiation from the earth or its atmosphere. The axis of the scan mirror must be at least 6.5 inches in front of the paraboloid mirror for the rays from the 28° view angle to clear the bottom edge of the paraboloid mirror (Figure 57).

Table 52 lists the length, L, of scan mirror required for each of the four scan angles. The length, L, is also given for a view angle of 152° which is necessary for a view of space in front of the spectrometer rather than behind it. The spectrometer needs only one scan mirror angle for a view of space, and it is preferable to use the 28° view angle and a 3.6-inch long mirror area rather than the 152° view angle which uses a 14.5-inch long mirror area.

The scan mirror still requires a length of at least 6.3 inches for the 112° spectrometer view angle. The housing should not be made large enough to

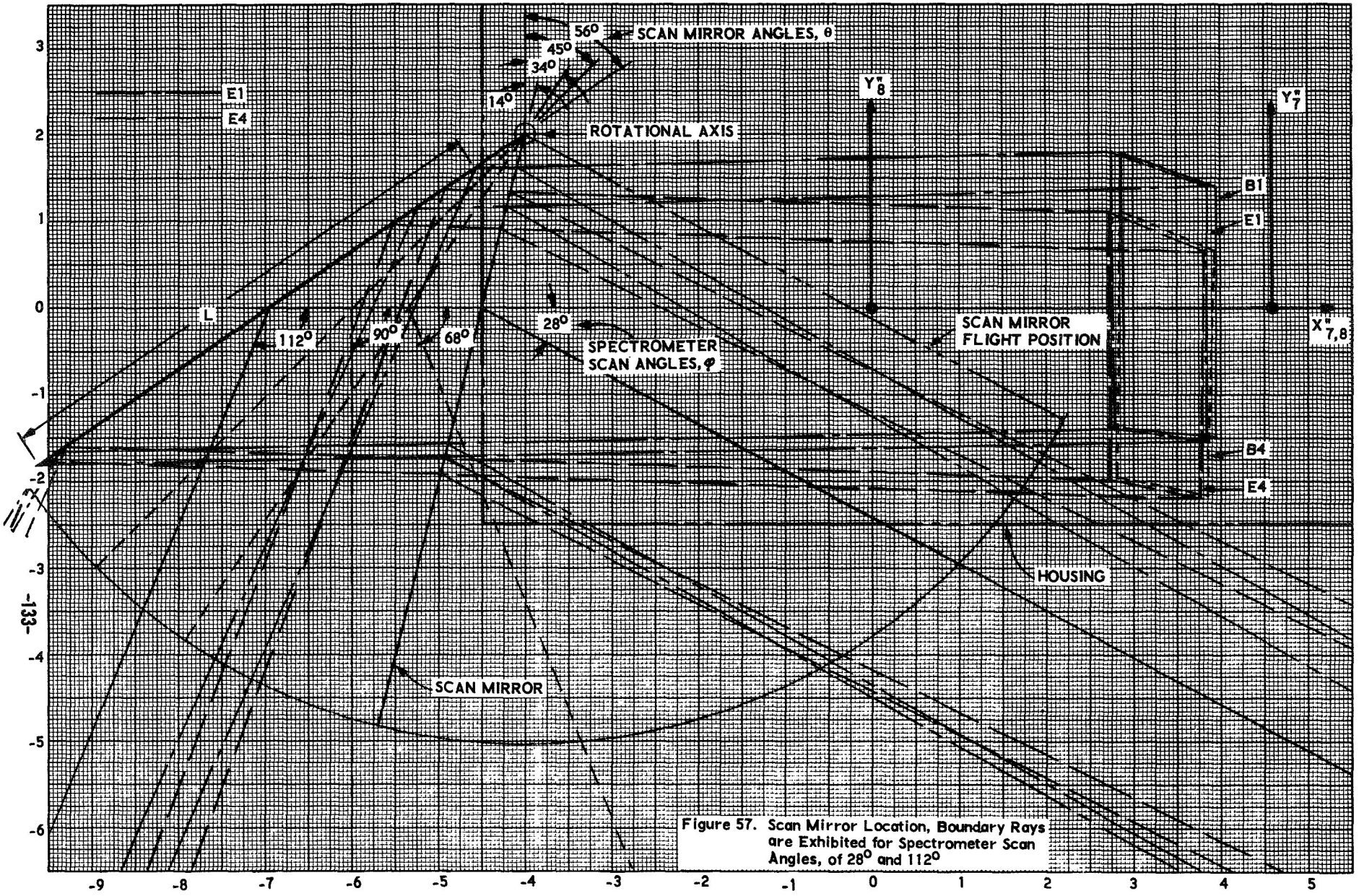

Figure 57. Scan Mirror Location, Boundary Rays are Exhibited for Spectrometer Scan Angles, of 28° and 112°

Table 52. Length of Scan Mirror Required for Mirror Spectrometer View Angles

Spectrometer View Angle θ	Scan Mirror Angle φ	Length of Scan Mirror Requirement L
28°	14°	3.6
68°	34°	4.2
90°	45°	5.0
112°	68°	6.3
152°	76°	14.5

enclose this scan mirror for all its scan angles. Rather, the scan mirror should be rotated into the flight position shown in Drawing 2. In this manner, the spectrometer housing does not need to be lower than that required to house the telescope paraboloid mirror.

SECTION 6

FIXED FIELD DETECTORS

The field-of-view areas of the earth for two monochromator entrance slits are long and narrow with aspect ratios of six to one. The Nimbus experiment requires a knowledge of the cloud patterns within the instantaneous fields-of-view of the entrance slits. This knowledge can be improved by dividing the entrance slit field-of-view images over an array of four or five infrared detectors having a 4 μ to 5 μ spectral band pass.

One method of accomplishing such images is to use a beam splitter following the entrance slits. The beam splitter reflects a portion of the monochromator input flux through an auxillary optical system and a 4 μ to 5 μ spectral band pass filter to an image of the entrance slit on an array of four or five detectors. The beam splitter, however, reduces the monochromator through-put and presents an additional optical element which could degrade or reduce the performance of all the spectral image surface detectors.

A second method of creating a separate image of the internal entrance slits is to use a greater numerical aperture than the F/3.5 aperture of the monochromator for the telescope system. Auxillary optics would be used to image the entrance slits on the four or five detectors so as not to disturb the detectors on the spectral image surface. However, to create the required zones of greater numerical aperture requires substantially larger telescope mirrors. Also, added optics are required inside the monochromator.

The simplest and most practical method of accomplishing an earth image on a four or five detector array corresponding to the entrance slit's fields-of-view is to mount the array of detectors directly on the entrance slit's defining structure so the detectors are adjacent to the two entrance slits. There is a

.05-inch spacing between the two entrance slits providing an ideal location for the detector array.

Figure 47 shows the angular aberrations produced by the telescope for four points on the inside edges of the two entrance slits: points C1, C2, C3, C4, D1, D2, D3, and D4. These angular aberrations are still slightly smaller between the two entrance slits where the detectors may be mounted. The detectors, however, can be covered with a 4 μ to 5 μ spectral band pass coating.

The area viewed on the earth by the entrance slits and the detector array is made identical for each sampling period by time-phasing the use of each entrance slit and the detector array relative to the satellite's orbital motion.

SECTION 7

RADIATION COOLING SHIELD

A radiation cooling shield should be mounted to the front of the spectrometer. A shield which is capable of removing .66 watt of internal heat from both the chopper assembly located at the entrance slits and the detectors on the spectral image surface, and radiate this heat to space. The cooling shield must be efficient enough to maintain the detector temperatures at between 200° K and 210° K, with long-term temperature variations of less than ±1° K.

The radiation cooling shield required has been designed and developed by Smith (8) for the multidetector spectrometer designed for the Nimbus F experiment. This radiation cooling shield is in the form of a truncated, four-sided prism with an open-end cross section of 9.4375 inches by 5.925 inches, a closed-end cross section of 6.875 inches by 3.25 inches, and a depth of 3.75 inches. The walls of this cooling shield are multilayered, consisting of, in sequence from the outside face: a thin quartz plate with a second surfaced mirror coating, cemented to a copper or aluminum conductive structure. Super insulation encloses all parts of this structure except where it contacts the chopper and the detectors.

This shield design is directly applicable to the final spectrometer design which has been described in this report. However, the 3.75-inch depth of that shield design would increase the length of the spectrometer to more than 17 inches, which is 2 inches greater than the 15-inch maximum length which has been the goal of this study.

Drawings 1 and 2 show a suggested shape for the outer surfaces of a radiation cooling shield which will fit within the specified spectrometer dimensions. It is assumed that construction details of this shield would follow Smith's (8) design. No thermal analysis has been performed for this suggested shield design.

Two criteria have been followed in developing this design:

1. The cross sectional area of the front opening of this shield has been maximized for the greatest housing dimensions permitted by the specifications.

2. The angular orientation of the four faces are perpendicular to those smallest incident angles (measure about the X_o-axis of the monochromator) for earth and solar radiation. The lower face and the two side faces of the cooling shield have angles of 30° relative to the X_o-axis. The upper face is at 60° to the X_o-axis. These four angles prevent double specular reflection between any two faces of the cooling shield for direct earth or solar rays. The earth and solar rays which are specularly reflected are in turn reflected directly to space.

The distance of the detectors from the front of the spectrometer vary by 1.75 inches (Drawing 1). Therefore, the back of the cooling shield has been positioned diagonally with respect to the front of the spectrometer, so it is as near to all the detectors as possible.

Drawing 1 shows the suggested overall spectrometer housing width of 10 inches, and the open-end of the radiant cooling shield also has this 10-inch width.

Drawing 2 shows that the back edge of the cooling shield is horizontal with respect to the earth so that its full width presents the same angular orientation to the earth's radiation. Drawing 2 also shows a suggested height for the spectrometer housing with a caged scan mirror which is 8.75 inches. Thus, the top of the radiation shield can project 4.25 inches above the spectrometer housing and still be within the 13-inch overall maximum height specified for the spectrometer.

The height for the open end of the cooling shield varies from roughly 4.0 inches on one side of the spectrometer to roughly 8 inches on the other. The open-end cross sectional area of this cooling shield design is, then

$$\frac{8 \text{ in.} + 4 \text{ in.}}{2} \times 10 \text{ in.} = 60 \text{ in.}^2$$

which is slightly greater than the open-end cross sectional area for the design described by Smith (8).

SECTION 8

MONOCHROMATOR ERROR ANALYSES

The optical ray trace results which have been presented in this report assume both perfect optical elements and perfect placement within the spectrometer.

The spectrometer which has been analyzed in this report is very complex, so in constructing it every effort should be made to reproduce the entrance slit, grating, and collimating mirror dimensional parameters as accurately as possible. For only then will the detector foreoptics be correct, as defined in this report.

The discussion which follows describes the spectral image surface errors which arise due to a single dimensional parameter error. The dimensional parameters are described by Figure 2 and Table 11.

1. Entrance Slit Locational Accuracy

The monochromator images the two entrance slits on the detector lens array with roughly unity magnification. Thus, if the entrance slits are moved .001 inch along the positive X_o-axis, then their spectral images will move .001 inch along the negative X_5-axis and the negative X_3'-axis of each detector lens. A .001-inch movement of the entrance slits along the positive Y_o-axis results in a .001-inch movement of all their spectral images along the negative Y_5-axis and the negative Y_3' axes.

Similarly, a .001-inch movement of the entrance slits along the positive Z_o-axis results in a .001-inch movement of all their spectral images along the negative Z_5-axis and the negative Z_3'-axes.

This one-to-one reciprocal relationship for the two entrance slits and their spectral images can be used to correct the combined errors that arise from imperfect positioning of the grating and the collimating mirror. In other words, the substrate which defines the entrance slits can be moved to correct the alignment errors of the grating and collimating mirrors, if these errors are reasonably small.

2. Grating Locational Accuracy

The grating locational error parameters which affect the spectral image location noticeably are α_2, β_2, and γ_2. Locational parameters a_2, b_2, and c_2 have negligible effects on the spectral image unless these values are greater than .1 inch. Table 53 shows the Y_5 and Z_5 errors at the 3.7 μ, 4.3 μ, and 6.0 μ spectral images for three different error angles for each α_2, β_2, and γ_2. These error angles are .001°, .01°, and .1°. Figure 2 and Table 11 define α_2, β_2, and γ_2.

3. Collimating Mirror Locational Accuracy

Table 53 also shows the Y_5 and Z_5 errors at the same three spectral images for a lateral offset of the collimating mirror of .1 inch along the $Z_{1,4}$-axis; that is, $c_{1,4}$ = .1 inch, a corresponding result would be obtained for $b_{1,4}$ = .1 inch, where the roles of Y_5 and Z_5 are interchanged.

4. Collimating Mirror Focal Length

The resultant spectral image error for a collimating mirror focal length error of .020 inch is shown in Table 54. The collimating mirror focal length is increased to 10.020 inches, and the resultant a_5, Centroid Y_5, and Centroid Z_5 values are given for the spectral images at 3.7 μ, 4.3 μ, and 6.0 μ. This error can be partly corrected for by increasing a to 10.040 inches.

Table 53. Axial Ray Error Analysis for Final Monochromator

	W →	.777 (3.7μ)		.930 (4.3μ)		1.260 (6.0μ)	
	Description of Error	Y_5	Z_5	Y_5	Z_5	Y_5	Z_5
1	(Zero Error)	-.0028	.9060	-.0047	-.4959	.1033	-5.5809
2	$C_{1,4}$=.1; $C_{2,5}$= -.1	-.0020	1.1016	-.0049	-.2941	.0982	-5.3110
3	2 minus 1	.0008	.1956	-.0002	.2018	-.0051	.2699
4	α_2=26.001°; α_3= -26.001°	-.0028	.9064	-.0047	-.4956	.1033	-5.5804
5	4 minus 1	0	.0004	0	.0003	0	.0005
6	α_2=26.01°; α_3= -26.01°	-.0028	.9094	-.0047	-.4924	.1031	-5.5761
7	6 minus 1	0	.0034	0	.0035	-.0002	.0048
8	α_2=26.1°; α_3= -26.1°	-.0026	.9399	-.0048	-.4609	.1014	-5.5325
9	8 minus 1	.0002	.0339	-.0001	.0350	-.0019	.0484
10	β_2=.001°; β_3= -.001°	-.0025	.9060	-.0044	-.4959	.1036	-5.5810
11	10 minus 1	.0003	0	.0003	0	.0003	- .0001
12	β_2=.01°; β_3= -.01°	.0004	.9057	-.0016	-.4962	.1060	-5.5816
13	12 minus 1	.0032	- .0003	.0031	-.0003	.0027	- .0007
14	β_2=.1°; β_3= -.1°	.0293	.9032	.0264	-.4992	.1304	-5.5876
15	14 minus 1	.0321	- .0028	.0311	-.0033	.0271	- .0067
16	γ_2=.001°; γ_3= -.001°	-.0030	.9060	-.0049	-.4959	.1031	-5.5809
17	16 minus 1	-.0002	0	-.0002	0	-.0002	0
18	γ_2=.01°; γ_3= -.01°	-.0042	.9061	-.0063	-.4957	.1009	-5.5803
19	18 minus 1	-.0014	.0001	-.0016	.0002	-.0024	.0006
20	γ_2=.1°; γ_3= -.1°	-.0167	.9072	-.0209	-.4942	.0790	-5.5750
21	20 minus 1	-.0139	.0012	-.0162	.0017	-.0243	.0059

Table 54. 100-Ray Error Analysis for Final Monochromator

W (λ)	.777 (3.7 μ)			.930 (4.3 μ)			1.260 (6.0 μ)		
Description of Error	a_5	Centroid Y_5	Centroid Z_5	a_5	Centroid Y_5	Centroid Z_5	a_5	Centroid Y_5	Centroid Z_5
1 Zero Errors	-10.3715	.0122	.9204	-10.3769	.0088	-.4976	-11.9214	.1655	-5.6868
2 Focal Lens -10.020	-10.4092	.0131	.9230	-10.4171	.0098	-.4980	-11.9940	.1672	-5.6998
3 2 Minus 1	- .0377	.0009	.0026	- .0402	.0010	-.0004	- .0726	.0017	- .0130

SECTION 9

CONCLUSION

The final design for an infrared Multidetector Spectrometer for the Nimbus "F" experiment described in this report is capable of meeting all the requested performance specifications listed in Section 2.0, Final Performance Requirements. In addition, the modification to the Multidetector Spectrometer will be housed within the requested overall dimensions. Drawings 1 and 2 which are located at the end of this section illustrate the overall spectrometer housing design.

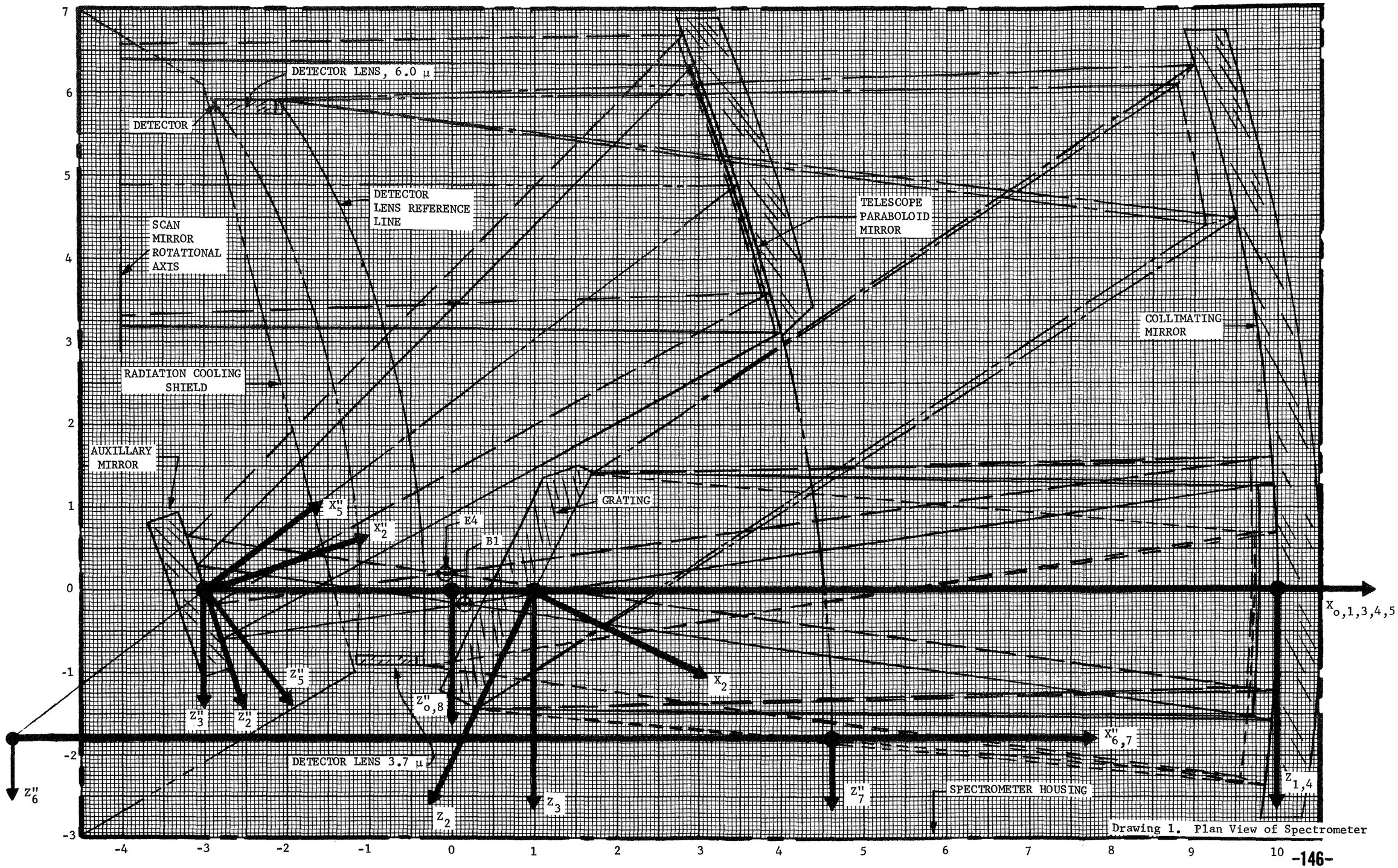

Drawing 1. Plan View of Spectrometer

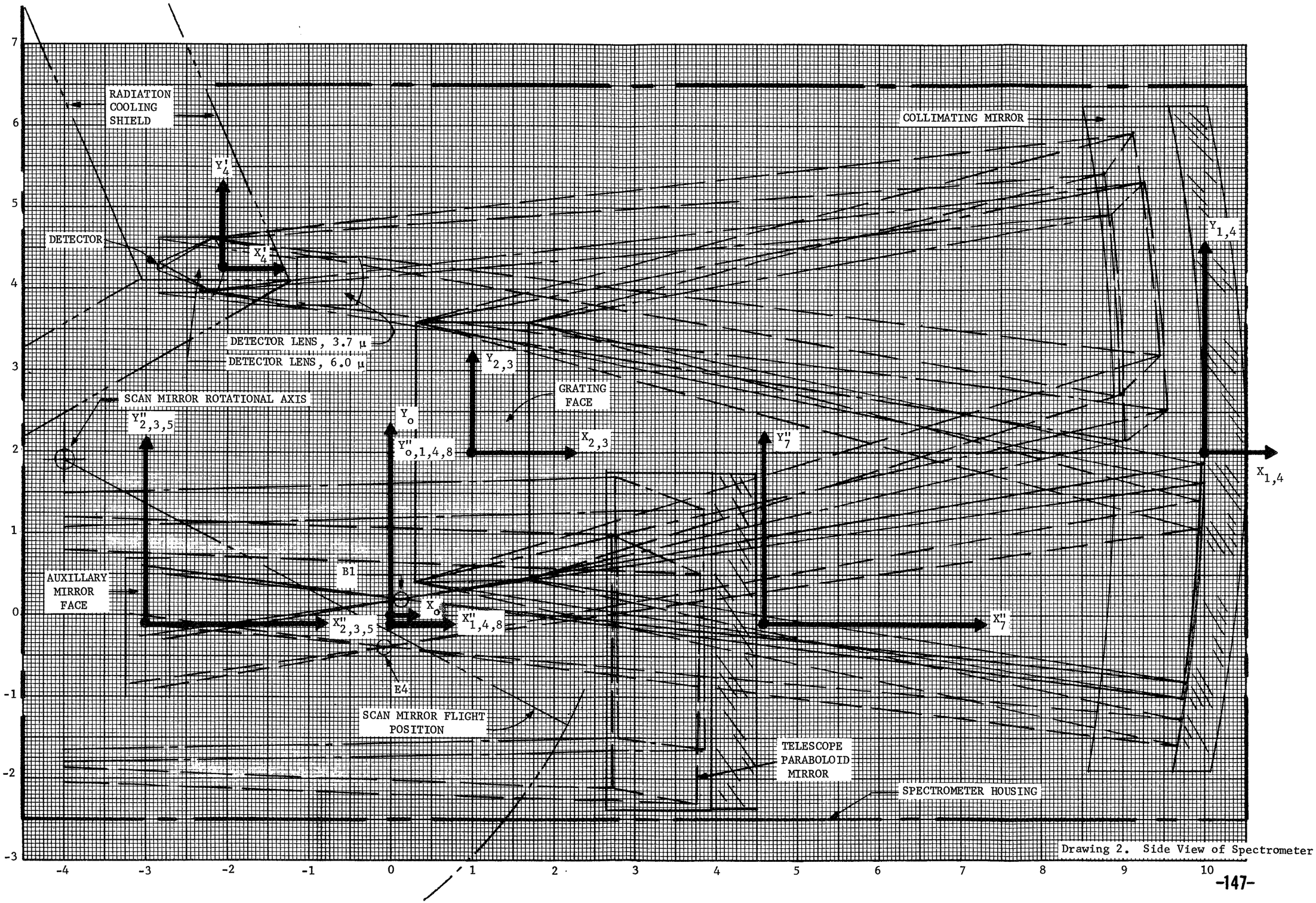

Drawing 2. Side View of Spectrometer

SECTION 10

REFERENCES

1. Henderson, B.D., "Study and Investigation of Optical System," Phase I Final Report. JPL Contract 950880, 14 May 1964.

2. Henderson, B.D., and J. Zerucha, "Study and Investigation of Optical System, Phase II Final Report. JPL Contract 950880, 14 August 1964.

3. Henderson, B.D., and J. Zerucha, "Infrared Spectrophotometer Calibration Monochromator Study," Final Report. JPL Contract 950975, 11 November 1964.

4. Schaper, P.W., and D.D. LaPorte, "Infrared Spectrometer for High Altitude Balloon Experiments," JPL SPS 37-36, IV, 195-202 (1965).

5. Schaper, P.W., "An Infrared Multidetector Spectrometer for Absolute Radiometric Measurements," JPL SPS 37-43, 239-248 (1967).

6. Shaw, J.H., R.A. McClatchey, and P.W. Schaper, "Balloon Observations of the Radiance of the Earth Between 2100 and 2700 cm^{-11}," Applied Optics 6, 227-30 (1967).

7. McClatchey, R.A., and J.H. Shaw, "A Spectrometric Measurement of the Atmospheric Temperature Above 30 Km Near Sunrise," J. Atmos. Science, 26, 1350-1353 (1969).

8. Smith, J.W., "Thermal Study of a Passive Cooling Device for an IR Spectrometer in a Normal Nimbus Orbit," JPL July 15, 1969.